Proteomic analysis of redox-dependent AGR2 complexes reveals a novel mucin quality control system in oesophageal adenocarcinoma

JACK CHRISTOPHER PETER WORFOLK

Proteomic analysis of redox-dependent AGR2 complexes reveals a novel mucin quality control system in oesophageal adenocarcinoma

Jack Christopher Peter Worfolk

Abstract: Disulphide bonds covalently linking cysteine residues, intramolecularly or intermolecularly, are often essential in ensuring the stability of secreted and cell surface proteins as well as facilitating correct spatial positioning of protein active sites. The protein disulphide isomerase (PDI) family of proteins catalyse the oxidation, reduction and isomerisation of these disulphide bonds. PDI proteins are vital for protein quality control and most are found ubiquitously. Anterior gradient-2 (AGR2) is an unusual tissue-restricted member of the PDI family that has gained considerable attention in the last 15 years because of its overexpression in a variety of different cancer types, including oesophageal adenocarcinoma. In this thesis it has been demonstrated that the OE19 late stage oesophageal adenocarcinoma cell line strongly expresses AGR2, and that in this cell line AGR2 can form redox-inducible, disulphide bond dependent complexes. It has also been shown, through the development and use of a novel, unbiased trapping and immunoprecipitation approach, that these AGR2 interacting proteins can be identified and compared. This approach has identified mucin isoforms that AGR2 preferentially binds as its primary clients and has revealed a host of ER chaperones involved in this quality control complex. This thesis lays the groundwork for the elucidation and definition of an AGR2-mucin quality control system within oesophageal adenocarcinoma and provides biomarkers and potential therapeutic targets for identification and treatment of AGR2-positive cancers.

Proteomic analysis of redox-dependent AGR2 complexes reveals a novel mucin quality control system in oesophageal adenocarcinoma

Jack Christopher Peter Worfolk

A Thesis submitted for the degree of Master of Science

Department of Biosciences, Durham University

March 2018

Table of contents

List of figures and tables

Section 1: Introduction

Section 2: Materials and Methods

Section 3: Results

Section 4: Discussion

List of Abbreviations

ACN	Acetonitrile
AGR2	Anterior gradient-2
APS	Ammonium persulphate
ATP	Adenosine triphosphate
BiP	Binding immunoglobulin protein
BSA	Bovine Serum Albumin
cDNA	Complimentary DNA
CID	Collision-induced dissociation
CNX	Calnexin
CRT	Calreticulin
D	Denaturing
DAB	3,3'-dianimobenzidine
DAG-1	Dystroglycan 1
DAPI	4',6-diamino-2-phenylindole
dH_2O	De-ionised water
DMSO	Dimethyl sulphoxide
DNA	Deoxyribonucleic acid
DTT	Dithiothreitol
DUSP10	Dual specificity phosphatase
ECL	Enhanced chemiluminescence
eIF2α	Eukaryotic translation initiation factor 2
ER	Endoplasmic reticulum
Ero1α	Endoplasmic reticulum oxidoreductase 1 alpha
ERp29	Endoplasmic reticulum protein 29
ERp44	Endoplasmic reticulum protein 44

ERp57	Endoplasmic reticulum protein 57
EtOH	Ethanol
FASP	Filter aided sample prep
FBS	Fetal bovine serum
GAL4	Galectin-4
GAMPO	Goat anti-mouse peroxidase
GFP	Green fluorescent protein
GPI	Glycosylphosphatidylinositol
HCl	Hydrochloric acid
HRP	Horse radish peroxidase
H_2O_2	Hydrogen peroxide
IgG	Immunoglobulin G
IP	Immunoprecipitation
KCl	Potassium chloride
L	Untreated lysate
LC-MS/MS	Liquid chromatography tandem mass spectrometry
mAb	Monoclonal antibody
MAPK	Mitogen-activated protein kinase
MEM	Minimum essential medium
MeOH	Methanol
mRNA	Messenger ribonucleic acid
MS	Mass spectrometry
MS-MS	Tandem mass spectrometry
MSC	Membrane contact site
MUC1	Mucin 1
MUC2	Mucin 2

MUC5AC	Mucin 5AC
MUC5B	Mucin 5B
NaOH	Sodium hydroxide
ND	Non-denaturing
NEM	N-ethylmaleimide
NR	Non-reducing
OG	Oesophageal
pAb	Polyclonal antibody
PBS	Phosphate buffered saline
PDI	Protein disulphide isomerase
PDIA3	Protein disulphide isomerase family A member 3
PFA	Paraformaldehyde
PNGase F	Peptide-N-glycosidase F
Prdx1	Peroxiredoxin 1
PrdxIV	Peroxiredoxin-4
PVDF	Polyvinylidene fluoride
R	Reducing
RPMI	Rosewell Park Memorial Institute medium
RT	Room temperature
SARPO	Swine anti-rabbit peroxidase
SBTI	Soybean trypsin inhibitor
SDS	Sodium dodecyl sulphate
SDS-PAGE	Sodium dodecyl sulphate polyacrylamide gel electrophoresis
TBS	Tris-buffered saline
TEMED	N,N,N’,N’-Tetramethylethylenediamine
TFA	Trifluoroacetic acid

UV	Ultraviolet
YFP	Yellow fluorescent protein
ZG16B	Zymogen granule protein 16B

Declaration

I declare that the contents and all data presented in this thesis, is the result of my own work. No part of the material offered has previously been submitted for a higher degree. The body of work has been achieved under the supervision of Dr. Adam M. Benham.

Jack Christopher Peter Worfolk

March 2018

Statement of Copyright

Acknowledgements

I would first like to thank Dr Adam Benham for providing me with this opportunity, supervising me through this project and always providing helpful guidance when needed.

I would also like to thank YKS Viswaneth and Dr Julie Walker from South Tees Hospitals NHS foundation trust for their doctoral advice and tissue samples respectively.

Additionally, I would like to thank Steven Bell, Naomi Carne and the rest of the members of Lab 8, as well as Adrian Brown from the Proteomics Facility, for their advice and assistance throughout this project.

Finally, I would like to thank my family for funding me throughout this project and for their continued support.

1. Introduction

1.1 The endoplasmic reticulum and chaperones

The major defining feature of eukaryotic cells, distinguishing them from prokaryotic cells, is the presence of organelles - membrane bound compartments which allow our cells to organise themselves and provide specialised microenvironments for specific purposes. While the textbook examples of organelles described them as individual and sperate compartments each with their own microenvironment, research in recent years has shed light on the importance of membrane contact sites (MCSs) (Wu et al., 2018). MScs are sites where organelles do not fuse but tether to one another, allowing highly regulated interorganelle communication and facilitating such complex processes as lipid and ion transfer as well as organelle division. These recent developments have highlighted the dynamic nature of organelles and the importance of interorganelle communication for regulating homeostasis. The secretory pathway within eukaryotic cells is comprised of a series of these organelles that process and transport a wide variety of products to various locations, including secretion outside of the cell. The secretory pathway provides a sophisticated processing and delivery system for complex protein structures to a variety of target locations. Proteins processed through the secretory pathway include secreted proteins, membrane bound proteins, lysosomal enzymes and proteins residing with the secretory pathway itself.

The endoplasmic reticulum (ER) is located at the start of the secretory pathway and is involved in a variety of different processes including lipid synthesis, Ca^{2+} handling as well as protein synthesis, folding, modification and transport (Baumann and Walz, 2001). While protein folding and maturation does occur in the cytosol, it is not optimized to the same extent as the lumen of the ER. Upon translation into the ER lumen, proteins must acquire the correct folding conformation if they are to function properly. Proteins which are persistently incorrectly folded are not transported to their correct destination and are instead degraded. This process of protein quality control is essential as not only are misfolded proteins unlikely to function properly, they are prone to aggregation. Aggregated proteins are involved in a range of neurodegenerative diseases such as ALS, Alzheimer's, Huntington's, Parkinson's and prion diseases (Ross and Poirier, 2004).

Assisting in the process of protein quality control are the protein chaperones. These proteins reside in the ER at high concentrations and recognise misfolded proteins, either promoting folding to the correct conformation, or directing improperly folded proteins for destruction. The chaperone proteins are vital for protein quality control, and ensuring only native conformers are allowed to exit the ER is essential as protein quality control takes place within the ER, but not in the ER-Golgi intermediate

compartment or the Golgi complex itself (Mezzacasa and Helenius, 2002). Several processes involved in protein folding occur only in the ER. These include signal peptide cleavage, GPI-anchor attachment, N-linked glycosylation and, most importantly for this thesis, disulphide bond oxidation, isomerisation and reduction.

1.2 Disulphide bonds, bridges and isomerases

Disulphide bonds play a pivotal role in protein maturation and are often essential for the stability and function of final protein structures. Disulphide bond formation takes place within the oxidising environment of the ER when two free thiol (SH) groups from the side chains of cysteine residues are covalently linked, either intramolecularly or intermolecularly, through an oxidation reaction. This process is known as oxidative protein folding and is often prone to error, resulting in non-native disulphide bonds. When this occurs the disulphide must be reduced before the correct bond can be formed. Catalysing the oxidation, reduction and isomerisation of these disulphide bonds are the protein disulphide isomerase (PDI) family of proteins.

PDI family members are defined by the presence of one or more thioredoxin-like domains, similar to the small 10 kDa oxidoreductase thioredoxin, and an active site CXXC motif (or similar) from which transient disulphide bonds are formed with their interaction partners. In humans, there are 21 known members of the PDI family. Some of these proteins are ubiquitous and essential for normal cellular function, such as Protein Disulphide Isomerase (PDI) (crystal structure shown in Figure 1), while others are tissue-restricted and adapted to catalyse the correct folding and secretion of specific client proteins, such as Anterior gradient-2.

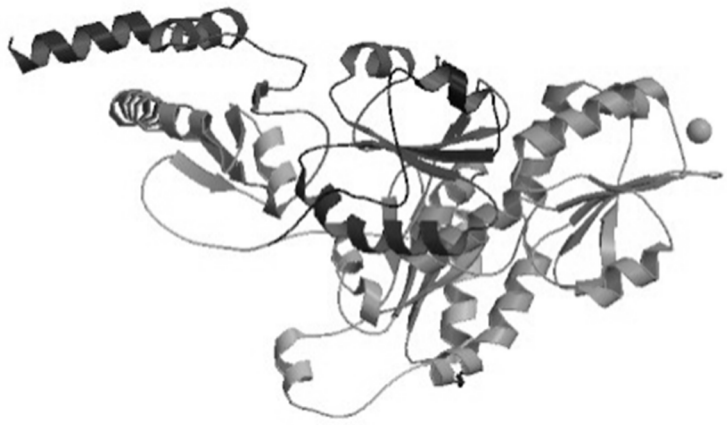

Figure 1: **Crystal structure of Yeast Protein Disulphide Isomerase** (2B5E from the protein databank (PDB) database). The four thioredoxin domains of PDI are displayed, as well as a Ba^{2+} barium ion shown as a circle to the right of the structure.

1.3 Anterior gradient-2 (AGR2)

Anterior gradient-2 (AGR2) is an unusual member of the PDI family of proteins but has gained considerable attention in the last 15 years due to its derepression and oncogenic properties in a variety of different cancer types. The first discovery of the anterior gradient proteins came when studying the embryogenesis of *Xenopus laevis*, where Xenopus anterior gradient-2 (XAG-2) was found to be a secreted protein expressed in the cement gland, an ectoderm-derived organ aiding anteroposterior development (Aberger et al., 1998). Shortly after, the human homologue hAG-2 (later referred to as AGR2) was found to be coexpressed with the estrogen receptor in several breast cancer cell lines, suggesting a possible role for AGR2 in breast tumour biology (Thompson and Weigel, 1998). Since then overexpression of AGR2 has been found in a variety of other types of adenocarcinomas including prostate (Zhang et al., 2005), oesophageal (Pohler et al., 2004), pancreatic (Ramachandran et al., 2008), ovarian (Park et al., 2011) and lung (Zhu et al., 2007). The exact role of AGR2 in tumour cell biology is slowly being elucidated, but already it has been shown to play key roles in cell growth, proliferation (Pohler et al., 2004), adhesion and metastasis (Liu et al., 2005).

As well as its role in cancer progression, AGR2 performs a physiological role as a protein chaperone, and is natively expressed in tissue such as lung, prostate, bladder, as well as the gastro-intestinal tract (Fagerberg et al., 2014). In these tissues it has been shown to be required for the correct folding and secretion of mucins, the large gel-forming glycoproteins that give mucus its viscoelastic properties (Park et al., 2009; Schroeder et al., 2012). Mucins contain large numbers of cysteine residues that form intra and interchain disulphide bonds which give mucus its structure. AGR2 is required for the correct synthesis of these disulphide bonds, although the exact mechanism by which it performs its function is unknown.

As mentioned previously, PDI family members are classified by the presence of at least one thioredoxin-like domain, whether it be enzymatically active or not. Unlike most other PDI family members AGR2 contains only one thioredoxin-like domain with an unusual CXXS motif. The primary structure of AGR2 is displayed in Figure 2. This motif has been shown to lack the catalytic oxidase activity found in other members of the PDI family (Nørgaard and Winther, 2001). The absence of oxidase activity in this motif suggests that AGR2 is not a typical PDI and leads to the possibility that it relies on other interacting partners to perform its biological function.

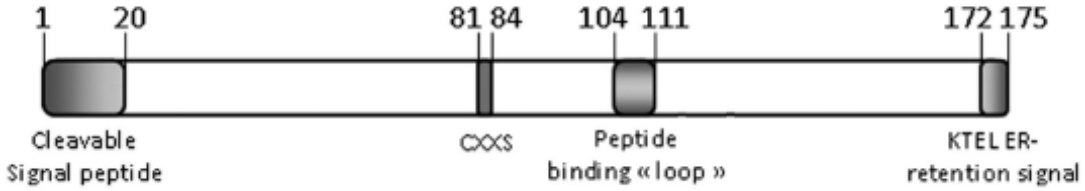

Figure 2: **The primary structure of AGR2.**
Shaded boxes indicate identified domains and motifs involved in the function and regulation of AGR2. Taken from Chevet et al. 2013 doi:10.1038/onc.2012.346.

Additionally, AGR2 contains a non-optimal KTEL ER localisation signal, removal or alteration of which will affect its localisation and function (Gupta et al., 2012). Normally, ER resident proteins possess a KDEL ER localisation signal at their C terminal which is recognised by the KDEL receptors in the cis Golgi. Proteins with this KDEL motif that have travelled to the cis Golgi are recognised by the KDEL receptors and are transported back to the ER, thus maintaining their concentrations without the need for fast translation rates. The presence of the non-optimal KTEL ER localisation signal at the C terminal of AGR2 prompts the question of where exactly within the cell it is localised. Multiple studies have shown that AGR2 is primarily localised to the ER (Gupta et al., 2012; Higa et al., 2011; Park et al., 2009; Zhao et al., 2010), however the non-optimal KTEL motif still may allow AGR2 to travel beyond the ER.

More recently a substrate binding loop has also been identified in AGR2 (Maslon et al., 2010). This was shown to be involved with its interaction with the nuclear DNA binding protein Reptin and is a possible route for AGR2 interactions to take place. This will be expanded upon later in section 1.5.

1.4 The physiological role of AGR2

As mentioned previously, one of the more significant roles of AGR2 involves its interaction with the mucin proteins, a major component of mucus. A study by Park et al., (2009) showed that $Agr2^{-/-}$ mice lacked intestinal mucus and had undetectable levels of the MUC2 protein and little to no MUC2 synthesis in the small intestine. It was also shown in this study that AGR2 deficient mice had increased susceptibility to intestinal disease, and with aging these mice often developed symptoms of colitis, including rectal prolapse. Knockout studies with other PDI family members such as ERp57 have resulted in embryonic lethality (Garbi et al., 2006). Although AGR2 knockout in mice produces a disease prone phenotype, it does not result in embryonic lethality and demonstrates AGR2's role as a highly specific PDI member primarily involved in mucus production.

AGR2 has also been shown to interact with airway mucins MUC5AC and MUC5B, as demonstrated by Schroeder et al., (2012). Co-immunoprecipitation experiments showed that AGR2 interacts with immature MUC5AC in airway cells, and analysis of airway epithelial gene expression showed a correlation between AGR2 and MUC5AC expression. In this study they also demonstrated that germline $Agr2^{-/-}$ mice had a greater than 50% reduction in MUC5AC and MUC5B protein levels compared to wild type mice, suggesting AGR2 plays a crucial role in the processing of MUC5AC and MUC5B. Taken together, these studies highlight the crucial role of AGR2 in the synthesis of certain mucin isoforms and opens up the question of how exactly it mediates this role.

Another study, this time using germline and inducible $Agr2^{-/-}$ mice, demonstrated the importance of AGR2 in both the goblet and Paneth cells of the intestinal crypts (Zhao et al., 2010). It was observed that in both germline and inducible $Agr2^{-/-}$ mice goblet cell lineage remains; however, they lose their normal morphology and intestinal mucus is decreased. In the same $Agr2^{-/-}$ mice they showed several abnormalities in Paneth cells. An enlargement of the Paneth cell compartment was observed as well as mislocalized Paneth cells in the upper crypt and villi. $Agr2^{-/-}$ mice were also found to be highly susceptible to experimentally induced ileitis and colitis. The phenotype observed in this study was compared to Crohn's disease, and in another study genetic variants of the *Agr2* gene that decrease its mRNA expression induce the ulcerative colitis phenotype (Zheng et al., 2006) suggesting AGR2 plays a key role in regulating inflammatory bowel disease. These knockout mice studies have shown the importance of AGR2 in mucus secretion and demonstrated the vital role it plays in regulating gastrointestinal diseases.

1.5 Interacting partners for AGR2

Through the use of yeast two-hybrid screens and a variety of other studies AGR2 has been shown to interact, directly or indirectly, with a large number of other proteins in the human body. The first and perhaps the most important for determining its direct role in humans, previously mentioned in section 1.4, was the discovery of its interaction with mucin 2 (MUC2) (Park et al., 2009). It was shown that MUC2, an integral component of intestinal mucus, requires AGR2 to fold properly and therefore function. In co-immunoprecipitation experiments AGR2 was shown to co-immunoprecipitate with MUC2, an interaction that disappeared when the single cysteine residue in AGR2 was mutated. From this they concluded AGR2 forms mixed disulphide bonds with MUC2, establishing AGR2 as a highly specific PDI family member.

The ability of AGR2 to interact with itself to form homodimers was first shown by Ryu et al., (2013) who provided evidence that this ability is facilitated by the formation of

an intermolecular disulphide bond, and that the dimerization is required for interaction with BiP. Paradoxically, shortly afterwards Patel et al., (2013) showed AGR2 existed in a monomer-dimer equilibrium within the ER at a K(d) of 8.83 μM, but provided data suggesting that the only cysteine residue within AGR2 was not necessary for dimer formation. They instead provided evidence that the dimer interaction was provided by salt bridges connecting the antiparallel arrangement of the alpha1 helices of the two molecules. If the dimer interaction does not require the CXXS motif cysteine residue it opens the possibility that the dimer conformation is used in interactions involving intermolecular disulphide bonds, such as MUC2 folding.

Using yeast two-hybrid screening in breast tumour tissues it was found that both metastasis-associated GPI-anchored C4.4a protein and extracellular alpha-dystroglycan (DAG-1) acted as binding partners for AGR2 (Fletcher et al., 2003). With both proteins involved in interactions with the extracellular matrix this has been suggested as a possible route for AGR2 to affect tumour cell metastasis, migration and invasion. Another protein found to interact with AGR2 through the use of yeast two-hybrid screening was the nuclear DNA binding protein Reptin (Maslon et al., 2010). With the use of site directed mutagenesis, a small substrate binding loop in AGR2 was determined to be the docking site for its interaction with Reptin and two ATP binding motifs on Reptin were found to be involved in regulation of the AGR2:Reptin complex. As Reptin can act as a regulator of tumour suppressor genes, this interaction suggests that a possible route for AGR2 as a prometastatic factor could be through gene regulation.

Almost all cancers, when they reach a certain stage, have either a mutated dysfunctional p53 gene or p53 activity is suppressed in one way or another. It is therefore not surprising that in 2003 AGR2 was shown to suppress p53 activity (Pohler et al., 2004). Cells transfected with AGR2 showed distinctly less p53 phosphorylation at both Ser15 and Ser392, after UV-induced DNA damage, compared to cells without AGR2. This was determined later to be mediated through AGR2's upregulation of DUSP10, a phosphatase that inactivates p53 along with another regulator of apoptosis, p38 MAPK (Hrstka et al., 2016). AGR2's ability to suppress p53 activity gives strong evidence towards its role as a regulator of tumour growth.

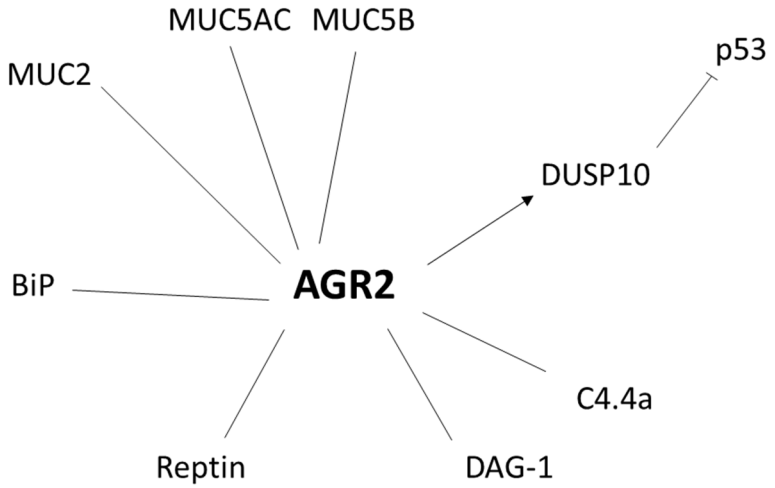

Figure 3: **Major interacting partners for AGR2.**
A diagram summarizing the major known interacting partners for AGR2 described in sections 1.4 and 1.5. Straight lines indicate binding interactions (whether direct or indirect), arrows indicate upregulation of activity and flat ended lines indicate inhibition of activity.

A wide variety interacting partners for AGR2 have been discovered and even more processes and pathways have been shown to be regulated by AGR2 (Figure 3) indicating the importance of AGR2 in the environments in which it is expressed.

1.6 Barrett's oesophagus and oesophageal adenocarcinoma

The development of oesophageal adenocarcinomas is often preceded by a condition called Barrett's oesophagus. Repeated gastro-oesophageal reflux and chronic exposure of the normal squamous oesophageal epithelium to gastric and duodenal contents can result in an adaptive response in some individuals. A metaplasia and dysplasia of the oesophageal epithelium can occur, activating glycoprotein synthesis machinery to produce mucus as a defence mechanism against the change in environment. This transition to a mucus secreting columnar epithelium results in a condition known as Barrett's oesophagus, or Barrett's epithelium. Although not cancerous, Barrett's oesophagus is considered a pre-malignant condition as there is a high chance (estimated between 0.5-2% per year) patients with Barrett's will develop oesophageal adenocarcinoma (Nancarrow et al., 2011). Patients with Barrett's oesophagus are estimated to have a 30-fold higher chance of developing oesophageal adenocarcinoma when compared to the general population (Solaymani-Dodaran et al., 2004).

The transition to Barrett's oesophagus is accompanied by a whole host of changes to gene expression, including the elevated expression of mucins such as MUC2 and MUC5AC (DiMaio et al., 2012). Along with mucins, AGR2 has been shown to be universally upregulated in Barrett's oesophagus (Pizzi et al., 2012; Pohler et al.,

2004). Unlike other cancers that overexpress and secrete AGR2, the overexpression of AGR2 in Barrett's oesophagus is assumed to be involved in the glycoprotein synthesis machinery. This aberrant expression of AGR2 has been proposed as a biomarker for Barrett's oesophagus (DiMaio et al., 2012).

1.7 Thesis Aims

Previous work by Simpson and Benham (unpublished data) showed that AGR2 is strongly expressed in the OE19 late stage oesophageal adenocarcinoma immortalised cell line, used as a model for Barrett's oesophagus. Their work suggested AGR2 complex formation was affected by treatment with the reductant dithiothreitol (DTT), visible through non-reducing western blotting. The aims of this thesis are to determine whether these changes observed were the result of an altered redox state, or due to the ER stress induced by DTT. Additionally, through the use of immunoprecipitation and mass spectrometry, the interactions AGR2 makes to form these complexes and the interacting partners involved will be investigated.

2. Materials and methods

2.1 Chemicals

Chemicals were from Sigma-Aldrich unless otherwise stated.

2.2 Antibodies

Rabbit polyclonal PDI antibody from our laboratory has previously been described (Benham 2000). Rabbit polyclonal calnexin antibody was a gift from Prof. Masuru Okabe, Osaka University. Rabbit monoclonal anti-AGR2 (D9V2F) XP (13062), rabbit polyclonal anti-Phospho-eIF2α (Ser51) (9721), rabbit polyclonal anti-BiP (3183), rabbit polyclonal anti-ERp57 (G117), rabbit monoclonal anti-ERp44 (D17A6) XP (3798) and mouse monoclonal anti-Myc-Tag (9B11) were purchased from Cell Signaling Technologies. Rabbit monoclonal anti-AGR2 (EPR3278/ab76473), mouse monoclonal anti-β-actin (ab8224), rabbit monoclonal anti-MUC5AC (EPR16904/ab198294), rabbit polyclonal anti-ERp29 (ab11420), mouse monoclonal anti-PrdxIV (7A1) (ab16943) and rabbit monoclonal anti-GAL4 (EPR12710(B)/ab175185) were purchased from abcam. Mouse monoclonal anti-PDI RL-90 (MA3-019) was purchased from ThermoFisher Scientific. Mouse monoclonal anti-PAUF/ZG16B (817310) was purchased from Nous Biologicals. Rabbit polyclonal anti-PDI was produced in our laboratory and has previously been described (Benham 2000). Secondary antibodies used in western blotting were swine anti-rabbit HRP (SARPO P0217) and goat anti-mouse HRP (GAMPO P0447) conjugates from DAKO. Donkey anti-rabbit Alexa Fluor 488 (A21206) and donkey anti-rabbit Alexa Fluor 594 (A21207) from ThermoFisher Scientific were used in immunofluorescence.

Antibody dilutions for western blotting were as follows: anti-AGR2 (D9V2F), 1:1000; anti-BiP, 1:1000; anti-β-actin, 1:10,000; anti-CNX, 1:2000; anti-ERp29, 1:1000; anti-ERp44, 1:1000; anti-ERp57, 1:1000; anti-GAL4, 1:1000; anti-MUC5AC, 1:10,000; anti-Myc, 1:1000; anti-PAUF/ZG16B, 1 μg/ml; anti-PDI pAb, 1:1000; anti-PDI (RL-90), 1:1000; anti-PrdxIV, 1:2000; anti-P-eIF2α, 1:500. Secondary antibody dilutions for western blotting were as follows: swine anti-rabbit HRP, 1:3000; goat anti-mouse HRP, 1:3000. Antibody dilutions for immunofluorescence were as follows: anti-PDI pAb, 1:200; anti-AGR2 (D9V2F), 1:200; anti-PrdxIV, 1:200. Secondary antibody dilutions for immunofluorescence were as follows: donkey anti-rabbit Alexa Fluor 488, 1:1000; donkey anti-rabbit Alexa Fluor 594, 1:1000. Antibody dilutions for immunoprecipitation were as follows: anti-AGR2 (EPR3278/ab76473), 1:20; anti-PDI pAb, 1:25; anti-ERp29 (ab11420), 1:500.

2.3 Cell culture

OE19 (JROECL19) and OE33 (JROECL33) cells were obtained from ECACC, both at passage number p6. The OE19 cell line was established from an adenocarcinoma of gastric cardia/oesophageal gastric junction from a 72-year-old male patient. The tumor was identified as pathological stage III (UICC) and showed moderate differentiation. The OE33 cell line was established from an adenocarcinoma of the lower oesophagus (Barrett's metaplasia) from a 73-year-old female patient. The tumor from which the cells were taken was identified as pathological stage IIA (UICC) and showed poor differentiation. The OE cell lines were subcultured twice weekly in Rosewell Park Memorial Institute medium (RPMI) 1640 (Invitrogen) supplemented with fetal bovine serum (FBS) to a final concentration of 8%, 2mM glutamax (Invitrogen) and 100 µg/mL Penicillin/Streptomycin (Invitrogen).

HT0180 cells were subcultured twice weekly in Dulbecco's Modified Eagle's Medium (DMEM, Gibco, Thermofisher Scientific) supplemented with with fetal bovine serum (FBS) to a final concentration of 8%, 2mM glutamax (Invitrogen) and 100 µg/mL Penicillin/Streptomycin (Invitrogen).

All cell lines were kept in a humidified incubator at 37°C and 5% CO_2. Treatments were carried out when the cells reached ~70% confluence, in 6 cm dishes.

2.4 Immunofluorescence

OE19 cells grown on coverslips were fixed with 4% paraformaldehyde (PFA) (agar scientific) in phosphate buffered saline with magnesium and calcium (PBS++) for 10 min, free aldehyde groups were quenched with 50 mM ammonium chloride in PBS++ for 10 min then the cells were permeabilised with 0.1% Triton X-100 in PBS++ for 10 min. Samples were then blocked in 0.2% bovine serum albumin (BSA) in PBS++ twice for 5 min each then incubated with 25 µL primary antibody solution, diluted in 0.2% BSA in PBS++, for either 1 hour (PDI) or overnight (AGR2, PrdxIV). Following primary incubation, samples were washed three times with PBS++ then incubated with secondary antibody solution, diluted in 0.2% BSA in PBS++, for 25 mins in the dark. Following secondary incubation, samples were washed twice with BSA, twice with PBS++ then incubated with 50 µL 5 µg/mL DAPI solution for 5 mins, rinsed briefly in PBS++ and dH_2O then mounted on microscope slides with Vectashield mounting medium (vectorlabs). Before imaging slides were left at 4°C overnight to allow the Vectashield to set. The slides were imaged on either a brightfield fluorescence microscope (Zeiss ApoTome) or a confocal microscope (Zeiss 880). When using two primary antibodies for co-staining both were applied simultaneously.

2.5 Preparation of cell culture medium for treatment

Stock solids of the chemicals, diamide, bile acids and thapsigargin were dissolved in dH_2O to produce stock solutions that were aliquoted and frozen at -20°C. Immediately prior to treatment stock solutions were defrosted and an appropriate volume was added to an aliquot of sterile RPMI media to give the desired final concentration. If media was required at a specific pH then media was aliquoted, adjusted to the desired pH dropwise with HCl or NaOH and tested with a calibrated pH meter. The pH-adjusted media was then sterilised by filtration through a 0.22 µm syringe filter (MILLIPORE) and stored at 4°C until needed.

2.6 Cell treatments

Cells were treated with fresh RPMI media (as described above) supplemented with the desired chemical and concentration and returned to the 37°C incubator for the required time course. Following treatment cells were washed twice with phosphate buffered saline (PBS) for 5 minutes. The first PBS wash was supplemented with 20 mM N-ethylmaleimide (NEM) in experiments using NEM. Cells were lysed immediately after treatment.

2.7 Cell lysis

Cells were lysed on ice in 300 µl of MNT lysis buffer (20 mM 4-morpholineethanesulfonic acid, 30 mM Tris, 100 mM NaCl, pH 7.4) with 1% Triton X-100, supplemented with 10 µg/ml each of the protease inhibitors chymostatin, leupeptin, antipain, and pepstatin A. Lysis buffer also contained 20 mM NEM in experiments using NEM. Lysed cells were scraped and the lysates were collected in Eppendorf tubes. The cell nuclei were removed by centrifugation at 16,100g (Eppendorf microcentrifuge) for 10 min at 4°C and the supernatants were collected in fresh Eppendorf tubes and flash frozen in liquid nitrogen and stored at -20°C.

2.8 Protein determination

Protein concentrations for equal loading were determined using the Bio-Rad Protein Assay procedure with BSA used as a standard. Standards were produced by combining the Bradford dye with dH_2O, HCl, BSA and lysis buffer. A 1 mg/mL stock solution of BSA was diluted in lysis buffer to produce final concentrations ranging from 0-10 µg/mL. Samples were produced by combining the Bradford dye with dH_2O, HCl, lysis buffer and 2 µL of lysate. Mixtures were left for 10 minutes then vortexed and their absorbances measured at 595 nm in an Eppendorf Biophotometer.

2.9 SDS-PAGE

For protein detection, samples were analysed under either reducing or non-reducing conditions in SDS-PAGE. Samples for SDS-PAGE were prepared by adding 2x Laemmli sample buffer to cell lysates. For samples ran under reducing conditions 50 mM DTT was also added. To denature the proteins within the sample they were heated at 95°C for 5 mins, then centrifuged at 16,100 g for 5 mins to collect the liquid at the bottom of the tube. Prepared samples were analysed using either 8%, 10% or 12% acrylamide gels. The resolving gel was comprised of: acrylamide (variable percentage) (Severn Biotech), 0.375 M Tris (pH 8.8), 0.1% SDS, 0.1% ammonium persulphate (APS) and 0.04% N,N,N',N'-Tetramethylethylenediamine (TEMED). The stacking gel was comprised of: 5% acrylamide, 0.125 M Tris (pH 6.8), 0.1% SDS, 0.075% APS, 0.1% TEMED.

Acrylamide gel were cast in the Hoefer mini gel casting system. The resolving gel was first cast and left to polymerise, with water to cover the gel. The water was then removed and replaced with the stacking gel, followed by insertion of either a 10 well or a 15 well comb. Once the gel fully polymerised samples were loaded alongside a protein stained marker (Bio-Rad). Gels were run at 10-50 mA for approximately one hour in a Hoefer mighty small II mini vertical electrophoresis unit containing 1x Tris-Glycine buffer (25 mM Tris, 192 mM glycine, 0.1% SDS, pH 8.3). Analysis was done either via western blotting or Coomassie blue staining.

2.10 Coomassie gel staining

After SDS-PAGE, gels were fixed in a fixing solution (7% acetic acid and 40% methanol in dH_2O) for 10 minutes. To stain the gels, fixing solution was removed and the Coomassie stain was applied (80% Brilliant blue G-colloidal concentrate in methanol). Staining took place overnight with gels placed on a rocker. To destain the gels, the first destaining solution (25% methanol, 10% acetic acid in dH_2O) was applied for 10 minutes, followed by the second destaining solution (25% methanol in dH_2O) which was applied for another 10 minutes. Gels were scanned into an office computer.

2.11 Western blotting

Following SDS-PAGE separation, proteins were transferred to polyvinylidene fluoride (PVDF) membrane. For transfer, membranes were first submerged in methanol for 20 seconds to activate them, then placed in transfer buffer (25 mM Tris base, 190 mM glycine and 20% methanol in dH_2O) and transferred at either 150 mA for 2 hours or at 30V overnight. Membranes were then blocked in 5% non-fat dry milk in TBS-T (Tris-buffered saline (10 mM Tris base, 70 mM NaCl, 1.34 mM KCl) containing 0.1% Tween 20) for 1h at room temperature. Membranes were washed 5 times with TBS-

T before either a 1-hour incubation at RT or an overnight incubation at 4°C with primary antibody (dependent on antibody), followed by another 5 washes and incubation for 1 hour at room temperature with either swine anti-rabbit HRP (SARPO) or goat anti-mouse HRP (GAMPO). Antibody concentrations are listed in section 2.2. To visualise protein localisation, 500 µL of enhanced chemiluminescence (ECL) solution per membrane was used. Membranes were exposed to photographic light sensitive film in a dark room and subsequently developed in an X-ray developer machine (XOMAT).

Western blot quantification through densitometry was performed on scanned immunoblot images with the ImageJ image processing program.

2.12 Immunoprecipitation

Immunoprecipitation of target proteins was performed using Protein A-Sepharose beads (Sigma). Protein A-Sepharose beads were incubated with the indicated antibodies (concentrations in section 2.2) for 1h at 4°C followed by three washes with lysis buffer (20 mM 4-morpholineethanesulfonic acid, 30 mM Tris, 100 mM NaCl, pH 7.4) with 1% Triton X-100. The bead-antibody mixture was then incubated with 200 µl cell lysate overnight at 4°C and washed with lysis buffer another five times, keeping the supernatant from the first wash for Western blotting analysis. The last four of these washes were performed without 1% Triton X-100 when preparing samples for mass spectrometry. Samples were eluted using either 50 µl Laemmli 2x sample buffer if intended for Western blotting or 30 µl elution buffer (4% SDS, 100 mM DTT, 100 mM Tris-Cl) if intended for mass spectrometry. In each experiment an IgG control was performed where Protein A-Sepharose beads and antibody were incubated together without cell lysate to identify any signal arising that was not directly resulting from the cell lysate, such as antibody-antibody interactions.

2.13 Proteomics

Immunoprecipitated samples, eluted in elution buffer as described above, require digestion in short peptides before they are suitable for analysis by mass spectrometry. The Filter Aided Sample Prep (FASP) Protein Digestion Kit from expedeon (44250) was used for this purpose. Of the 30 µL of elute sample produced from the IP, 2 µL was used in a Bradford protein determination assay as information about the amount of total protein in each sample was required for MS analysis.

Immediately prior to FASP digestion DTT was added to samples for a final concentration of 5 mM. FASP digestion was performed by adding 28 µL of protein extract to a spin filter followed by washing in urea to reduce the concentration of SDS in the filter. Samples were then alkylated with iodoacetamide and transferred to

ammonium bicarbonate for enzymatic digestion with trypsin (used at a 1:100 enzyme-to-protein ratio) and acidified with trifluoroacetic acid (TFA).

Peptides generated by FASP digestion were analysed by data-dependent LC-MS/MS on a TripleTOF 6600 mass spectrometer (Sciex) linked to an Eksigent 425 liquid chromatography system via a Sciex Nano-spray III source. The peptide mass in each of the final FASP-eluates was assumed to be the same as the mass of protein digested. Final eluates were freeze-dried and the residue re-suspended at 1 µg/µl in 2% ACN, 0.1% formic acid. Nano-flow chromatographic separation of peptides used a trap-and-elute method with an Acquity M-class Symmetry C18 Trap column, 100Å, 5 µm, 180 µm x 20 mm (Waters), and a PicoFrit packed emitter column 75 µm x 250 mm - 10 µm tip - containing Reprosil-PUR 3µm (New Objective). One microgram peptide samples were transferred onto the trap column within a 25 µL volume of 0.1% formic acid at 5 µL/min before injection-valve-switching and running of the following gradient at 300 nL/min. Buffer A = 0.1% formic acid in water, buffer B 0.1% formic acid in ACN. Sequential linear gradients of 1 to 28% B over 50 minutes and 28 to 80% B over 5 minutes were followed by a 5-minute column wash in 80% B. Return to 1% B was over 3 minutes and the column was then re-equilibrated in this buffer for 27 minutes.

Data-dependent top-30 MS-MS acquisition started immediately upon gradient initiation and was for 80 minutes. Throughout this period, precursor-ion scans (400 to 1600 m/z) of 250 ms enabled selection of up to 30 multiply-charged ions for CID fragmentation and MS/MS spectrum acquisition (m/z 100-1600) for 33 ms. Rolling precursor exclusion of 15 seconds was applied throughout to limit multiple fragmentation of the same peptide.

Precursor- and fragment-ion lists in mgf format were generated from wiff format raw MS data-files using MSConvert, available as part of the ProteoWizard software suite. Protein identification used the database search engine Mascot 2.5.1. and a database containing Uniprot human db download (6-4-17) plus 9 protease/GFP/YFP sequences. The peptide false discovery rate from a target decoy database was set at ≤1% and a filter of >1 unique peptide sequence per protein applied.

2.14 Transfection

Transfection of OE19 cells with Myc-tagged ERp29 cDNA (OriGene, CAT#: RC210918) was performed following the Lipofectamine 3000 Reagent Protocol from ThermoFisher Scientific. OE19 cells were grown to ~70% confluence and transfections were performed under sterile conditions within a flow hood. Ero1α cDNA was used as a positive control as this had previously been tested in our laboratory and a mock transfection without cDNA added was used as a negative

control. Prior to transfection, 5 µL of lipofectamine was added to 125 µL of Opti-MEM and vortexed to mix. Additionally, 5 µL of P3000 and either 12.5 µL or 25 µL of ERp29 cDNA (1.25 µL for Ero1α cDNA, 0 µL for mock) was added to another 125 µL of Opti-MEM. These two solutions were mixed together and allowed to incubate at RT for 10 minutes, during which time the cells were washed with 2 mL PBS twice. The DNA-lipofectamine-Opti-MEM mixture was then added to the cells, followed by an additional 250 µL of Opti-MEM and incubation for 1 hour at 37°C. Following this, an extra 1 mL of Opti-MEM was added to each dish and cells were incubated at 37°C for 24 hours to allow the transfection to take place. Cells were then washed in PBS twice and lysed in MNT lysis buffer as described previously.

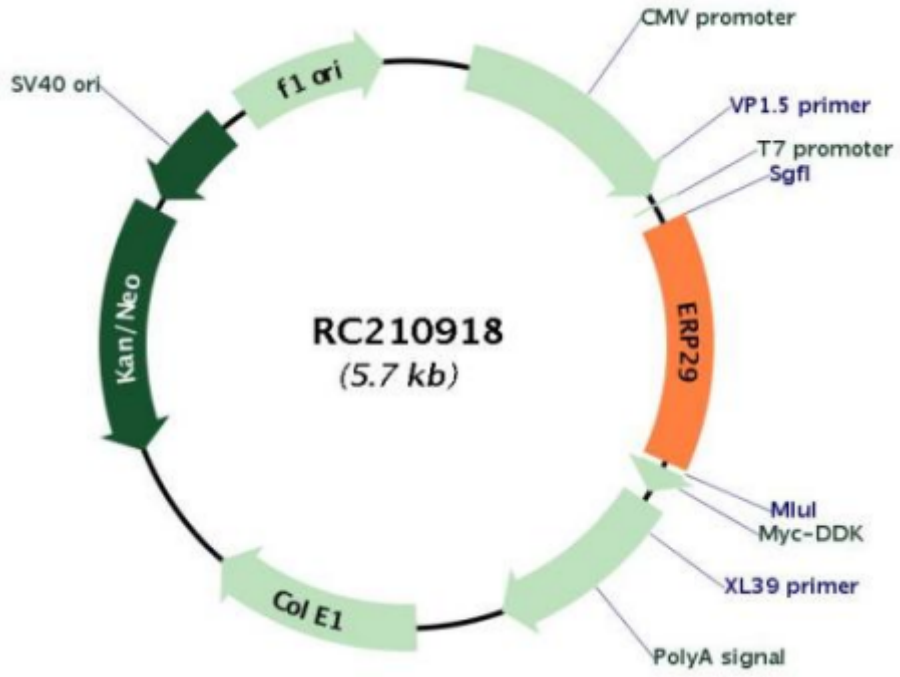

Figure 4: **Circular map for the RC210918 cDNA construct.**
Transfection of OE19 cells was attempted through the use of the RC210918 cDNA construct containing a ERp29 sequence with a Myc-tag at its C-terminal and a kanamycin resistance gene.

2.15 Deglycosylation

Deglycosylation was attempted as a method for more clearly visualising mucins on an SDS-PAGE gel. To achieve this the New England Biolabs PNGase F protocol was used. Lysates were prepared as described previously, without treatment with NEM, and protein concentrations were determined via Bradford assay. Both denaturing reaction conditions and non-denaturing reaction conditions were tested to allow comparison and to determine the extent of reaction completion.

Denaturing deglycosylation was achieved by combining cell lysates and Glycoprotein Denaturing Buffer, heating the mixture at 100°C for 10 minutes followed by chilling on ice and centrifuging to collect the solution. This was then supplemented with GlycoBuffer 2, 10% NP-40 and PNGase F and incubated at 37°C for 1 hour. Non-denaturing deglycosylation was achieved by combining cell lysate, GlycoBuffer 2 and PNGase F and incubating the reaction at 37°C for 4 hours. Samples were then analysed by reducing western blotting as described previously.

2.16 Alcian Blue gel staining

The Alcian Blue gel staining method was used in an attempt to visualise mucins on an SDS-PAGE gel. After samples were separated on an SDS-PAGE gel, as described previously, gels were moved to a pH 2.5, 0.5% Alcian Blue solution in 2% aqueous acetic acid and left to stain for 45 minutes. This was followed by a destain in 2% aqueous acetic acid for 15 minutes. Gels were scanned into an office computer.

2.17 Partial trypsinisation

OE19 lysates were subjected to limited proteolysis through the addition of varying trypsin concentrations. A stock solution of trypsin was added to each lysate to achieve final trypsin concentrations of 0, 0.25, 1.25 and 2.5 µg/mL. Lysates were incubated for 30 minutes at 4°C to allow for digestion, followed by digestion termination with the addition of soybean trypsin inhibitor (SBTI) for a final concentration of 200 µg/mL. Lysates were then analysed on 8% acrylamide gels by SDS-PAGE and western blotting as described previously.

2.18 Mouse stomach lysis

Male mice aged 8-12 weeks were sacrificed in accordance with the Animals (Scientific Procedures) Act (1986) by trained personnel in the Life Sciences Support Unit at Durham University.

After removal from the body of the mouse the stomach was cut into four similarly sized pieces and thoroughly cleaned in PBS. Each piece of the mouse stomach was treated in either RPMI media containing 5 mM diamide or diamide free media for 5 minutes, and subsequently washed in either PBS or PBS supplemented with 20 mM NEM for 5 minutes. This produced four different conditions. All pieces were then washed in PBS for 5 minutes and cells were scraped from the tissue with the use of a scalpel. Solutions containing the cells were centrifuged at 1200 rpm for 5 minutes to pellet the cells. The PBS supernatant was removed and replaced with 300 µL MNT lysis buffer (containing 20 mM NEM in NEM treated samples). This solution was left for 5 minutes at 4°C, centrifuged at 16,100 g for 10 min at 4°C and the supernatants were collected in fresh Eppendorf tubes and flash frozen in liquid nitrogen and stored

at -20°C. Samples were analysed by SDS-PAGE and western blotting as described in sections 2.9 & 2.11.

2.19 Immunohistochemistry

Paraffinized oesophageal tissue sections were provided by YKS Viswanath and Julie Walker, James Cook University Hospital, Middlesbrough and stained for AGR2 using the 3,3'-dianimobenzidine (DAB) staining method.

Tissue sections embedded in paraffin were incubated at 50°C overnight prior to staining. Sections were deparaffinised with two 7-minute washes in Histoclear, one 7-minute wash in 100% ethanol, one 5-minute wash in 95% ethanol and finally one 5-minute wash in 70% ethanol. Sections were then hydrated in dH_2O for 3 minutes. Antigen retrieval was achieved by treating the sections with 3% H_2O_2 in MeOH for 15 min followed by 20 min in 10 mM Na-citrate (pH 6.0) at 90°C. Slides were then cooled on ice, followed by a 5-minute wash in 0.2% BSA in PBS and a 30-minute blocking incubation in 0.2% BSA + 5% normal goat serum (DAKO, X0907) in PBS. Long incubations such as this blocking step were performed in a moist chamber to reduce evaporation. Sections were then incubated with an AGR2 mAb (ab76473) at a 1:250 dilution in PBS + 0.2% BSA + 2% normal goat serum for 1-hour RT. After primary incubation, sections were washed in 0.2% BSA in PBS for 5 minutes, followed by a 45-minute RT incubation with secondary antibody goat anti-mouse/rabbit biotin (made by mixing 2 mL PBS with 20 µL reagent C from Dako kit, K0492). After which they were again washed in 0.2% BSA in PBS for 5 minutes and then incubated with a reagent A/B mixture (made by mixing 2 mL PBS with 20 µL reagent A and 20 µL reagent B) for 30 minutes RT. This mixture required making 15 minutes before use. For the next step a DAB solution was required, comprising of 5 mL PBS, a H_2O_2 tablet and a DAB tablet. This solution was applied to the sections and they were allowed to develop before submersion in dH_2O to stop development. Slides were then stained with haematoxylin for 4 minutes, followed rinsing in dH_2O, 1% HCl in MeOH, dH_2O again, tap water, 70% EtOH, 95% EtOH, a 5-minute wash in 100% EtOH, two 7-minute washes in Histoclear and finally mounting in DPX (Agar Scientific, R1340). Slides were imaged with a Leica ICC50 microscope.

2.20 Alcian Blue tissue section staining

Alcian Blue was also used on the paraffinized oesophageal tissue sections as a stain for mucin. Tissue sections embedded in paraffin were incubated at 50°C overnight prior to staining. Sections were deparaffinised with two 7-minute washes in Histoclear, one 7-minute wash in 100% ethanol, one 5-minute wash in 95% ethanol and finally one 5-minute wash in 70% ethanol. Sections were then hydrated in dH_2O for 3 minutes, rinsed in dH_2O, washed in 3% acetic acid for 3 minutes then stained

with a pH 2.5, 0.5% Alcian Blue solution in 2% aqueous acetic acid for 30 minutes. Following staining, sections were rinsed in a gentle flow of tap water for 10 minutes and then rinsed briefly in dH_2O. Slides were then stained with haematoxylin for 6 minutes, then subsequently rinsed in dH2O, 1% HCl in MeOH, dH_2O again, tap water, 70% EtOH, 95% EtOH, a 5-minute wash in 100% EtOH, two 7-minute washes in Histoclear and finally mounting in DPX (Agar Scientific, R1340). Slides were imaged with a Leica ICC50 microscope.

3 Results

3.1 AGR2 expression and localisation in OE19 cells

Barrett's Oesophagus is a pre-malignant condition leading to oesophageal adenocarcinoma in which the appearance of the oesophageal epithelium changes to more resemble that of the stomach. With this metaplasia comes the induction of mucin synthesis, mucous production and the derepression of the mucin specific protein disulphide isomerase AGR2 (Pohler et al., 2004). In order to study AGR2's role within Barrett's Oesophagus, the OE19 oesophageal adenocarcinoma immortalised cell line was chosen. Previous work in the laboratory had suggested that AGR2 was expressed in this oesophageal cell line (Simpson and Benham, unpublished data).

To check expression of AGR2 in this cell line and to determine the subcellular localisation of AGR2 within OE19 cells, immunofluorescence was performed. Cells were grown on coverslips, fixed with 4% PFA in PBS++, permeabilised with Triton X-100 and stained with either the AGR2 D9V2F rabbit mAb or a PDI pAb, and co-stained with DAPI. The secondary antibody used was the donkey anti-rabbit Alexa Fluor 594 (red). Images were taken on a Zeiss Apitome Brightfield microscope. As PDI is known to be localised and retained in the ER, a polyclonal PDI antibody was used to stain the ER of the OE19 cells. This visualisation of the ER can then be used as a point of reference when observing the localisation of other proteins via immunofluorescence, for example AGR2.

PDI localisation in OE19 cells is shown in Figure 5 as a ring around the DAPI (blue) stained nuclei. Cells stained with the AGR2 mAb shown in Figure 5 demonstrate the strong expression of AGR2 in this cell line. These cells had a similar pattern of AGR2 localisation to the PDI stained cells, implying they are both localised to the ER, although higher resolution images and co-staining would be required to confirm this observation.

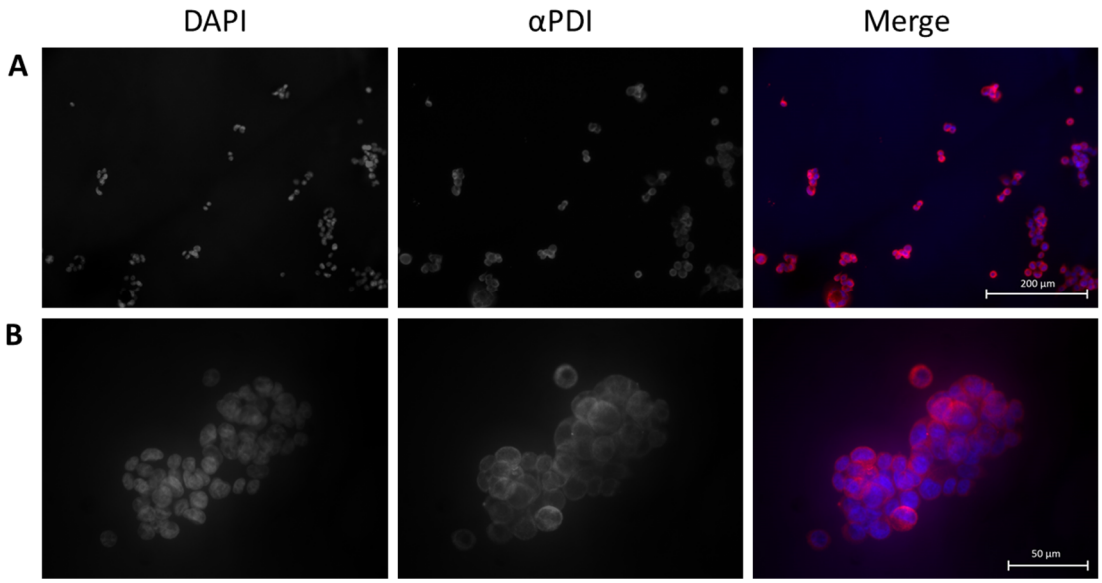

Figure 5: **PDI expression and localization in OE19 cells.**
OE19 cells were stained with a polyclonal PDI antibody and anti-rabbit Alexa Fluor 594 in order to observe expression and ER localization. DAPI (blue) was used to stain the nuclei of cells. Perinuclear expression of PDI (red) indicates ER localisation. Images were taken on a Zeiss ApoTome brightfield microscope. (**A**) x20 magnification. (**B**) x63 magnification.

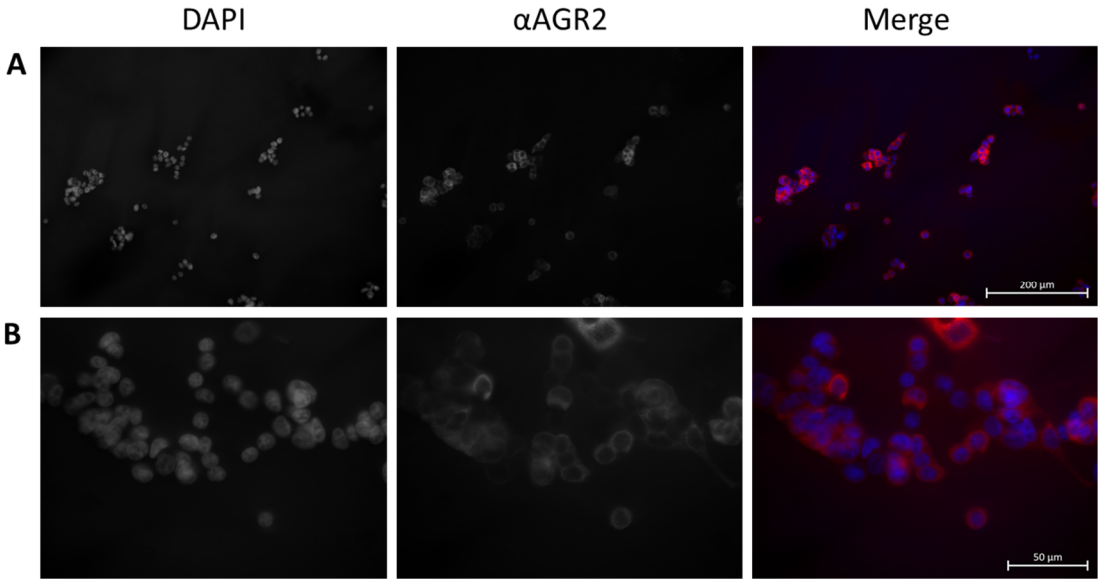

Figure 6: **AGR2 expression and localization in OE19 cells.**
OE19 cells were stained with the D9V2F AGR2 mAb and anti-rabbit Alexa Fluor 594 in order to observe expression and subcellular localization. DAPI (blue) was used to stain the nuclei of cells. Similarly to PDI expression, AGR2 expression displays perinuclear localisation, indicating ER localisation. Images were taken on a Zeiss ApoTome brightfield microscope. (**A**) x20 magnification. (**B**) x63 magnification.

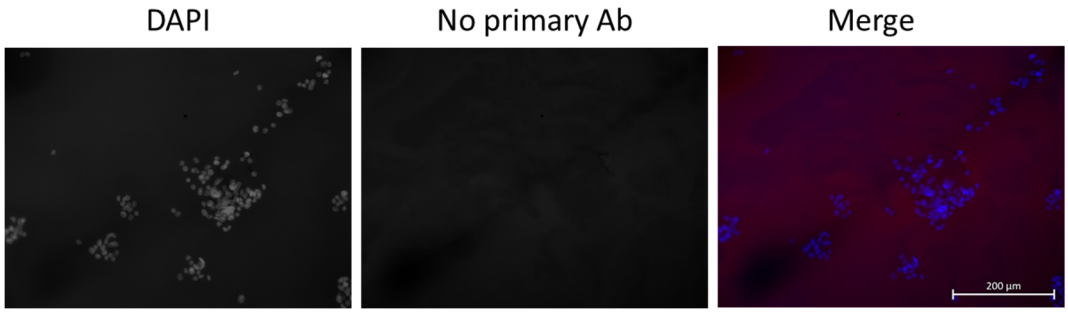

Figure 7: **No primary antibody on OE19 cells.**
OE19 cells only stained with anti-rabbit Alexa Fluor 594. No primary antibody was used. Images were taken on a Zeiss ApoTome brightfield microscope. (**A**) x20 magnification.

Although images taken on the Zeiss ApoTome microscope indicate perinuclear expression of AGR2, this could not be confirmed due to low image resolution. Therefore, it was decided to switch the microscope to a laser-scanning confocal microscope. Confocal microscopy makes use of a pinhole between the sample and detector, blocking out-of-focus light and allowing the image to be acquired from a single focal plane. This technique allows much higher resolutions than standard brightfield imaging and is better suited to the OE19 cells as they tend to adhere to each other and form masses of cells rather than spreading out and creating a flat monolayer.

The Zeiss LSM 880 Confocal Microscope was used to obtain higher resolution images, as shown in Figure 8. In a separate experiment to the one described previously, cells were again grown on coverslips, fixed with 4% PFA in PBS++, permeabilised with Triton X-100 and stained with either the AGR2 D9V2F rabbit mAb or a PDI pAb, and co-stained with DAPI. The secondary antibody used was donkey anti-rabbit Alexa Fluor 594 (red). Perinuclear staining can be observed clearly when staining for PDI (Figure 8A), and AGR2 (Figure 8B), which again shows a similar profile of expression localisation when compared to PDI, indicating that in OE19 cells AGR2 is found within the ER.

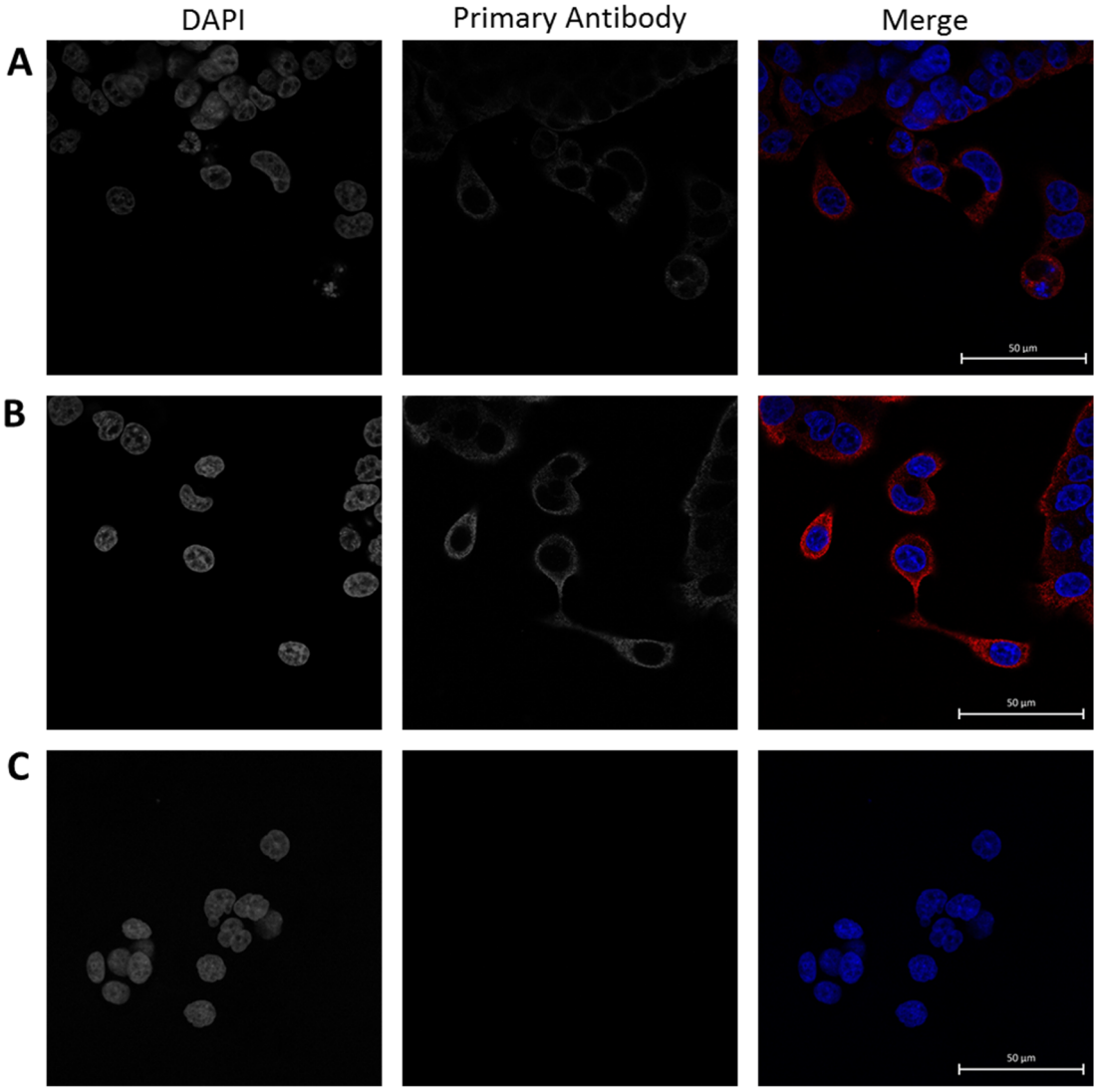

Figure 8: **Expression and localization of PDI and AGR2 in OE19 cells.**
(**A**) Cells stained with polyclonal PDI show the typical ER expression within OE19 cells. (**B**) Cells stained with the D9V2F AGR2 mAb showed subcellular localisation of AGR2 within OE19 cells. (**C**) OE19 cells stained with only anti-rabbit Alexa Fluor 594 (no primary antibody). Images were taken on a Zeiss LSM 880 confocal microscope at x63 magnification.

3.2 The effect of redox on AGR2 complex formation

Experimental work performed in the lab previously by Simpson and Benham (unpublished data) showed evidence that, in the OE19 oesophageal adenocarcinoma cell line, treatment of the cells with DTT (5 mM) - a reducing agent and ER stress inducer – altered the ability of AGR2 to form protein complexes. In these experiments the alkylating agent N-ethylmaleimide (NEM) was used to sequester free thiol groups and therefore trap disulphide bonds in their native conformation, allowing visualisation of disulphide bond dependent complexes through non-reducing western blotting. These observations indicated that AGR2, in oesophageal adenocarcinoma, forms complexes that are either redox dependent, indicating that these interactions require disulphide bonds, ER stress dependent and the changes observed are due to the extra stress put on the ER by the addition of DTT, or a combination of the two.

To test whether the complexes previously observed are redox dependent, the oxidising agent diamide was chosen. As an oxidising agent diamide will alter the redox state of a living cell it is added to, inducing a change to more oxidising conditions and therefore promote the formation of disulphide bonds. If the complexes AGR2 forms with partner proteins are redox dependent, as was theorised by Simpson and Benham, then diamide should promote AGR2 interactions and induce complex formation, and these complexes should be visible through non-reducing western blotting.

Diamide treatments were performed on the OE19 cell line using 5 mM diamide in RPMI medium for either 0, 5 or 10 minutes, followed by washing with PBS supplemented with 20 mM NEM to trap disulphide bonds. Lysates were made using an MNT lysis buffer supplemented with 20 mM NEM and the lysates were analysed by SDS-PAGE and western blotting using the D9V2F AGR2 mAb. The results of this experiment (Figure 9) show an immediate induction of AGR2 complexes under non-reducing conditions when diamide is present in the treatment. Multiple overlapping bands appear at higher molecular weights along with a clear band appearing at ~37 kDa which is assumed to be AGR2 in its homodimeric form; this is consistent with the literature (Ryu et al., 2013). This result clearly shows that AGR2 can form redox dependent and therefore disulphide bond dependent complexes, and that these complexes can be trapped with NEM for later analysis.

The combination of diamide to induce disulphide bond formation and NEM to trap and prevent disulphide bonds reshuffling demonstrates a method for trapping disulphide dependent interactions that will be used later in this project.

After inducing AGR2 complexes with diamide, the question was asked whether these complexes are stable or transient. To determine whether the induction of AGR2 complexes by diamide could be reversed, a recovery experiment was performed. Following a 5-minute treatment with diamide, OE19 cells were exposed to diamide-free media for varying lengths of time before NEM treatment and lysis as previously described. Figure 9C shows a western blotting analysis of these treatments.

Complexes were again induced rapidly after the addition of diamide to the media. A possible transfer inefficiency of higher molecular weight complexes from the acrylamide gel to the PVDF membrane may be the reason why bands appear fainter in the 5-minute recovery lane (labelled 5r in Figure 9C). Despite that, it is still clear that some bands disappeared after recovery and some persisted. Most notable is the single well-defined band that appeared above the dimer band in the 5-minute treatment but was then absent in the recovery lanes. This is likely to be the same band seen in the 5-minute treatment but absent from the 10-minute treatment in Figure 9A.

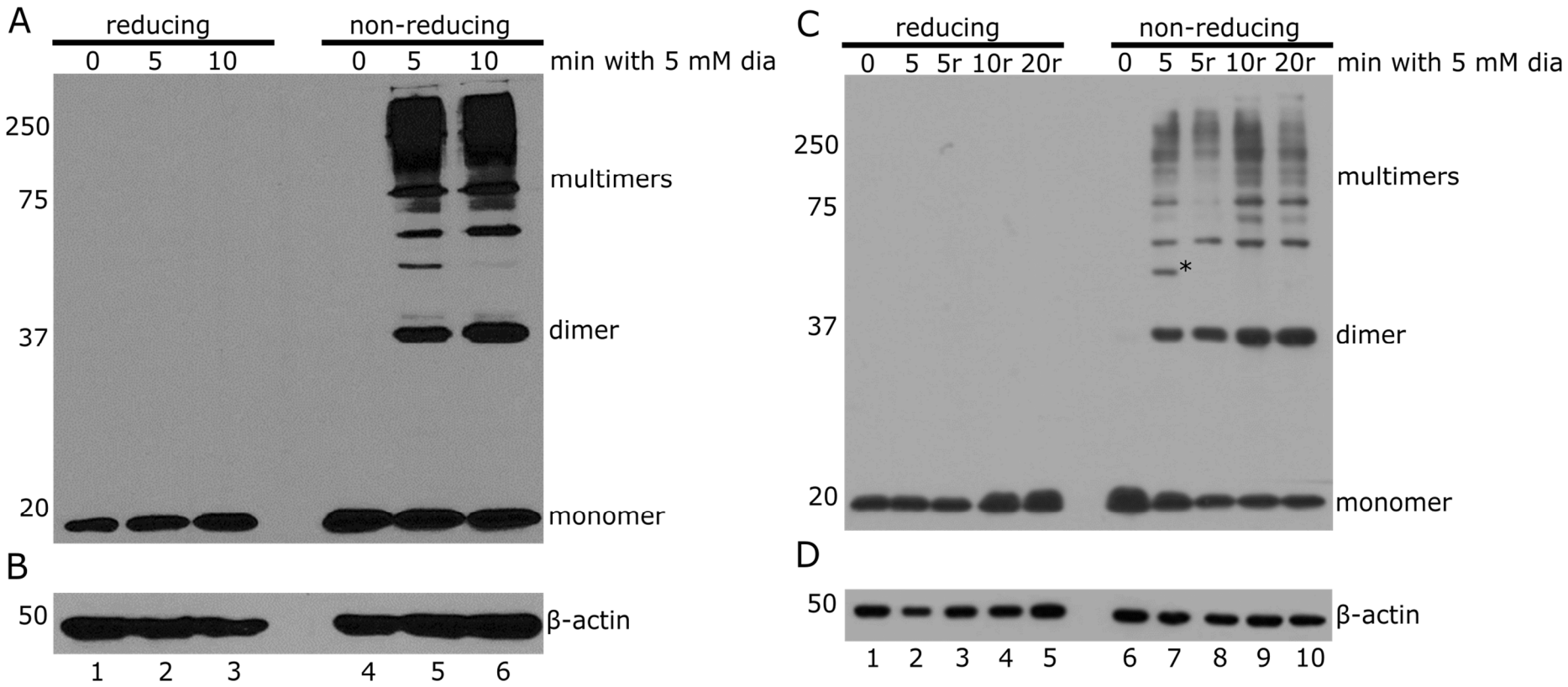

Figure 9: **Diamide treatment promotes AGR2 complex formation in OE19 cells.**
(**A**) OE19 cells, treated with 5mM diamide for either 0, 5 or 10 minutes, were lysed and run on a 12% poly-acrylamide gel, transferred to a PVDF membrane and probed using the D9V2F AGR2 mAb. Complexes appear in diamide treated lanes under non-reducing conditions. (**B**) β-actin loading control for diamide treatment samples. (**C**) OE19 cells treated with diamide as before, but also allowed to recover for 5, 10 and 20 minutes prior to lysis. Recovery lanes show most complexes persist, however some (*) were reduced after recovery. (**D**) β-actin loading control for diamide treatment and recovery samples. Dia = diamide treatment. Molecular weight markers were used, as marked on the left of the gels, and were in kDa.

3.3 The effect of ER stress on AGR2 complex formation

Previous work by Simpson and Benham showed evidence that AGR2 complex formation, in OE19 cells, is affected by DTT treatment (unpublished). DTT is a known inducer of ER stress so one possibility is that the change in AGR2 complex formation observed after DTT treatment could be due to the ER stress caused by DTT treatment on OE19 cells. In order to test the effect ER stress had on AGR2 complex formation, independent of the redox changes induced by DTT, other non-redox-active inducers of ER stress were tested. Thapsigargin was chosen as it is a potent inducer of ER stress and it is also not redox-active.

OE19 cells were treated with media containing 2 µM thapsigargin for 0, 30 and 60 minutes and 6 hours, treated with 20 mM NEM in PBS and lysed in MNT lysis buffer containing 20 mM NEM. Lysates were analysed via SDS-PAGE and western blotting using the D9V2F AGR2 mAb (Figure 10A). A diamide treated OE19 sample was loaded onto the gel as a positive control for AGR2 complexes. Reducing samples were also probed with a P-eIF2α antibody to test for the induction of ER stress (Figure 10C). After 60 minutes thapsigargin treatment a signal could be seen when using a P-eIF2 antibody, and a stronger signal seen after 360 minutes, indicating ER stress was being inducted.

No complexes were observed in any of the thapsigargin treated samples when immunostaining for AGR2, indicating that there was no strong induction of AGR2 complexes. However, the diamide treated sample also did not show the same strong induction of higher molecular weight bands as shown in previous experiments. This may be due to an issue in transferring higher molecular weight complexes to the PVDF membrane. Therefore, it cannot be said definitively whether thapsigargin has an effect on AGR2 complex formation.

It was speculated that the conditions known to induce the transition from normal oesophageal epithelium to Barrett's epithelium may also play a role in AGR2 complex formation. During the transition into Barrett's epithelium, gastric reflux exposes oesophageal cells to low pH and a plethora of stomach bile acids. These conditions have previously been shown to induce oxidative stress and oxidative DNA damage in Barrett's oesophagus cells, and are theorised to be behind the development of Barrett's oesophagus and subsequent tumour progression (Dvorak et al., 2007). Therefore, it was decided to test the effect of low pH in combination with bile acids on AGR2 complex formation in OE19 cells.

A bile acid cocktail, as described in Dvorak et al., 2007 and also the materials and methods section of this thesis, was added to RPMI media and acidified to pH 4. OE19 cells were treated with this media for 0, 5 and 10 minutes as well as a longer 6-hour

time course before treatment with NEM in PBS and lysis with an MNT lysis buffer supplemented with NEM. Lysates were analysed by SDS-PAGE and western blotting using the D9V2F AGR2 mAb. A diamide treated OE19 sample was loaded onto each gel as a positive control for AGR2 complexes. Coomassie gel staining was also performed on separate gels alongside western blots as a secondary loading control. Coomassie stained gels are shown in Figure 11A and B.

Western blotting results from samples treated with low pH media only (Figure 11C) showed no evidence of AGR2 complex formation. Samples treated with low pH media supplemented with bile acids (Figure 11D) did however show some evidence of AGR2 complex formation despite excessive background signal on the blot that obscured some of the non-reducing samples in the 5 and 10 min lanes. Some, complexes also appeared in the reducing lane of the 10 min sample, possibly due to ineffective reducing agent or contamination from the diamide treated lane. Overall, low pH and bile acid treatments suggest that the bile acid environment does not promote the formation of disulphide dependent-complexes between AGR2 and itself or partner proteins; however, if more time was available, it would be worth extending this analysis to a wider range of bile acid combinations with additional controls.

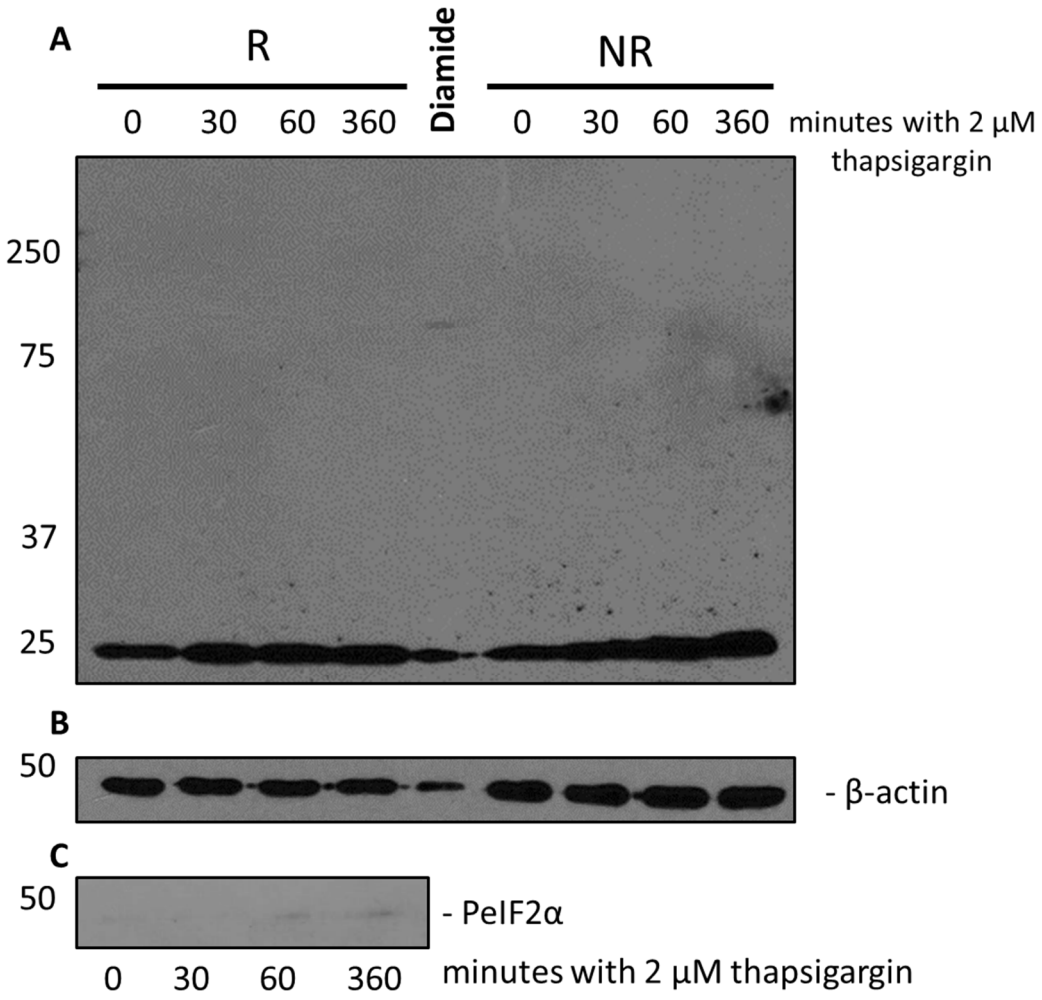

Figure 10: **The effect of thapsigargin on AGR2 complex formation in OE19 cells**.
(**A**) OE19 cells treated with 2 µM thapsigargin for 0, 30, 60 and 360 minutes showed no visible changes in disulphide-dependent complex formation under non-reducing conditions. An OE19 lysate treated with 5mM diamide for 5 minutes (as described in Figure 9) and ran under non-reducing conditions was used as a positive control for complexes (central lane). (**B**) β-actin loading control for thapsigargin treated samples. (**C**) Reducing thapsigargin treated samples were probed with an antibody for PeIF2α as this is a marker for ER stress. Weak bands appeared in lanes with longer treatments indicating the thapsigargin caused ER stress in the cells. R = gel ran under reducing conditions. NR = gel ran under non-reducing conditions. Molecular weight markers were used, as marked on the left of the gels, and were in kDa.

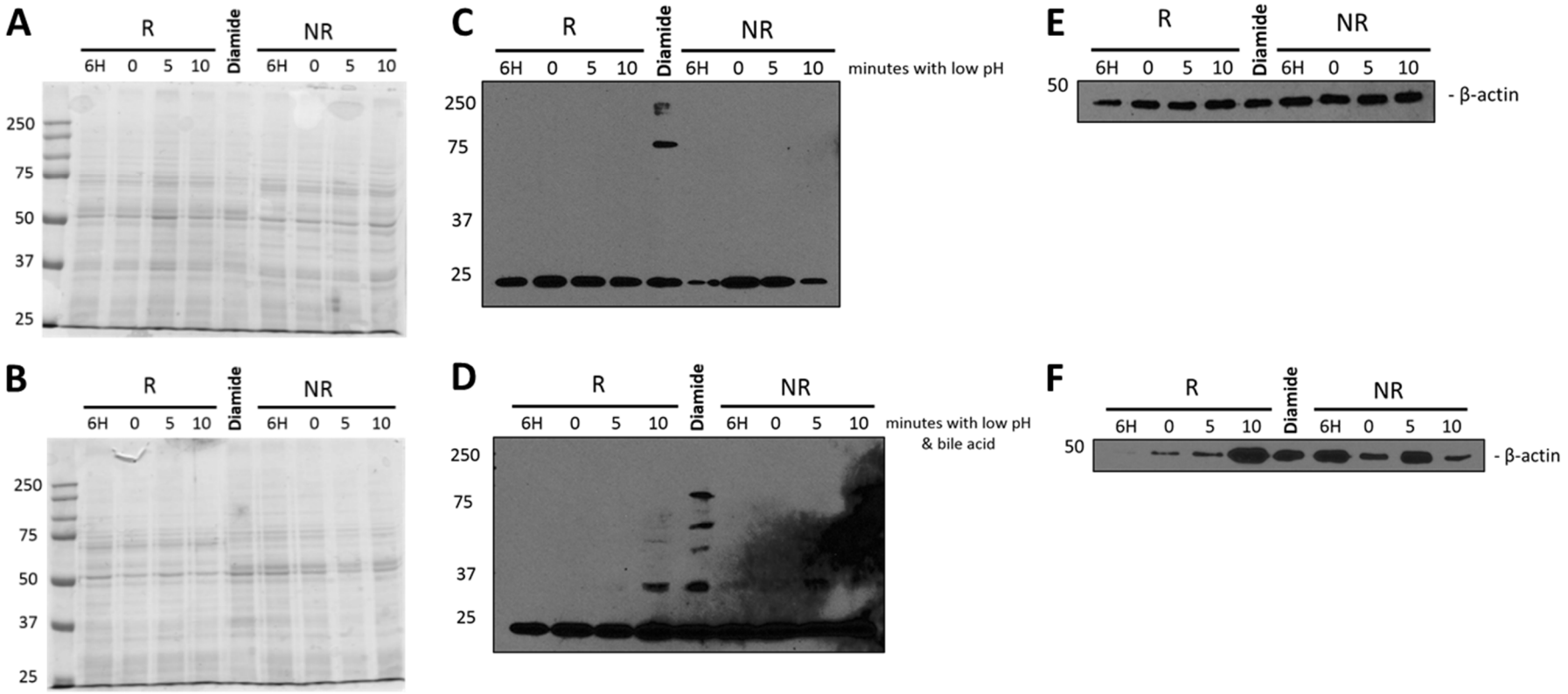

Figure 11: **The effect of low pH and bile acids on AGR2 complex formation in OE19 cells**.
OE19 cells were treated with pH 4 RPMI media supplemented with a cocktail of bile acids to test their effect on AGR2 complex formation. Coomassie stained SDS-PAGE gels showed that protein composition was not grossly altered by the treatments and serve as a protein recovery control. A single diamide treated sample was loaded onto each gel as a positive control for AGR2 complexes. (**A**) Coomassie gel showing samples treated with low pH media without bile acids. (**B**) Coomassie gel showing samples treated with low pH media and with bile acids. (**C**) Western blot showing samples treated with low pH media without bile acids probed for AGR2. (**D**) Western blot showing samples treated with low pH media with bile acids probed for AGR2. Some complexes appeared, although they were obscured by background signal. (**E**) β-actin loading control for samples treated with low pH media. (**F**) β-actin loading control for samples treated with low pH media supplemented with bile acids. R = gel ran under reducing conditions. NR = gel ran under non-reducing conditions. Molecular weight markers were used, as marked on the left of the gels, and were in kDa.

3.4 Identification of novel AGR2 interacting proteins

The western blotting results shown in Figure 9 demonstrate results obtained from using a trapping approach for retaining disulphide bonded complexes in the presence of diamide and NEM. Having demonstrated the effectiveness of this trapping approach through western blotting it was decided to use proteomic analysis to determine the identity of the proteins with which AGR2 interacted. Immunoprecipitation was used to separate AGR2 and its interactors from the remaining cell lysate, and mass spectrometry was employed to identify the proteins isolated by immunoprecipitation. However, before carrying out mass spectrometry analysis, immunoprecipitation was validated in our system with western blotting analysis.

An independent AGR2 antibody, the rabbit monoclonal anti-AGR2 (EPR3278/ab76473) antibody, was acquired for immunoprecipitation for two reasons. Firstly, the D9V2F AGR2 antibody did not support IP applications, and secondly, two different species of AGR2 antibodies are required to verify the presence of AGR2 in an AGR2 immunoprecipitated sample analysed by western blotting.

Immunoprecipitation was first carried out on fresh OE19 lysates, without treatment with diamide or NEM. This was to test the capability and efficiency of the AGR2 antibody to retain the AGR2 protein in our system. Two separate immunoprecipitations were performed, one with PDI and the other with AGR2. Both of these immunoprecipitations were then analysed via western blotting for both PDI and AGR2.

OE19 cells were grown to ~90% confluency before lysis to ensure there were sufficient protein concentrations for immunoprecipitation. Immunoprecipitation was performed by incubating Protein A-Sepharose beads with either the AGR2 mAb ab76473 or the in-house generated PDI pAb to allow the antibodies to associate with the beads, followed by washing in MNT lysis buffer with 1% Triton X-100. The beads/antibody mix was then incubated with 200 µL of OE19 cell lysate for an appropriate period of time to allow the protein in the lysate to associate with the antibody. To serve as a negative control, one sample was immunoprecipitated with lysis buffer (added instead of lysate) at this step. Supernatant removed after incubation with the lysate was stored and ran on the SDS-PAGE gel alongside immunoprecipitate samples. The mixture was then washed again and eluted in 2x sample buffer. Samples were run on 12% SDS-PAGE gels under reducing conditions and analysed via western blotting using both the D9V2F AGR2 mAb and the PDI mAb RL90 (MA3-019). Results are shown in Figure 12.

Both blots showed strong staining in the 50 kDa region. This was due to the HRP-conjugated secondary antibodies used in western blotting interacting with the IgG heavy chains of the antibodies used for immunoprecipitation. Supernatant samples taken after incubation with the lysate serves to show the effectiveness and efficiency of the immunoprecipitation. OE19 lysates immunoprecipitated with the ab76473 AGR2 mAb and blotted back with the D9V2F AGR2 mAb showed a single band in the 20 kDa region (Figure 12A). This band is the AGR2 monomer and its presence in both the OE19 lysate and the AGR2 immunoprecipitated eluate verifies that the AGR2 immunoprecipitation was successful in retaining the AGR2 protein. Samples immunoprecipitated with a PDI pAb and blotted back with an AGR2 mAb (Figure 12A) showed no band in the 20 kDa AGR2 monomer region indicating that the PDI immunoprecipitation did not pull down the AGR2 protein and therefore an interaction was not observed.

Figure 12B shows both immunoprecipitations blotted back with a PDI mAb. The PDI protein runs at ~50 kDa, similar to the IgG heavy chain. This overlapping range caused issues when interpreting the dense bands of the IgG heavy chain, which obscured the PDI signal. No clear PDI signals could be observed in Figure 12B and therefore no conclusion could be made as to the effectiveness of the immunoprecipitation. The identity of the dense bands that appeared in the OE19 lysate lane is uncertain but could be cross-linked PDI protein, or contamination from nuclear material.

Having demonstrated the ability of the AGR2 mAb ab76473 to bind and retain AGR2 during immunoprecipitation, it was decided to test AGR2 immunoprecipitation once more, this time in the presence of diamide and NEM. There is a possibility that diamide and/or NEM may interfere with the interaction between the AGR2 mAb and the AGR2 protein, therefore these conditions were tested first with western blotting before committing to mass spectrometry analysis.

Cells grown to ~90% confluency were treated either with media containing 5 mM diamide or control media for 5 minutes, treated with 20 mM NEM and lysed in MNT lysis buffer containing 20 mM NEM. Immunoprecipitation was performed on these lysates as described previously. Immunoprecipitated samples were analysed via reducing western blotting with the D9V2F AGR2 mAb.

Clear AGR2 monomer bands in the 20 kDa region could be seen in both the input and the AGR2 immunoprecipitated lanes and were entirely absent in the IgG lanes (Figure 13), demonstrating that immunoprecipitation with the ab76473 AGR2 mAb in the presence of diamide and NEM was successful. AGR2 bands in the supernatant samples appeared weaker than those in the immunoprecipitated lanes, showing that the majority of the AGR2 protein in the lysates was retained throughout the immunoprecipitation.

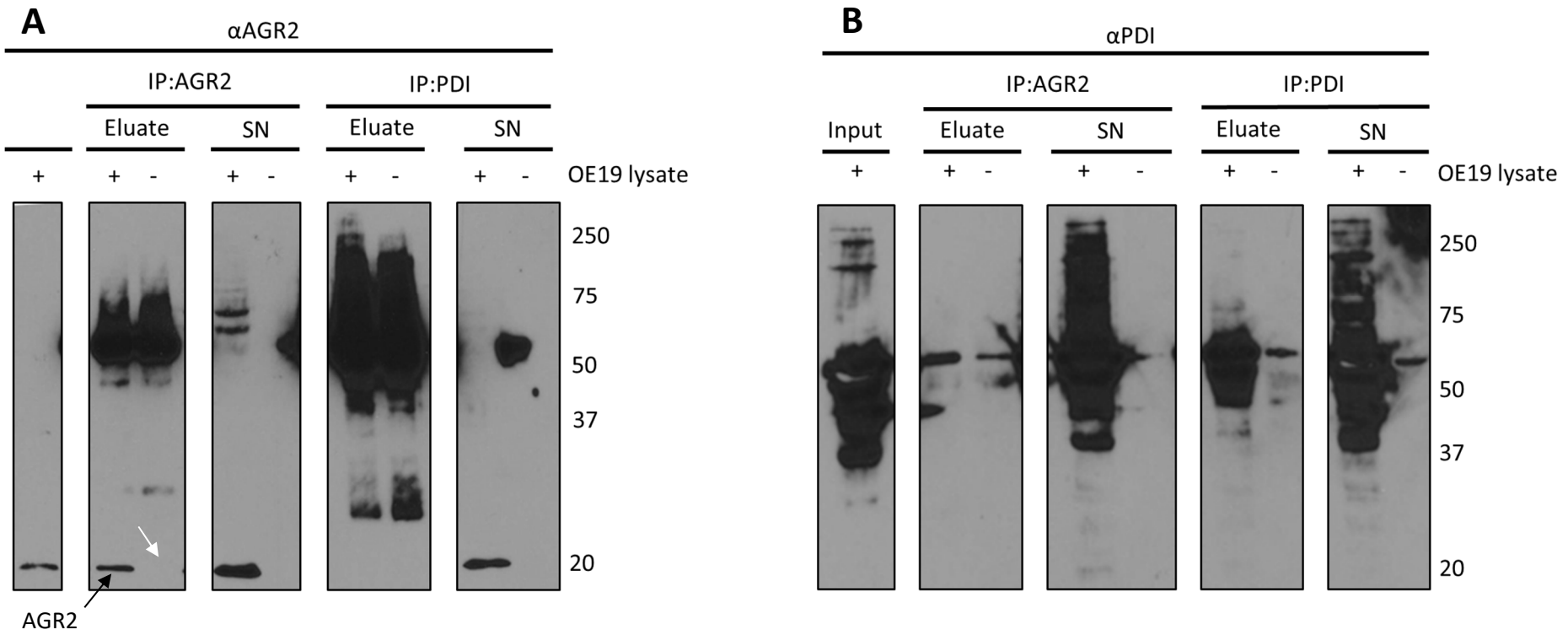

Figure 12: **OE19 cell lysates immunoprecipitated with PDI and AGR2 antibodies, blotted back for PDI and AGR2.**
OE19 cells were lysed and immunoprecipitated using either the AGR2 mAb ab76473 or an in-house generated PDI pAb. (**A**) Immunoprecipitated samples were blotted back with the D9V2F AGR2 mAb. Bands appearing in the 19 kDa range are the AGR2 monomer. The presence of the AGR2 monomer band in the OE19 positive IP:AGR2 eluate (black arrow) and absence in the OE19 negative eluate (white arrow) signifies that the immunoprecipitation was successful in extracting the AGR2 protein from the OE19 lysate. (**B**) Immunoprecipitated samples blotted back with the PDI mAb RL90. The PDI bands were obscured by IgG heavy chain. + = IP performed with OE19 lysate, - = IP performed without OE19 lysate, SN = supernatant (see IP method in section 2.12). Molecular weight markers were used, as marked on the left of the gels, and were in kDa.

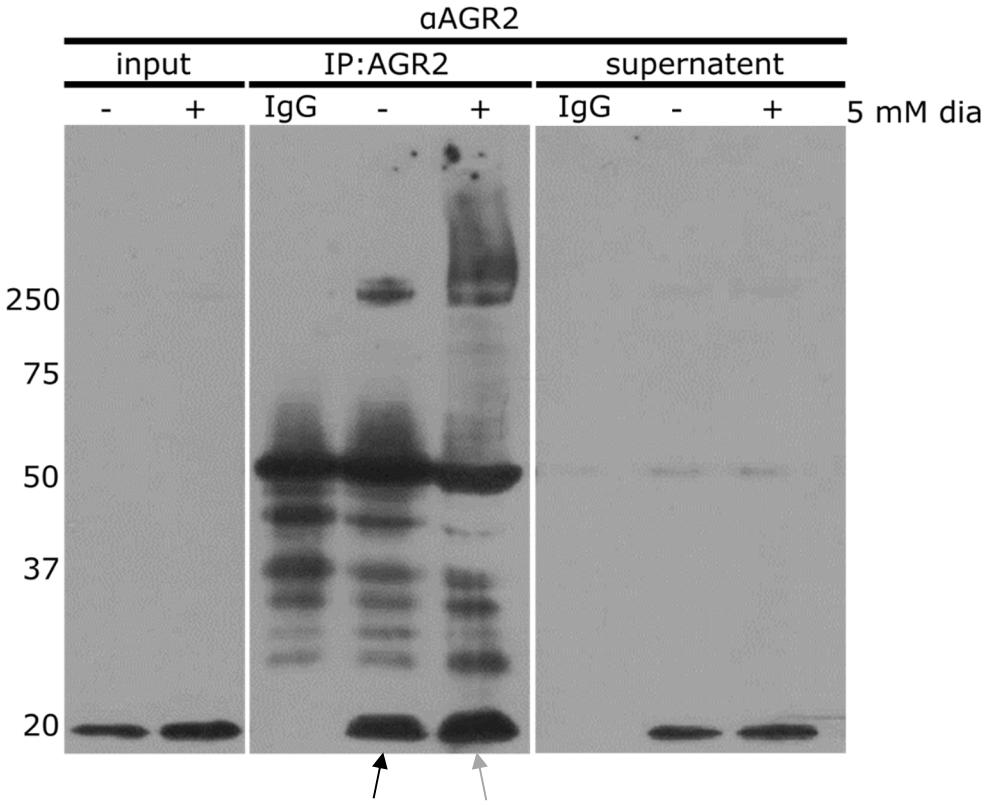

Figure 13: **OE19 immunoprecipitation with an AGR2 mAb in the presence of diamide and NEM.**

OE19 cells were treated with 5mM diamide and 20 mM NEM prior to lysis, immunoprecipitated with the AGR2 mAb EPR3278 and immunoblotted with the AGR2 mAb D9V2F. Bands appearing at 19 kDa in the IP:AGR2 diamide positive (grey arrow) and negative lane (black arrow) demonstrates the retrieval of AGR2 was successful. + = IP performed with OE19 lysate, - = IP performed without OE19 lysate and dia = diamide treatment. Molecular weight markers were used, as marked on the left of the gel, and were in kDa.

After demonstrating that AGR2, in the presence of diamide and NEM, could be detected by immunoprecipitation, the next step was to prepare samples for mass spectrometry analysis. Inducing and retaining these AGR2 complexes and then subsequently isolating these complexes from the OE19 lysate provides a sample that in theory only contains AGR2 and the proteins it is interacting with. Proteomic analysis of the proteins contained within that sample should then reveal proteins involved in these AGR2 complexes, first observed in Figure 9.

The immunoprecipitation conditions chosen for analysis by mass spectrometry were identical to those shown in Figure 13. The samples taken for analysis were: an OE19 lysate treated with 5 mM diamide for 5 minutes prior to lysis, an OE19 lysate without diamide treatment and one immunoprecipitation with only lysis buffer to serve as a negative control. All samples were immunoprecipitated with the AGR2 mAb ab76473, all samples were supplemented with 20 mM NEM prior to lysis and all lysis buffer used contained 20 mM NEM. To prepare samples for mass spectrometry analysis the immunoprecipitation approach required slight adjustments. Removal of Triton X-100 from the final washes was required as it is not compatible with mass spectrometry. After immunoprecipitation, a Bradford protein determination assay was performed to divulge the protein concentrations in each sample and to check the success of the elution, followed by digestion with trypsin to produce peptide fragments suitable for detection by MS. This full process is detailed in Figure 14.

Data received from the Protein Pilot software were in the form of protein summaries detailing the proteins peptides could be matched with reasonable confidence. In initial experiments, samples contained high quantities of keratins, a common contaminate detected in mass spectrometry analysis, although these numbers were significantly reduced after a more careful approach was adopted in a second round of sample preparation. As mentioned previously, one sample analysed by mass spectrometry was immunoprecipitated with lysis buffer instead of OE19 lysate to serve as a negative control. Any proteins detected in this control sample were immediately discounted from the protein summaries of samples immunoprecipitated with OE19 lysates. These proteins included keratins, immunoglobulins and cytoskeletal components.

After subtracting hits also detected in the control sample and any extra keratins and obvious contaminants, proteins were selected that were deemed likely to be interacting with AGR2. These included proteins known to reside in the ER or secretory pathway and therefore would share the same intracellular localisation as AGR2. The most notable interactors were the mucins MUC5AC and MUC5B, which are known to be clients of AGR2, and lectins such as GAL4 and ZG16B, which may be involved in the AGR2-mucin interactions. Factors considered when evaluating the potential of a protein hit as a real AGR2 interactor included the peptide count – the number of

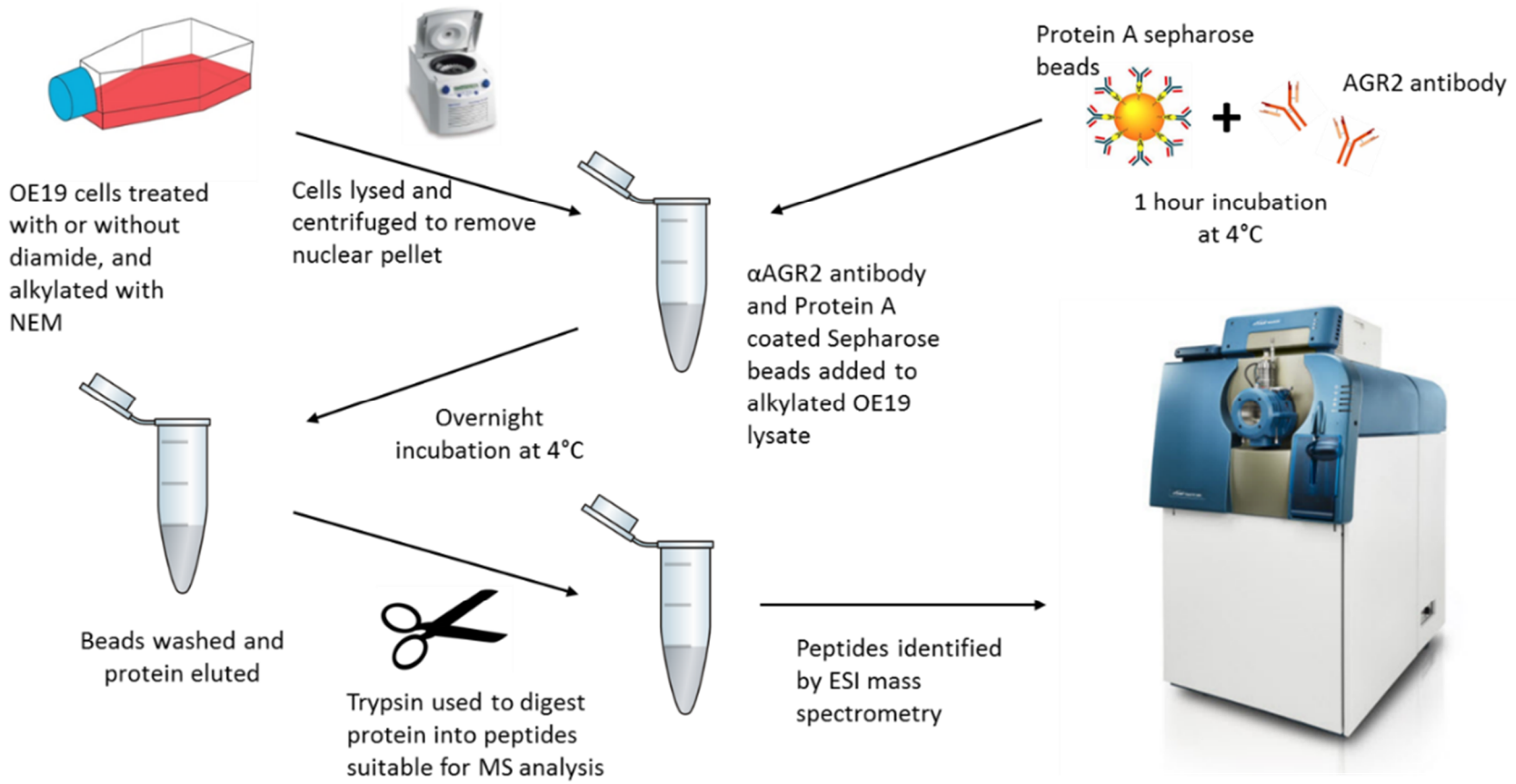

Figure 14: **Schematic diagram describing a trapping and immunoprecipitation approach for detecting interacting proteins.**
OE19 cells grown to ~90% confluency were treated with or without diamide to induce disulphide bond formation and alkylated with NEM to trap disulphide bonds. Cells were lysed and the lysate were immunoprecipitated with an AGR2 mAb (ab76473) and protein was eluted in an SDS elution buffer. Samples were digested with trypsin via the FASP digestion method and analysed by ESI mass spectrometry to identify the peptide fragments present in the sample. These peptide fragments contained AGR2 and proteins locked in complex with AGR2.

peptides detected that matched the protein database sequence, and the unused value – a description of the uniqueness of the peptide sequences detected. All of the proteins described above had two or more peptide hits as well as unused values above zero, indicating that they were unlikely to be similar sequences of a different protein. Non-human sequences were screened out by the software.

A curated list of proteins for each sample analysed by mass spectrometry are displayed in Tables 1-4. The unused score for a protein is a measure of the peptides detected during analysis that are unique to that protein, whereas the total score is a measure of the total peptides detected. Therefore, if a protein has an unused score lower than its total score it is possible that the peptides detected originated from another similar protein. Although included in the table, proteins with unused scores of 0 were not picked for further analysis. Percentage coverage (%Cov) was also displayed in the tables showing the percentage of the protein sequence that was covered by peptide matches. %Cov(50) and %Cov(95) refer to percentage coverage at 50% and 95% confidence respectively. %Cov was used as a measure of confidence that the protein was present in the sample, although ultimately proteins will low scores, such as calnexin (CNX), were investigated. Peptide counts were also used to determine protein confidence and initially a lower limit of 2 peptides was set. However, due to its known lectin binding abilities, ZG16B was investigated despite its peptide count of 1.

AGR2 was successfully detected in all but the control samples providing a crucial point of verification that the immunoprecipitation was successful and specific. Several known AGR2 interacting proteins were also detected at high peptide counts, including the mucins MUC5AC and MUC5B, known clients of AGR2 (Schroeder et al., 2012), as well as the ER resident chaperone BiP (Ryu et al., 2013). The presence of both MUC5AC and MUC5B at high peptide counts in the MS data suggests these are the primary clients of AGR2 in OE19 cells.

Additionally, several other ER resident chaperones were detected, including: ERp29, PrdxIV, Ero1α, ERp44, ERp57, Calnexin, PDIA3 and P5. These proteins are all ER resident chaperones and therefore are highly likely to be involved in the interactions of AGR2. Also detected were the lectins GAL4 and ZG16B. Lectins are of particular interest as they may be involved in the AGR2-mucin interactions. MUC1, PDI and Prdx1 were all also returned in the protein summaries although all had unused values of zero indicating the peptides detected could be similar peptides from related proteins. Prdx1 is also not an ER resident protein and therefore is unlikely to be interacting with AGR2.

To test and validate these interactions, antibodies specific to a selection of the proteins of interest were acquired where they were not already available and AGR2

immunoprecipitated samples were analysed by reducing western blotting using these new antibodies. MUC5AC was chosen as the mucin to test as it appeared at higher peptide counts overall, although MUC5B would also have been a suitable candidate.

Table 1: **List of protein identifications from the mass spectrometry analysis of an AGR2 immunoprecipitated, untreated OE19 lysate.**

Unused	Total	%Cov	%Cov(50)	%Cov(95)	Name	Abv. Name	Peptides(95%)
35.38	35.38	14.4	11.78	5.819	Mucin-5AC	MUC5AC	17
12.83	14.91	9.233	6.473	4.148	Mucin-5B	MUC5B	8
10.01	10.01	41.71	36.57	36.57	Anterior gradient-2	AGR2	8
17.24	17.24	27.22	22.02	14.53	78 kDa glucose-regulated protein	GRP78/BiP	7
2.03	2.03	16.83	10.1	10.1	Zymogen granule protein 16 homolog B	ZG16B	1

Table 2: **List of protein identifications from the mass spectrometry analysis of an AGR2 immunoprecipitated, diamide treated OE19 lysate.**

Unused	Total	%Cov	%Cov(50)	%Cov(95)	Name	Abv. Name	Peptides(95%)
61.77	61.77	20.25	17.72	13.41	Mucin-5AC	MUC5AC	33
50.03	53.53	19.66	16.31	12.1	Mucin-5B	MUC5B	28
38.46	38.46	48.17	48.17	35.47	78 kDa glucose-regulated protein	GRP78/BiP	19
13.49	13.52	46.86	44	44	Anterior gradient-2	AGR2	17
8.72	8.75	37.16	27.59	21.84	Endoplasmic reticulum resident protein 29	ERp29	5
3.11	3.23	22.91	13.93	5.263	Galectin-4	GAL4	2

Table 3: **List of protein identifications from mass spectrometry analysis of an AGR2 immunoprecipitated, untreated OE19 lysate replicate.**

Unused	Total	%Cov	%Cov(50)	%Cov(95)	Name	Abv. Name	Peptides(95%)
57.48	57.48	17.56	17.39	12.35	Mucin-5AC	MUC5AC	29
28.27	28.27	61.71	46.86	41.14	Anterior gradient-2	AGR2	27
42.8	42.8	40.06	38.99	38.99	78 kDa glucose-regulated protein	GRP78/BiP	22
18.73	21.07	8.487	7.671	7.15	Mucin-5B	MUC5B	11
0	11.57	41.21	32.66	29.15	Peroxiredoxin-1	Prdx1	6
0	4.11	5.709	5.709	3.937	Protein disulphide isomerase	PDI	2
0	4.03	2.948	2.231	2.231	Mucin-1	MUC1	2
3.51	3.79	12.48	12.48	4.752	Endoplasmic reticulum resident protein 57	ERp57	2
2.36	2.5	4.899	4.899	3.547	Calnexin	CNX	2

Table 4: **List of protein identifications from the mass spectrometry analysis of an AGR2 immunoprecipitated, diamide treated OE19 lysate replicate.**

Unused	Total	%Cov	%Cov(50)	%Cov(95)	Name	Abv. Name	Peptides(95%)
128.98	128.98	35.25	33.06	27.87	Mucin-5B	MUC5B	76
101.94	107.27	27.08	26	22.76	Mucin-5AC	MUC5AC	57
46.69	46.69	65.14	65.14	65.14	Anterior gradient-2	AGR2	50
55.17	55.17	49.85	49.85	47.09	78 kDa glucose-regulated protein	GRP78/BiP	31
17.42	17.42	43.68	43.68	40.61	Endoplasmic reticulum resident protein 29	ERp29	9
10.37	10.48	41.7	39.48	36.9	Peroxiredoxin-4	PrdxIV	7
0	8.51	18.7	15.16	8.268	Protein disulphide isomerase	PDI	4
7.43	7.49	17.31	13.68	10.47	ERO1-like protein alpha	ERO1A	4
4.65	5.23	18.61	18.61	8.515	Endoplasmic reticulum resident protein 57	ERp57	4
0	6.05	3.825	3.108	3.108	Mucin-1	MUC1	3
2.57	2.6	7.955	5.909	5.909	Protein disulphide isomerase P5	P5	2
4.07	4.08	11.58	8.128	8.128	Endoplasmic reticulum resident protein 44	ERp44	2
2.07	2.22	6.081	6.081	3.547	Calnexin	CNX	2

3.5 Verification of the expression of AGR2 interactors

Newly acquired antibodies for ERp29, GAL4, ZG16B and MUC5AC were tested with reducing western blotting of OE19 lysates to determine antibody effectiveness and protein expression (Figure 15). The ERp29 pAb (ab11420) showed a band in the 29 kDa region in both lanes which was assumed to be monomeric ERp29, as well as other higher molecular weight bands, which are likely to be non-specific (Figure 15A). The GAL4 mAb (ab175185) showed strong expression in both lanes in the expected 36 kDa region (Figure 15B). The ZG16B mAb (817310) did not show a band in the expected 22 kDa range yet did show a range of bands appearing at ~30-80 kDa (Figure 15C). These signals were assumed to be caused by cross-reactivity and thus further analysis with this protein was halted. The MUC5AC mAb (ab198294) yielded a non-distinct, smeary signal in the 250+ kDa, which was expected as MUC5AC is a large glycoprotein with many glycosylation sites and a high number of possible glycosylation variants (Figure 15D). These signals appeared in all OE19 lanes except the reducing diamide treated lane for unknown reasons. HT1080 cell lysates were used as a negative control as they are known to have little to no expression of mucins.

3.6 Validation of AGR2 interactors by immunoprecipitation and western blotting

In order to validate the results seen in the mass spectrometry data, AGR2 immunoprecipitated lysates were tested by immunoblotting with antibodies specific to the new potential interacting proteins. AGR2 Immunoprecipitated OE19 lysates were prepared as described previously with and without diamide treatment and with NEM trapping. Samples were run under reducing western blotting conditions and immunoblotted back for the protein of interest.

MUC5AC was successfully detected in AGR2 immunoprecipitated OE19 lysates analysed by western blotting (Figure 16A). Similar to results seen in Figure 15D, the MUC5AC signal again appeared as a smear in all lanes it was observed in. These included both the untreated and diamide treated lanes of the IP, appearing stronger in the diamide treated IP lane. Faint bands in the 50 kDa region of the IP lanes are assumed to be IgG heavy chain cross-reactivity. These results show clearly that MUC5AC is being retained after AGR2 immunoprecipitation of OE19 lysates. An AGR2 immunoprecipitation probed with a BiP pAb successfully detected a signal in the 78 kDa region in the diamide treated AGR2 IP lane (Figure 16B). This signal was very weak compared to the input and supernatant lanes, however it is clearly visible when compared to the untreated and IgG only IP lanes.

Like previous proteins, detection of ERp29 was first attempted after AGR2 immunoprecipitation using an ERp29 pAb (ab11420) in western blotting (Figure 17A).

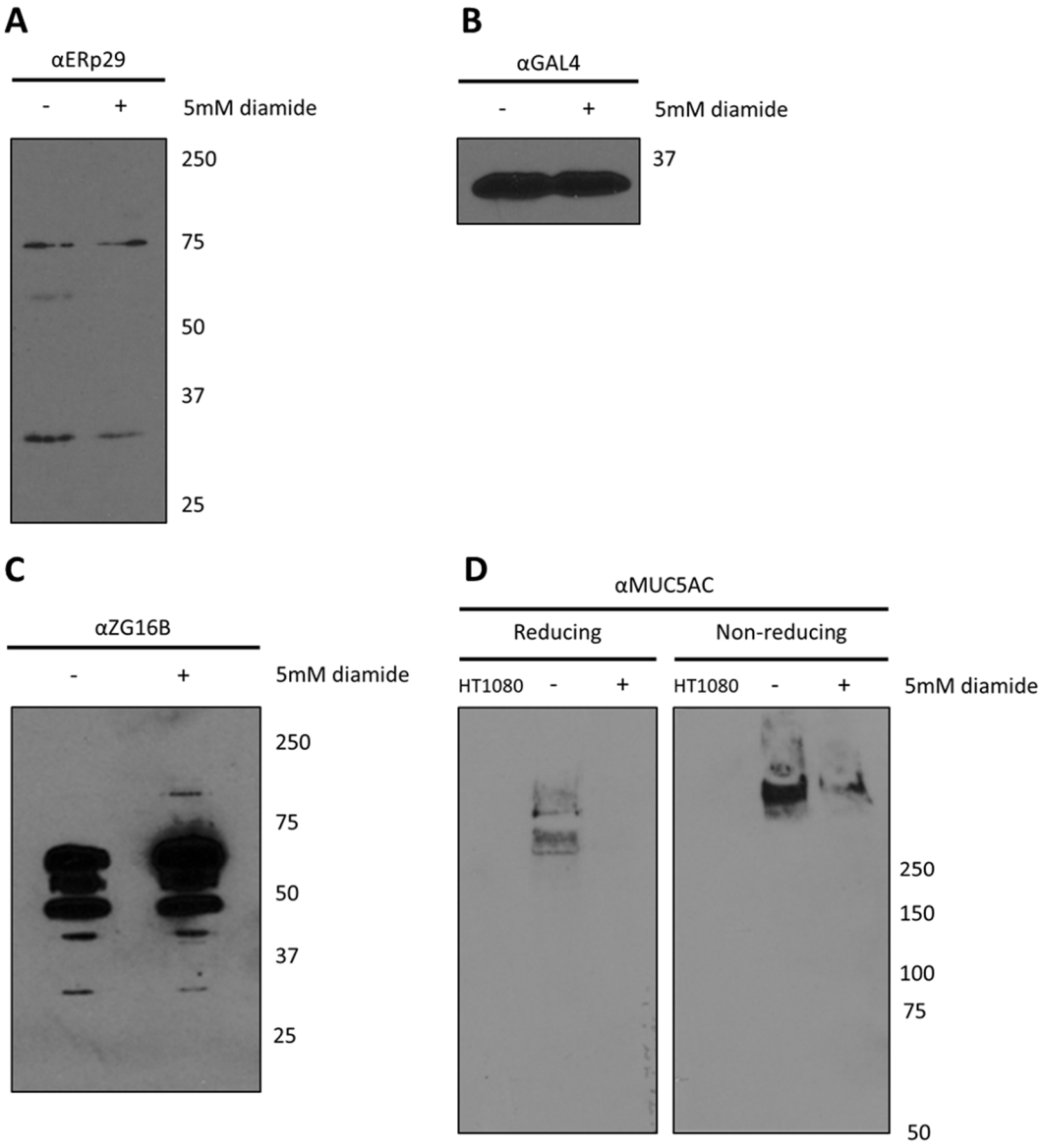

Figure 15: **Verification of expression of ERp29, GAL4, ZG16B and MUC5AC in OE19 cells.**

The expression of AGR2 interacting proteins detected from mass spectrometry was tested with reducing western blotting of OE19 lysates. (**A**) ERp29 pAb (ab11420) tested against OE19 lysates treated with and without diamide and with NEM. Bands in the 29 kDa region represent the ERp29 monomer. (**B**) GAL4 mAb (EPR12710(B)) tested against OE19 lysates treated with and without diamide and with NEM. Strong bands in the 36 kDa region represent the GAL4 protein. (**C**) ZG16B mAb (817310) tested against OE19 lysates treated with and without diamide and with NEM. No band appeared in the expected 22 kDa range and other bands are assumed to be unintentional cross-reactivity. (**D**) MUC5AC mAb (ab198294) tested against OE19 lysates, treated with and without diamide and with NEM. Non-distinct signals appeared at high molecular weights in almost all OE19 lanes. HT1080 lysates used as negative controls.

However, this attempt was unsuccessful and no ERp29 signal could be seen in the AGR2 IP lanes, partially due to excessive background on the blot. This experiment was attempted multiple times, with persistent background issues, without successfully detecting an ERp29 band in an AGR2 IP lane (data not shown). As the ERp29 pAb described as suitable for IP by the supplier, it was decided to immunoprecipitate with the ERp29 pAb and analyse through western blotting with the AGR2 mAb (D9V2F). The immunoprecipitation conditions used previously were applied to the ERp29 IP and the results of this experiment can be seen in Figure 17B. Signals were detected in the AGR2 monomer range, however, they were present in all IP lanes including the immunoprecipitate without lysate added, therefore it was concluded that the signal present was due to cross-reactivity with the IgG light chain and the interaction between ERp29 and AGR2 could not be independently verified.

After AGR2 immunoprecipitation, GAL4 could not be detected by western blotting (Figure 18A). Strong monomer bands could be seen in both the input and supernatant lanes but was entirely absent in the AGR2 IP lanes. Considering this data and the low peptide count observed in the MS data it was concluded that there was any interaction between AGR2 and GAL4 was weak, and further experiments on the putative interaction between GAL4 and AGR2 were discontinued. When probing an AGR2 IP with an ERp57 pAb it was observed that the ERp57 signal appeared at almost exactly the same height on the acrylamide gel as the IgG heavy chain (Figure 18B). This resulted in a similar issue to that observed in the ERp29 IP probed back for AGR2; the IgG cross-reactivity obscured any ERp57 signal and rendered the results inconclusive.

Probing an AGR2 IP with a PrdxIV mAb 7A1 revealed a signal in the diamide positive lane providing further evidence that an interaction occurred between AGR2 and PrdxIV (Figure 19A). The reason for the lack of heavy chain cross-reactivity on this blot is that the PrdxIV mAb was raised in mice and does not readily react with the AGR2 IP mAb ab76473 raised in rabbits. ERp44 was also successfully detected after AGR2 immunoprecipitation, as represented by a band in the expected 44 kDa region (Figure 19B). Again, this was most prominent in the diamide treated IP lane, although it could be argued that a very faint signal was present in the corresponding location of the untreated IP lane. Finally, probing an AGR2 IP for calnexin (CNX) produced a distinct band in the 90 kDa range where CNX migrates on an acrylamide gel (Figure 20). This was also only visible in the diamide treated AGR2 IP lane, however CNX was detected in both untreated and diamide treated MS samples indicating that this interaction may be strengthened by diamide but still occurs in its absence. Successful detection of PrdxIV, ERp44 and calnexin by western blotting analysis of AGR2 immunoprecipitated lysates supports the claim that these proteins are all involved in the interactions of AGR2.

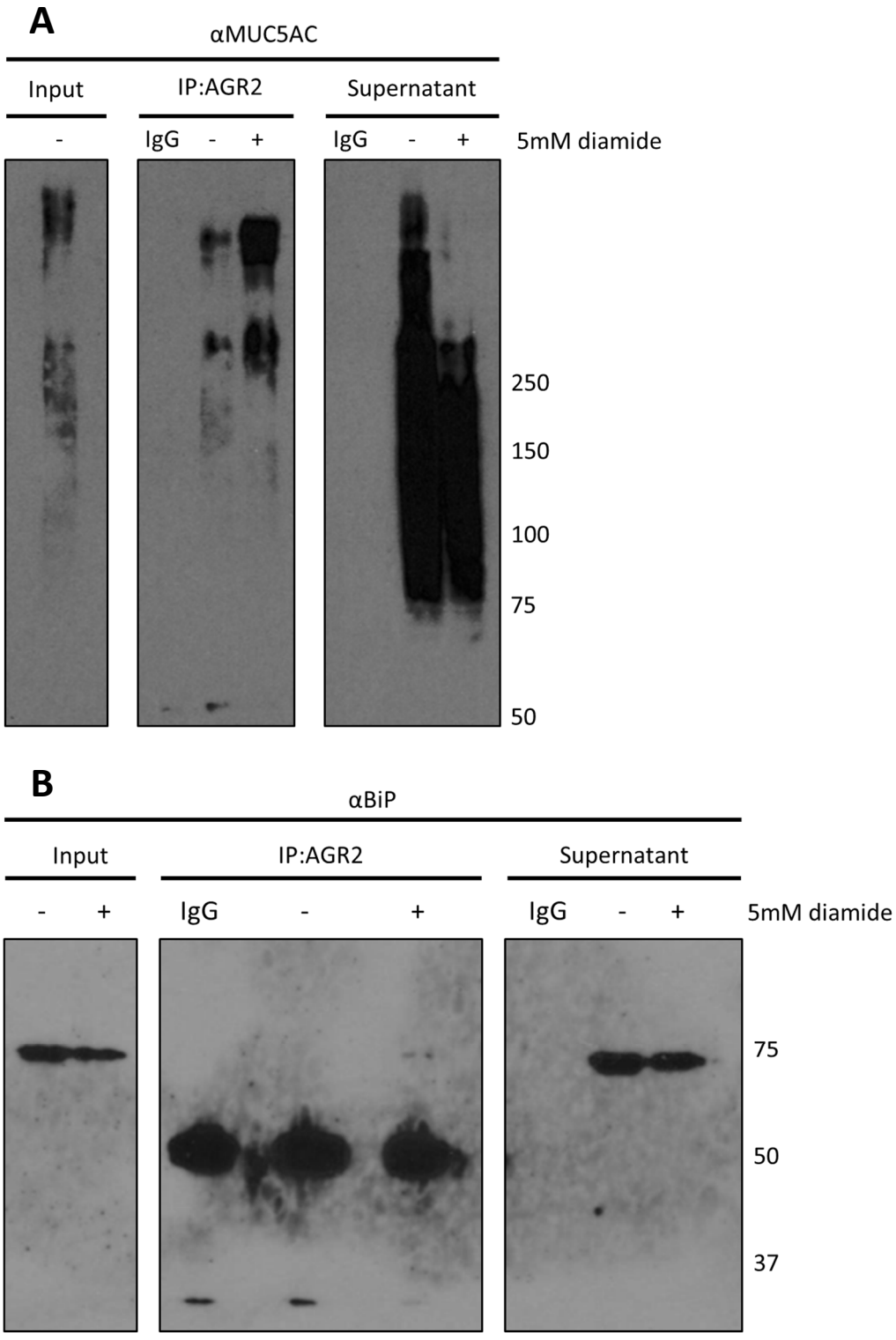

Figure 16: **Validation of AGR2 interactions with MUC5AC and BiP.**
OE19 lysates treated with and without diamide and with NEM were immunoprecipitated with the AGR2 mAb ab76473 and immunoblotted back for the protein of interest. (**A**) AGR2 immunoprecipitation probed with the MUC5AC mAb EPR16904. Strong signals in the IP:AGR2 lanes showed that MUC5AC was retained after AGR2 immunoprecipitation. (**B**) AGR2 immunoprecipitation probed back with BiP pAb 3183. A faint signal in the diamide treated AGR2 IP lane showed BiP was retained after AGR2 immunoprecipitation.

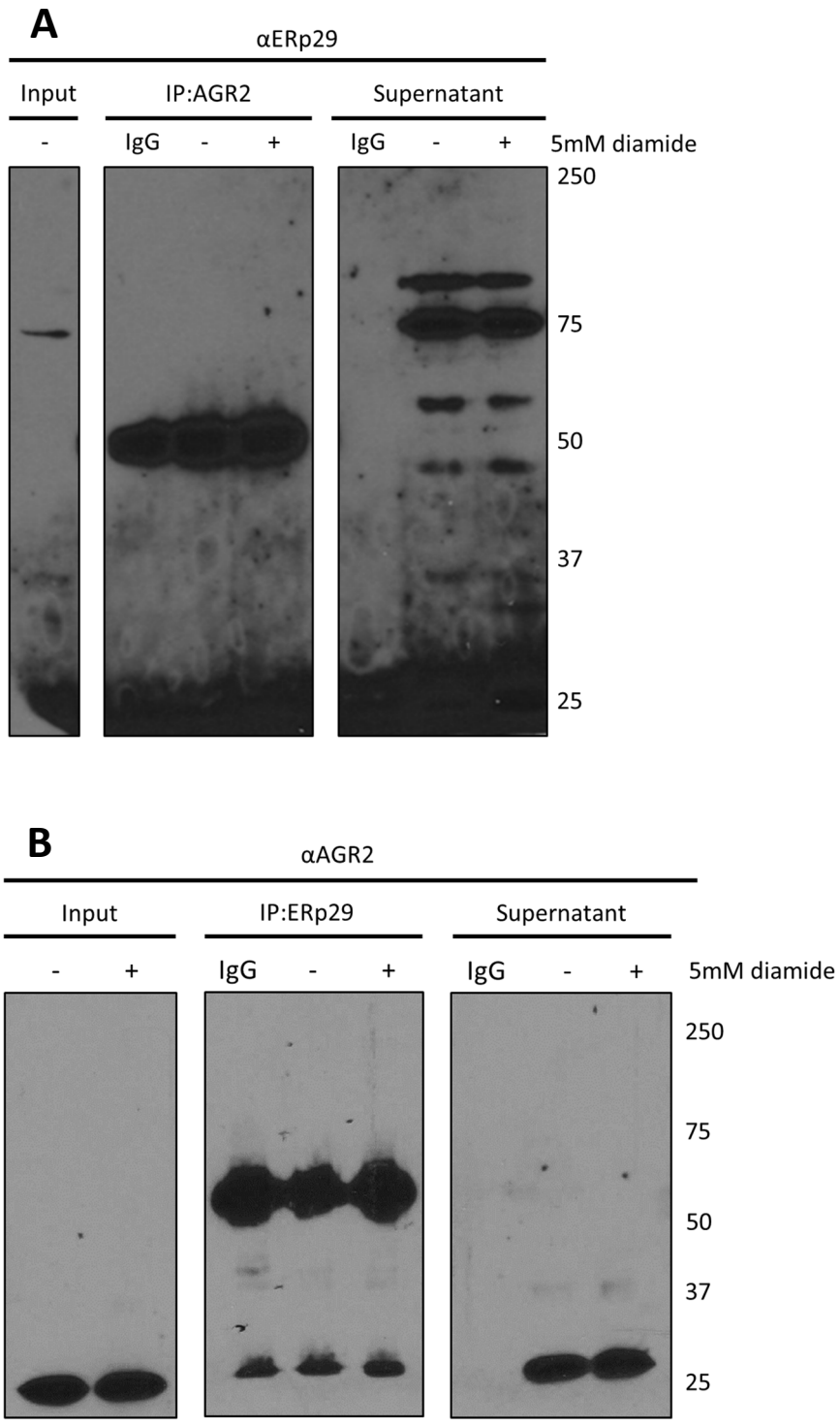

Figure 17: **Validation of AGR2-ERp29 interactions.**
OE19 lysates treated with and without diamide and with NEM were immunoprecipitated with the AGR2 mAb ab76473 and immunoblotted back for the protein of interest. (**A**) AGR2 immunoprecipitation probed back with the ERp29 pAb ab11420. High background and an overall weak ERp29 signal resulted in no interaction being observed. (**B**) ERp29 immunoprecipitation probed back with the AGR2 mAb D9V2F. Results inconclusive as bands appeared in all IP:ERp29 lanes including the IgG only and were therefore assumed to be the IgG light chain.

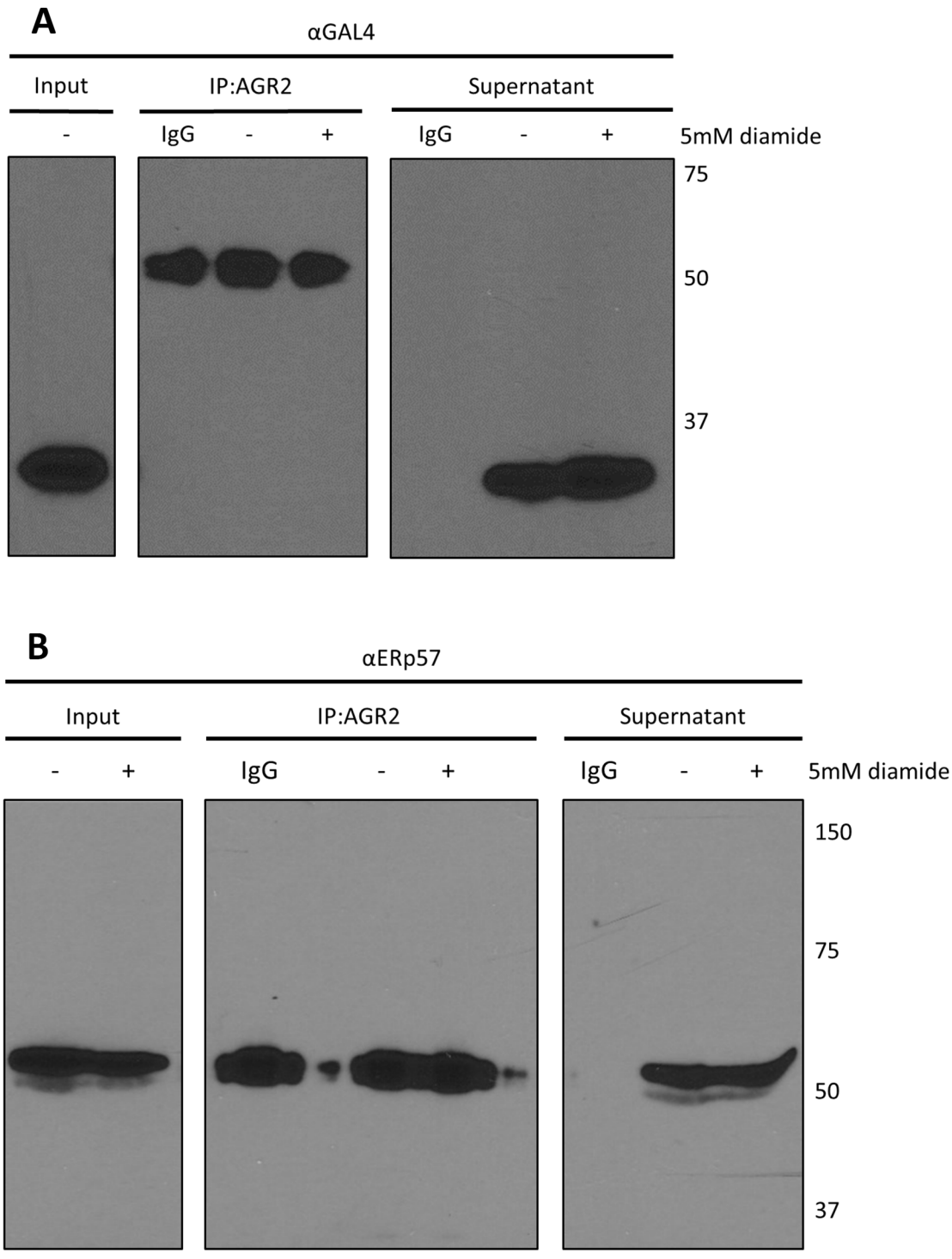

Figure 18: **Validation of AGR2 interactions with GAL4 and ERp57.**
OE19 lysates treated with and without diamide and with NEM were immunoprecipitated with the AGR2 mAb ab76473 and immunoblotted back for the protein of interest. (**A**) AGR2 immunoprecipitation probed back with the GAL4 mAb EPR12710(B). No signal was detected in the expected 36 kDa region of either AGR2 IP lane indicating that GAL4 was not retained after AGR2 immunoprecipitation. (**B**) AGR2 immunoprecipitation probed back with an ERp57 pAb G117. The IgG heavy chain obscured the signal in the expected 57 kDa region rendering the results inconclusive.

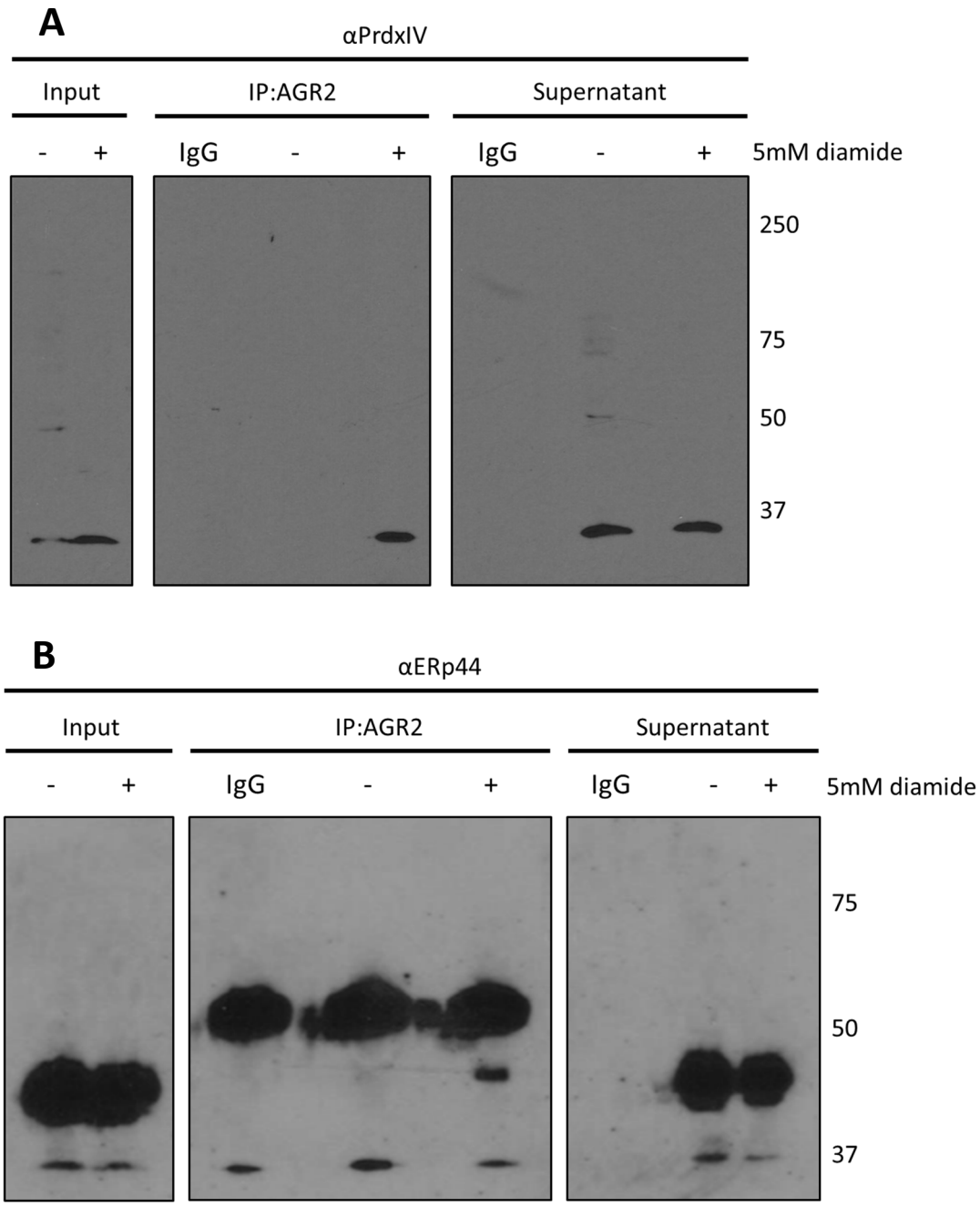

Figure 19: **Validation of AGR2 interactions with PrdxIV and ERp44.**
OE19 lysates treated with and without diamide and with NEM were immunoprecipitated with the AGR2 mAb ab76473 and immunoblotted back for the protein of interest. (**A**) AGR2 immunoprecipitation probed back with the PrdxIV mAb 7A1. The clear band appearing in the diamide treated AGR2 immunoprecipitated lane shows PrdxIV was retained after AGR2 immunoprecipitation. (**B**) AGR2 immunoprecipitation probed back with an ERp44 mAb D17A6. The band appearing in the expected 44 kDa region of the diamide treated AGR2 IP lane shows ERp44 was retained after AGR2 immunoprecipitation.

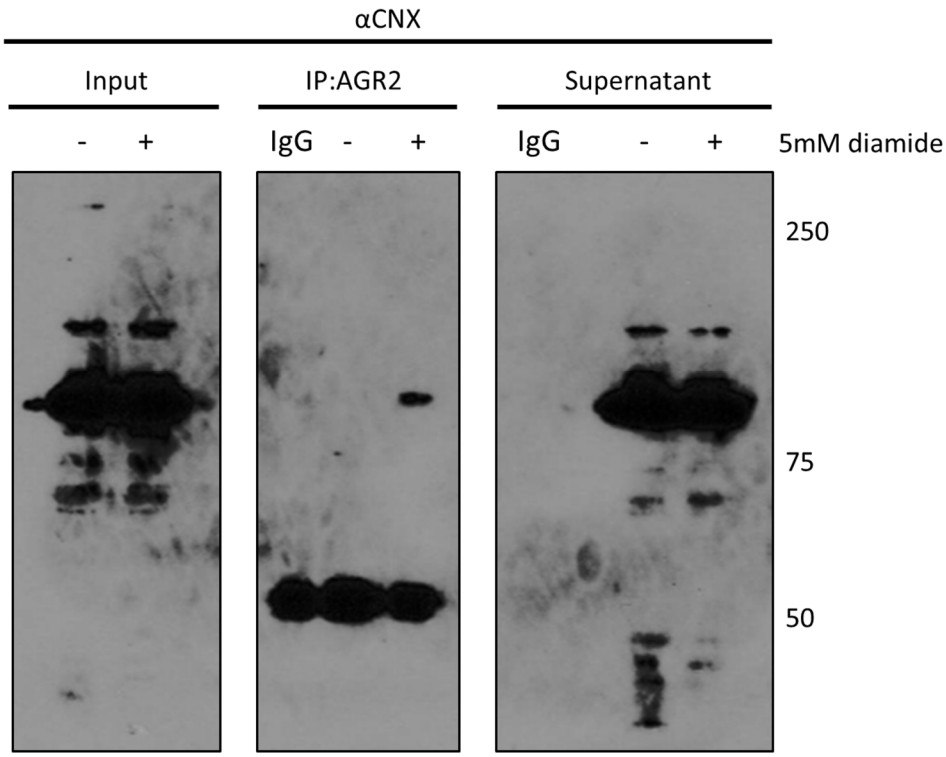

Figure 20: **Validation of an AGR2-CNX interaction.**
OE19 lysates treated with and without diamide and with NEM were immunoprecipitated with the AGR2 mAb ab76473 and immunoblotted back for CNX. AGR2 immunoprecipitation probed back with a CNX mAb. A single clear band was present in the diamide treated AGR2 immunoprecipitated lane indicating that CNX was retained after AGR2 immunoprecipitation.

3.7 Transfection of OE19 cells with a Myc-tagged ERp29 cDNA construct

Peptides corresponding to the ERp29 protein were detected in two of the four samples analysed by MS (Tables 1-4), providing convincing evidence that an interaction was taking place between AGR2 and ERp29. Attempts to validate this observation through western blotting of AGR2 and ERp29 immunoprecipitated lysates (Figure 17A & B) were unsuccessful. Therefore, a transfection experiment was initiated attempting to transiently express Myc-tagged ERp29 in OE19 cells. Once OE19 cells are expressing Myc-tagged ERp29 it will then be possible to use an anti-Myc antibody in place of the ERp29 antibody. Blotting an AGR2 immunoprecipitation with an anti-Myc antibody should remove the issues with excessive background signal previously encountered. Alternatively, immunoprecipitating with an anti-Myc antibody and probing back with an AGR2 antibody may reduce the issues with IgG light chain cross-reactivity as a different antibody will be used.

As the transfection protocol had not yet been fully optimised for Myc-tagged ERp29 cDNA, transfection of OE19 cells was tested with two different concentrations of cDNA. A mock transfection was also performed as well as an Ero1α transfection which had previously been optimised and therefore served as a positive control. After transfection, cells were lysed and run on a western blot probed with an anti-Myc mAb (Figure 21). Unfortunately, no signal was detected in either ERp29 transfected lane, showing that the OE19 cells did not express Myc-tagged ERp29. A band was detected in the Ero1α lane indicating that the transfection protocol was carried out successfully. A faint band also appeared in the mock treated lane, possibly due to some non-specific cross-reactivity. Transfection with Myc-tagged ERp29 cDNA was unsuccessful and it was decided to focus on other potential interacting partners.

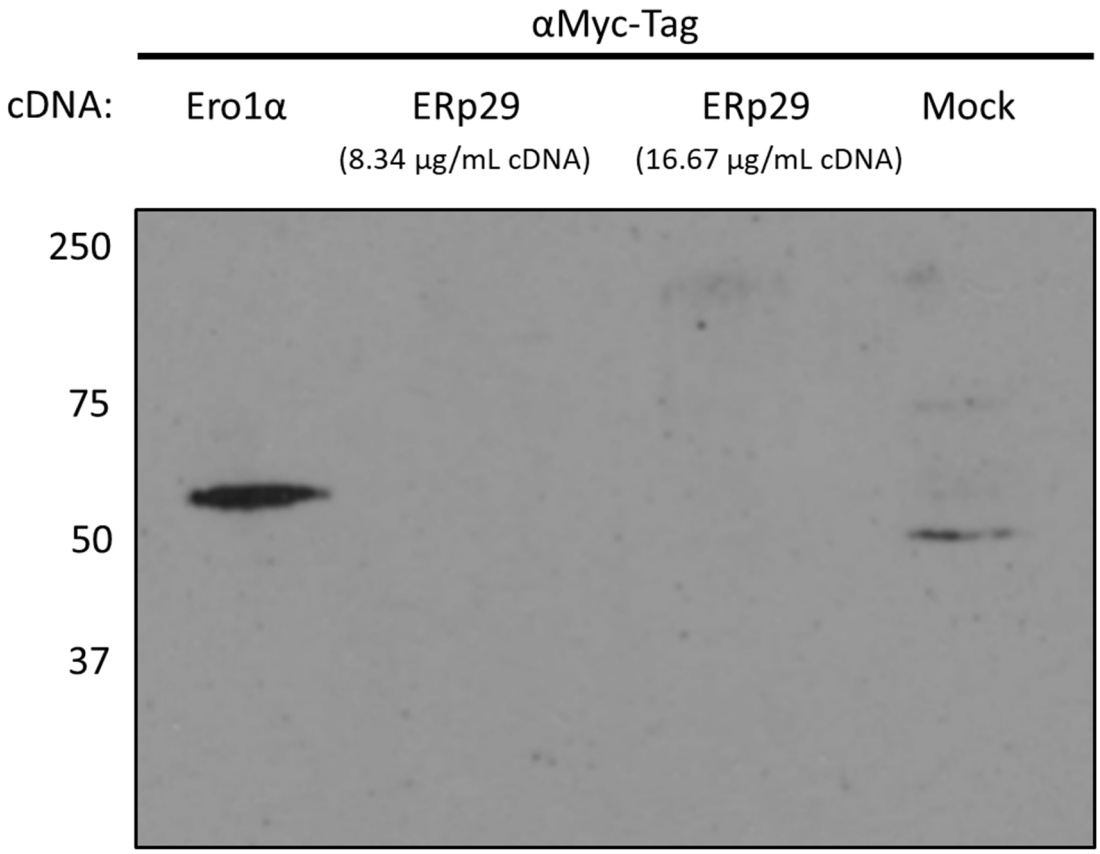

Figure 21: **Transfection of OE19 cells with Myc-tagged ERp29 cDNA.**
OE19 cells were transfected with a Myc-tagged ERp29 cDNA construct using the Lipofectamine 3000 Reagent. Ero1α cDNA served as a positive control. Western blotting with an anti-Myc mAb show a band in the Ero1α lane which was entirely absent in both ERp29 lanes, showing that the transfection was unsuccessful.

3.8 Co-localisation of AGR2 and PrdxIV in OE19 cells

PrdxIV was successfully detected in mass spectrometry analysis of AGR2 immunoprecipitated OE19 lysates and subsequently detected through western blotting analysis of AGR2 immunoprecipitated OE19 lysates. To provide further evidence that an interaction takes place between these two proteins a co-immunofluorescence experiments were set up. Utilising two different fluorophore-conjugated secondary antibodies it was possible to observe two different proteins simultaneously and from this determine their degree of co-localisation.

Cells were grown on coverslips, fixed in PFA, permeabilised in Triton X-100 and stained with either the AGR2 D9V2F rabbit mAb, the PrdxIV 7A1 mouse mAb or both. Fluorophore-conjugated secondary antibodies donkey anti-rabbit Alexa Fluor 594 (red) and donkey anti-mouse Alexa Fluor 488 (green) were applied to all coverslips, along with DAPI. Images were taken on the Zeiss LSM 880 Confocal Microscope. Both AGR2 (red) and PrdxIV (green) showed a similar perinuclear staining to the AGR2/PDI immunofluorescence presented in Figures 1-5. These results indicate that AGR2 and PrdxIV are both localised to the ER of OE19 cells. When merging both AGR2 and PrdxIV channels (Figure 22D), a very strong correlation between the AGR2 signal and the PrdxIV signal (yellow) was observed. This high degree of overlap between these two proteins supports the claim that AGR2 and PrdxIV are appropriately localised to interact with each other.

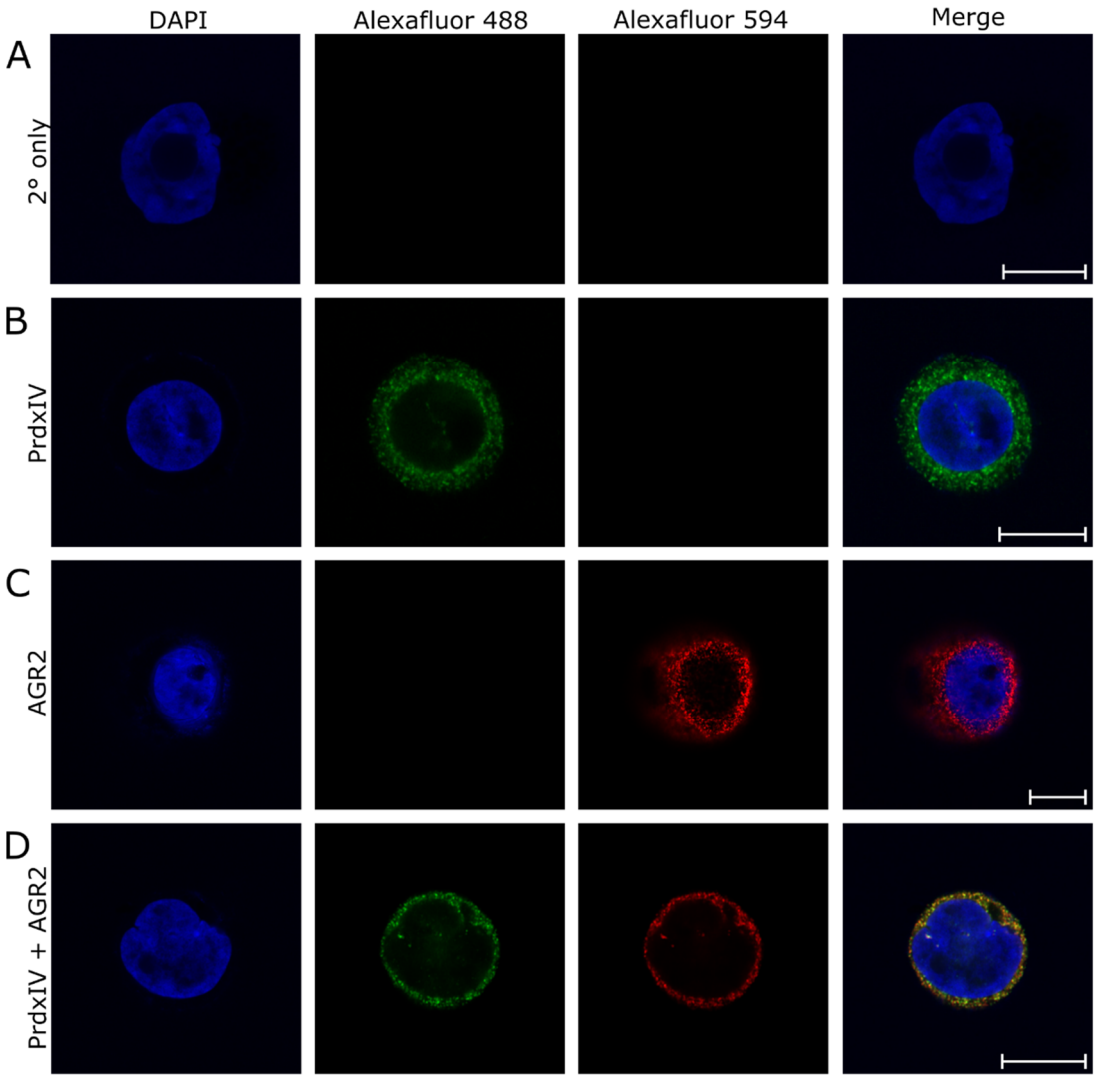

Figure 22: **AGR2 and PrdxIV co-localise in OE19 cells.**
Immunofluorescence was performed on OE19 cells with either the D9V2F AGR2 mAb, the 7A1 PrdxIV mAb or both. All slides were stained with both anti-rabbit ALEXAFluor 594 and anti-mouse Alexa Fluor 488. (A) Secondary antibody only. (B) 7A1 PrdxIV mAb. (C) D9V2F AGR2 mAb. (D) both 7A1 PrdxIV mAb and D9V2F AGR2 mAb. Strong co-localisation was observed when combining both AGR2 and PrdxIV (**D**) supporting the claim that these two proteins co-localise in the ER. White scale bars represent 10 µm.

3.9 Mucin visualisation

Western blotting is typically optimal for proteins between 20-200 kDa and therefore high molecular weight proteins such as the mucins can be difficult to visualise through standard gel electrophoresis and western blotting. Although a strong signal was observed previously when probing an AGR2 immunoprecipitation for MUC5AC (Figure 16A), this gave smeary and inconsistent results, so it was decided that other methods for visualising mucins should be explored.

3.9a Deglycosylation of mucins

During synthesis, secreted mucin proteins travel through the secretory pathway where they undergo extensive glycosylation before being ejected from the cell. These glycosylation events occur to varying extents on each molecule and result in a mucin population with variable molecular weights. When analysing MUC5AC after western blotting, this resulted in large non-distinct smears as seen in Figure 16A. The theory behind this experiment was that by deglycosylating an OE19 lysate it would be possible to remove some of the variation in mucin molecular weight and subsequently observe more distinct bands after western blotting analysis, allowing a clearer picture of the expression of mucins within a sample.

The New England Biolabs PNGase F protocol was chosen as the method for deglycosylation. Both denaturing reaction conditions and non-denaturing reaction conditions were tested. Under denaturing conditions, the sample is heated to 100°C for 10 minutes to remove the secondary structure of the folded protein and allow full deglycosylation. By comparing denaturing conditions to non-denaturing conditions, a comparison can be made to determine the extent of reaction completion. OE19 cell lysates without diamide or NEM treatment were subjected to protein determination using the Bradford assay and deglycosylated as per the New England Biolab protocol. Samples were then analysed by reducing and non-reducing western blotting (Figure 23).

After probing with a MUC5AC mAb distinct bands appeared in both the untreated OE19 lysate and the OE19 lysate treated under non-denaturing reaction conditions, under non-reducing western blotting conditions. Distinct bands were observed in the denaturing deglycosylated sample, indicating that the glycosylation was successful. However, these bands were also observed in the untreated sample and therefore these distinct bands were unlikely to be a product of the deglycosylation steps taken. Non-distinct smears could also still be seen at the top of the blot. The absence of any signal including background noise on the non-reducing denaturing sample and the lysate and non-denaturing samples run under reducing conditions was likely due to a transferring issue. Under reducing conditions, the majority of the denaturing sample lane could still be seen and the absence of any signal shows that the

deglycosylation was not successful. Overall, experiments to improve the detection of MUC5AC by deglycosylation were not successful.

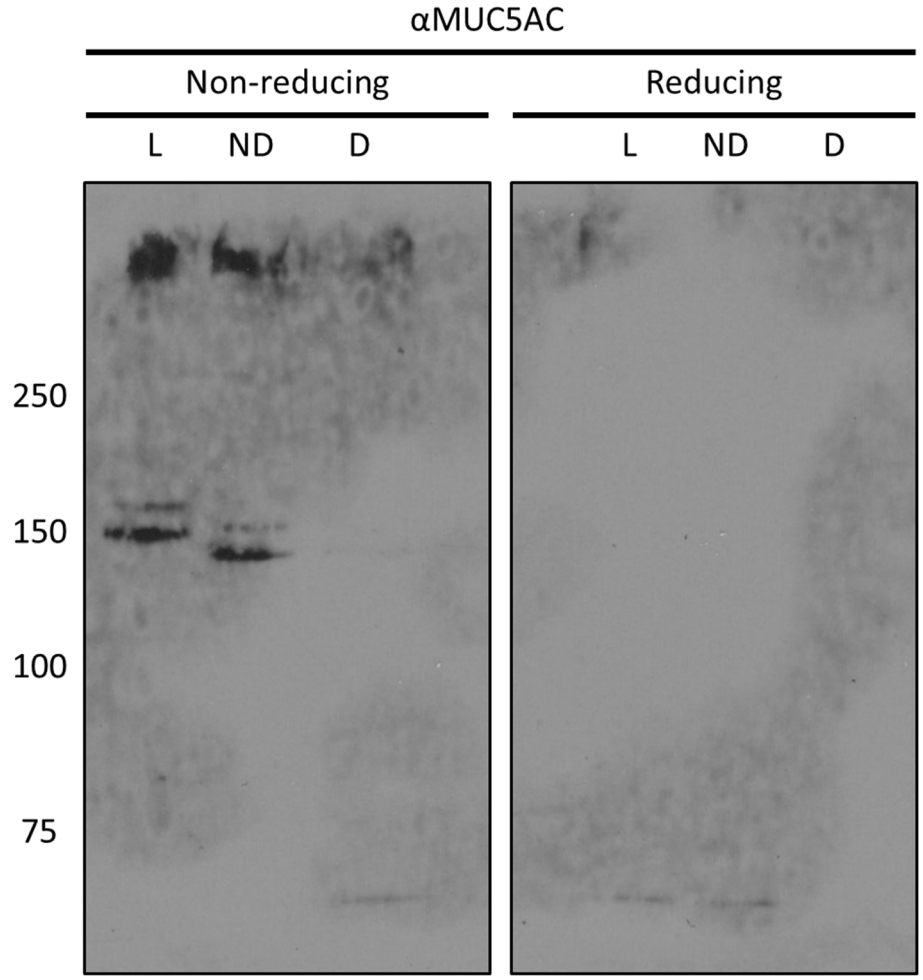

Figure 23: **MUC5AC deglycosylation using PNGase F.**
OE19 lysates were subjected to either denaturing or non-denaturing deglycosylation with PNGase F. Deglycosylated samples were run on 8% acrylamide gels and analysed by western blotting with a MUC5AC mAb. Distinct bands appeared in the lysate and non-denaturing non-reducing lanes but were absent from all other lanes. L = untreated lysate, ND = non-denaturing deglycosylated lysate, D = denaturing deglycosylated lysate.

3.9b Alcian Blue staining of mucins

Alcian Blue is a polyvalent basic dye used to stain acidic polysaccharides and has widely been used as a stain for mucins (Steedman, 1950). Use of the Alcian Blue stain in SDS-PAGE applications has previously been demonstrated as a method for visualising mucins separated on a gel (Cowman et al., 1984). It was therefore decided to test this visualisation method on OE19 and OE33 lysates.

OE19 and OE33 lysates were separated by 8% acrylamide SDS-PAGE, as described previously, followed by staining in 0.5% Alcian Blue plus 2% aqueous acetic acid for 45 minutes. Gels were then destained in 2% aqueous acetic acid for 15 minutes and an image of the gel was taken with a standard office scanner (Figure 24). It could be argued that the Alcian Blue stain was localised more towards the top of the gel in lanes OE19 and OE33 lysates were loaded – the location mucins have previously been observed. However, nothing more than diffuse non-specific staining was achieved in this and subsequent experiments.

Although through mass spectrometry analysis glycoproteins were detected in the OE19 cell line, if the experiment was to be repeated again it would benefit from the inclusion of a cell line with a high mucin content, or even a purified glycan, to serve as a positive control.

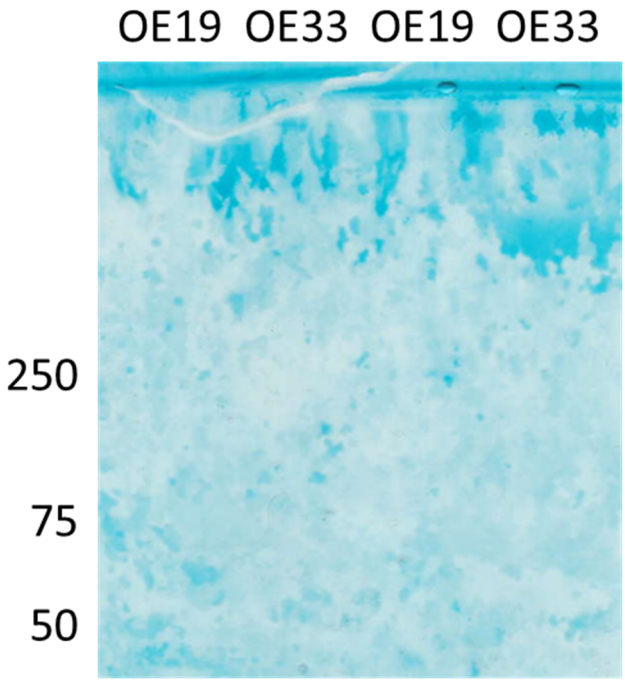

Figure 24: **OE19 and OE33 lysates separated by SDS-PAGE and stained with Alcian Blue.**
Duplicate OE19 and OE33 lysates were run on an 8% acrylamide gel and then stained for acidic polysaccharides with 0.5% Alcian Blue in 2% aqueous acetic acid. Alcian Blue stain did not stain specific proteins in the gel. Staining at the top of the gel could be due to the presence of mucins, however it is very non-specific.

3.9c Partial trypsinisation of mucins

Another method used to attempt to visualise MUC5AC was limited proteolysis through limited trypsin digestion. Trypsin is a serine protease which can be applied to cell lysates to digest the proteins into smaller peptide fragments (Dias-Gunasekara et al., 2006; Magnuson et al., 2005). As traditional western blotting is optimized for proteins in the 20-200 kDa range, this method can be applied to large proteins such as mucins, fragmenting them into peptides more easily detectable by western blotting analysis.

To test partial trypsinisation on OE19 lysates, trypsin concentrations of 0, 0.25, 1.25 and 2.5 µg/mL were used. After a 30-minute incubation digestion was terminated through the addition of soybean trypsin inhibitor (SBTI). Lysates were run on an 8% acrylamide gel and analysed by reducing western blotting. Probing the membrane with a MUC5AC mAb resulted in no signal being detected (data not shown). The membrane was then re-probed with a PDI pAb to test for trypsinisation (Figure 25). It is expected that trypsin would reduce the size of the 60 kDa band of PDI and produce new bands at lower molecular weights in the 35-45 kDa range (Wang et al., 2010). When probing with a PDI pAb no additional bands were observed at lower molecular weights. The only difference observed was in the 2.5 µg/mL lane where the band was reduced in size, however this band remained defined in the 60 kDa region. As an 8% acrylamide gel was used, it is possible that some PDI fragments may have migrated off the bottom of the gel and are therefore not visible. From these experiments we were not able to determine whether or not trypsinisation was successful, but due to time pressures we were forced to move on.

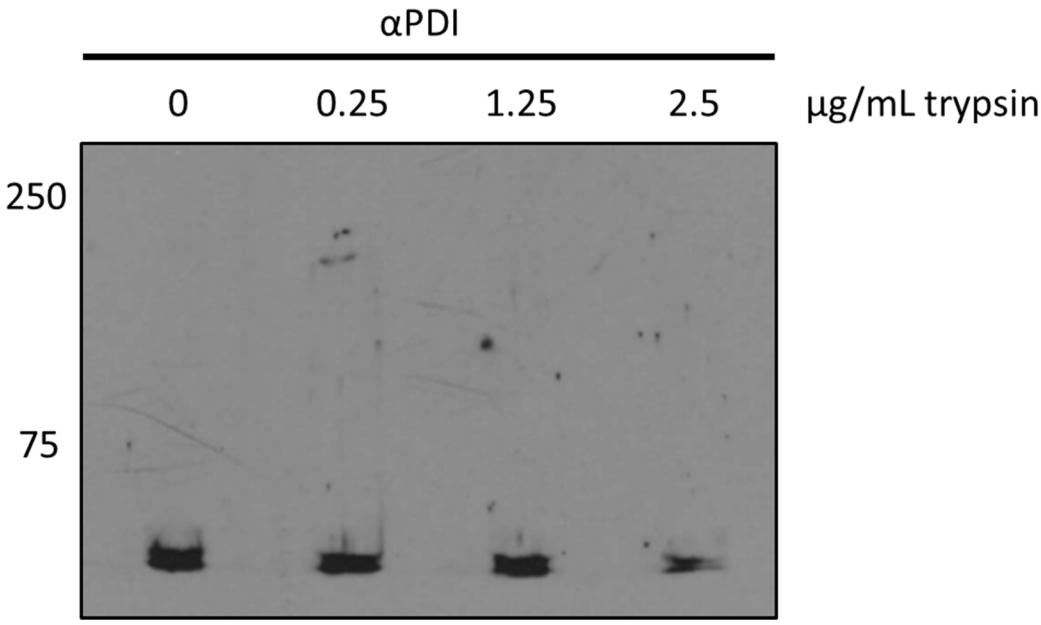

Figure 25: **Limited proteolysis of OE19 lysates through partial trypsinisation.**
OE19 lysates were subjected to limited proteolysis through the addition of varying concentrations of trypsin to digest samples. Lysates were separated by SDS-PAGE and western blotting and initially probed with a MUC5AC mAb. When no signal appeared, the membrane was re-probed with a PDI pAb. PDI bands did not show the expected fragmentation expected after trypsinisation.

3.10 In vivo AGR2-PrdxIV interaction testing using mouse stomach tissue

The OE19 cell line has provided a convenient cell culture model to test the interactions AGR2 makes with other proteins and has revealed multiple AGR2 interactions for follow up. However, an immortalised cell line does not replicate the complex environment of a tissue. Therefore, to provide further evidence to support the claim that AGR2 interacts with PrdxIV, and to test this claim in an in vivo system, a mouse model was chosen. Mouse stomach tissue was chosen to test this interaction as AGR2 and PrdxIV are both known to be expressed in stomach tissue.

Male mice aged 8-12 weeks were sacrificed in accordance with the Animals (Scientific Procedures) Act (1986) by trained personnel in the Life Sciences Support Unit at Durham University. After removal from the body of the mouse, the stomach was cut into 4 similarly sized pieces and thoroughly cleaned in PBS. These stomach sections were treated with or without diamide and with or without NEM creating four separate treatment conditions. After treatment cells were scraped into PBS, pelleted and transferring to lysis buffer (with or without NEM). Lysates were analysed by western blotting with an AGR2 mAb and then subsequently re-probed with a β-actin mAb (Figure 25). OE19 lysates were run as a positive control for AGR2.

Clear AGR2 bands were detected in two of the four mouse stomach lysates (+diamide, +NEM and -diamide, -NEM) and a faint band appeared in one of the other lanes (+diamide, -NEM), although this may have been due to sample over-spill. Reprobing for β-actin revealed there was limited protein in the two lanes lacking AGR2 signal (-diamide, +NEM and +diamide, -NEM). Lower molecular weight bands in the OE19 lanes of the β-actin reprobe were assumed to be persisting AGR2 signal. A positive AGR2 signal in two of the lanes demonstrated that lysates contained AGR2 and therefore it was decided to immunoprecipitate these lysates with an AGR2 mAb and attempt to detect PrdxIV within that AGR2 immunoprecipitate. Immunoprecipitation was carried out as previously described for OE19 lysates using the EPR3278 AGR2 mAb and a western blot probed with a PrdxIV mAb was used to detect a PrdxIV signal. When probing back with a PrdxIV mAb, background signal on the blot obscured any evidence of a signal in the immunoprecipitated lanes (data not shown). The lack of trapped complexes in the non-reducing stomach samples suggested that the procedure for isolating AGR2 complexes from tissues requires further optimisation. Taken together with the limited protein recovery that was achieved after tissue lysis, it was decided to focus on expression studies of AGR2 in cancer tissues.

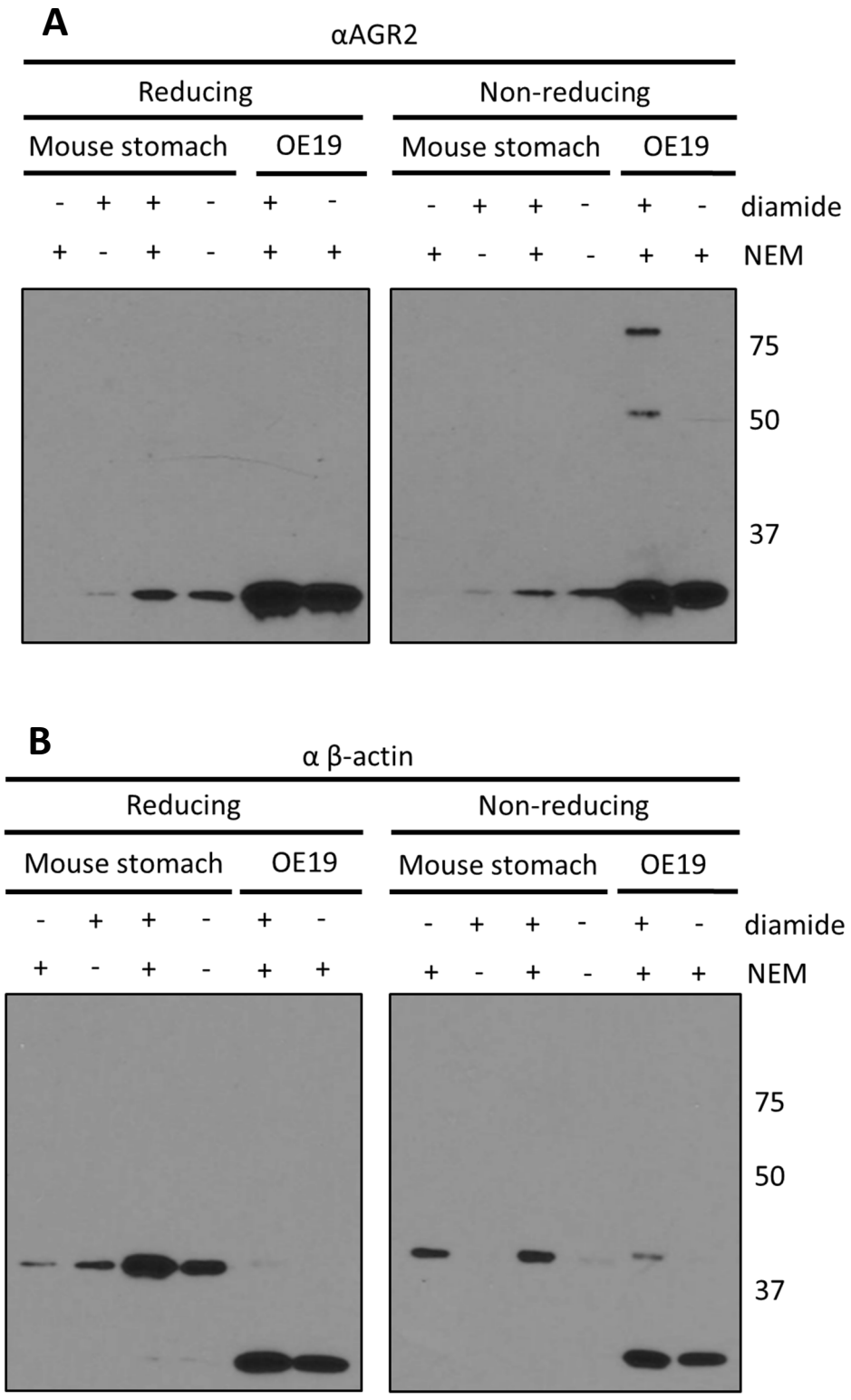

Figure 26: **AGR2 expression in lysates recovered from mouse stomach tissue.**
Stomach tissue was treated with and without diamide and NEM and lysed. Lysates were run under reducing and non-reducing conditions and probed for both AGR2 (**A**) and β-actin (**B**). OE19 lysates were run alongside mouse lysates as a positive control. Bands appearing in the +/+ and -/- lanes (**A**) show AGR2 is present in the mouse stomach. Reprobing for β-actin showed limited protein in -/+ and +/- lanes as well as AGR2 signal persisting (**B**).

3.11 Immunohistochemical analysis of oesophageal tissue sections

As explained previously the transition from normal oesophageal tissue to Barrett's oesophagus and eventually oesophageal adenocarcinoma is accompanied by changes in tissue morphology and mucin expression. Previous histological studies of Barrett's oesophagus and normal oesophageal tissue provided the basis for differentiating between the two tissue types (Hao et al., 2006). Normal oesophageal tissue is characterised as a simple squamous epithelium, homogeneous in nature and lacking glandular structures, whereas metaplasia induced in Barrett's oesophagus results in histology resembling that of the stomach, with glandular structures present. We sought to demonstrate this transition through staining of various paraffinized tissue sections, including both immunohistochemical staining for AGR2 as well as Alcian Blue staining of mucins. The following four different tissue sections were chosen: normal oesophagus, Barrett's oesophagus, oesophageal junction tumour and oesophageal tumour. These provide a range of cancer progression to test for both AGR2 and mucin expression.

Paraffinized sections on slides were provided by YKS Viswanath and Julie Walker, James Cook University Hospital, Middlesbrough. Slides were deparaffinized with xylene and ethanol, hydrated and either stained for AGR2 using the D9V2F AGR2 mAb through the DAB immunohistochemical staining method or stained for mucins with Alcian Blue.

AGR2 expression can be clearly seen in Barrett's tissue, OG junction tumour and oesophageal tumour tissue, visible as a brown stain (Figures 27 & 28). This staining is entirely absent from the normal oesophagus demonstrating the strong induction of AGR2 derepression in malignant and pre-malignant oesophageal tissue.

Similar to the distribution of AGR2 staining, mucin staining, visible as a blue colouration, was present in all tissue sections except the normal oesophagus (Figure 29 & 30). Alcian Blue staining was highly localised to clusters of secretory granules of varying size and shape, with little to no specific staining in the surrounding tissue. When comparing these Alcian Blue stained clusters to the same clusters on slides stained for AGR2 it is clear that they also contain AGR2 expression.

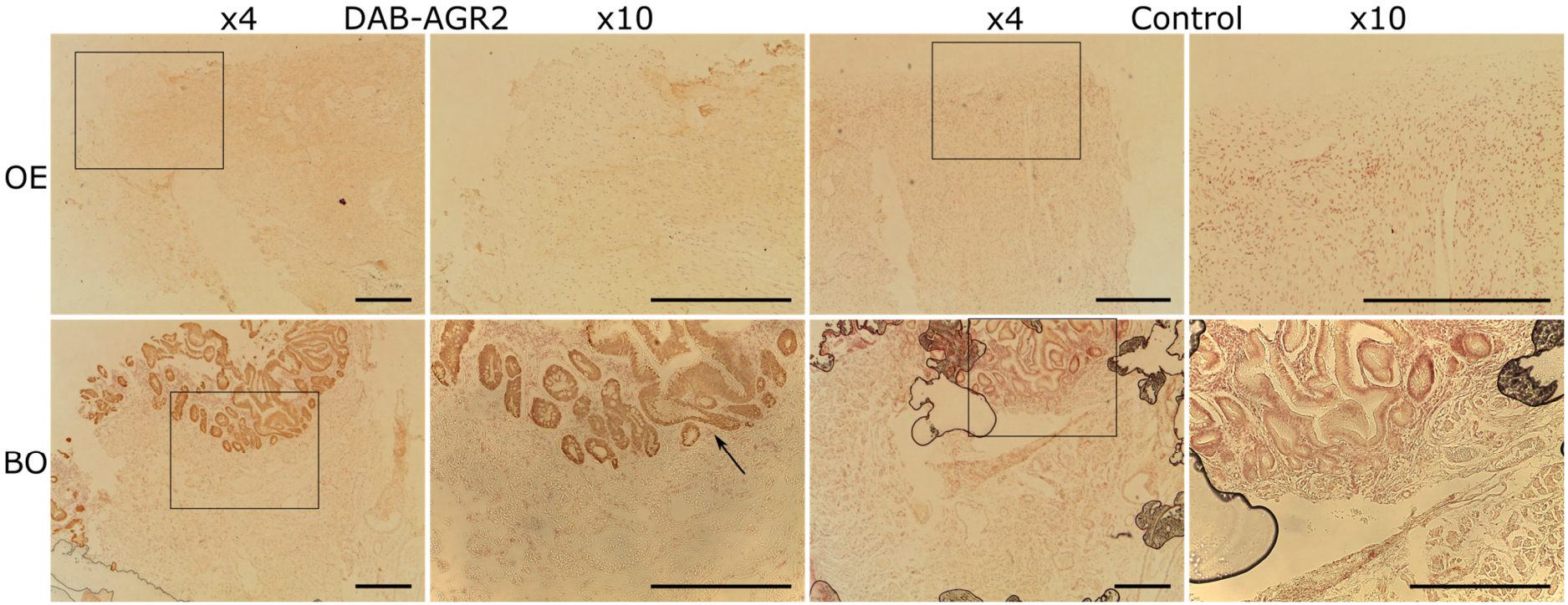

Figure 27: **Immunohistochemical staining of AGR2 in normal oesophagus and Barrett's oesophagus tissue sections.**
Human tissue sections from normal oesophagus (OE) and Barrett's oesophagus (BO) were immunohistochemically stained for AGR2 using the D9V2F AGR2 mAb (brown). Tissue was also stained with haematoxylin for cell nuclei. Controls were performed without the D9V2F AGR2 mAb. Barrett's oesophagus tissue sections show strong brown AGR2 staining (black arrow) representing strong AGR2 expression, which is entirely absent in normal oesophagus. Black squares on x4 magnification show areas magnified to x10. Scale bars represent 1 mm.

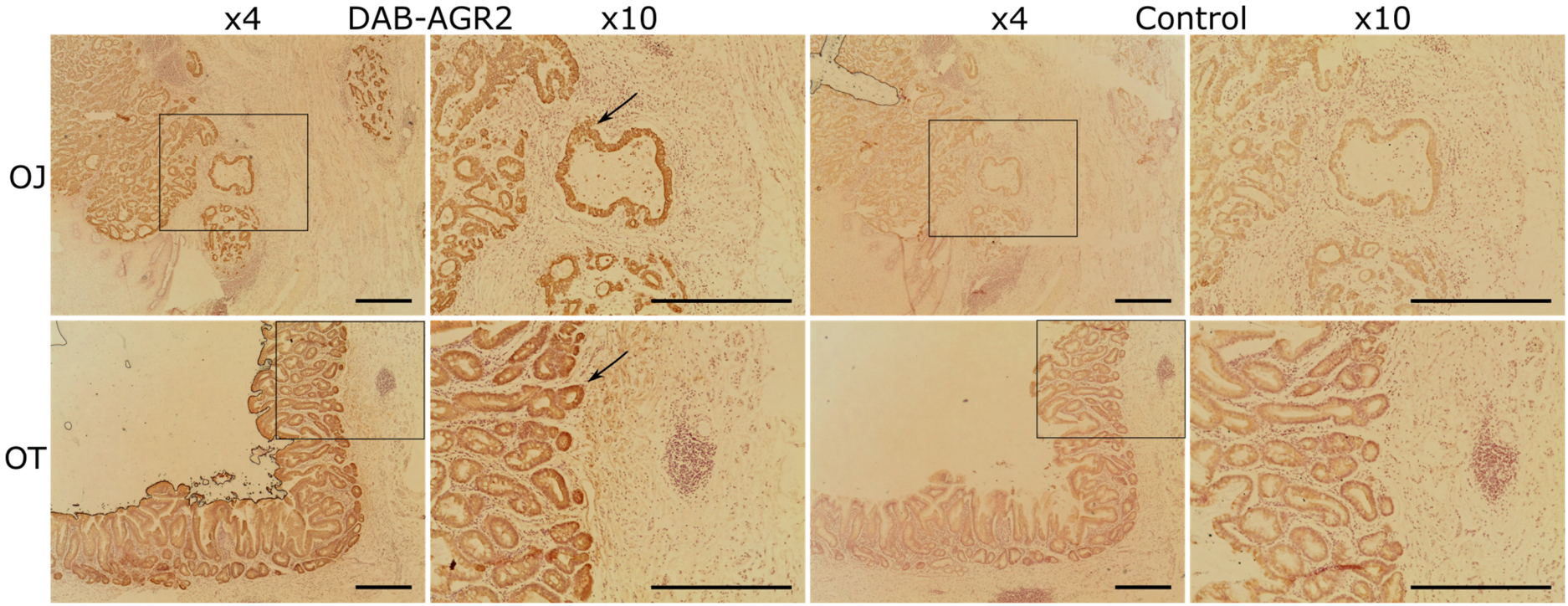

Figure 28: **Immunohistochemical staining of AGR2 in oesophageal junction tumour and oesophageal tumour tissue sections.**
Human tissue sections from oesophageal junction tumour (OJ) and oesophageal tumour (OT) were immunohistochemically stained for AGR2 using the D9V2F AGR2 mAb (brown). Tissue was also stained with haematoxylin for cell nuclei. Controls were performed without the D9V2F AGR2 mAb. Both tissue types show strong brown AGR2 staining (black arrows) representing strong AGR2 expression. Black squares on x4 magnification show areas magnified to x10. Scale bars represent 1 mm.

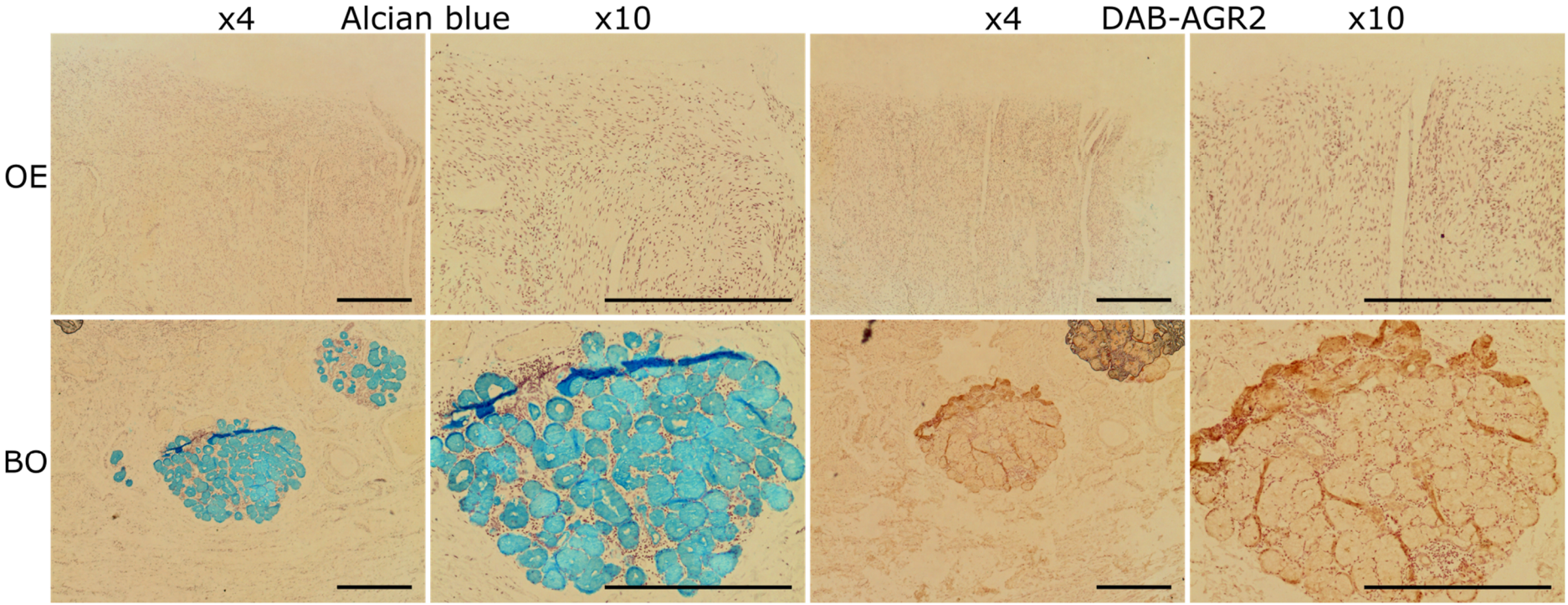

Figure 29: **Alcian Blue staining of mucins in normal oesophagus and Barrett's oesophagus tissue sections.**
Human tissue sections from normal oesophagus (OE) and Barrett's oesophagus (BO) were stained for mucin with Alcian Blue. Tissue was also stained with haematoxylin for cell nuclei. Highly localised Alcian Blue staining can be seen in glandular clusters in BO but is entirely absent in OE sections. Control sections displayed are Alcian Blue negative, but DAB stained for AGR2 as in Figures 27 & 28. Glandular structures in BO display both Alcian Blue staining as well as DAB-AGR2 staining showing similarities in expression localisation. Scale bars represent 1 mm.

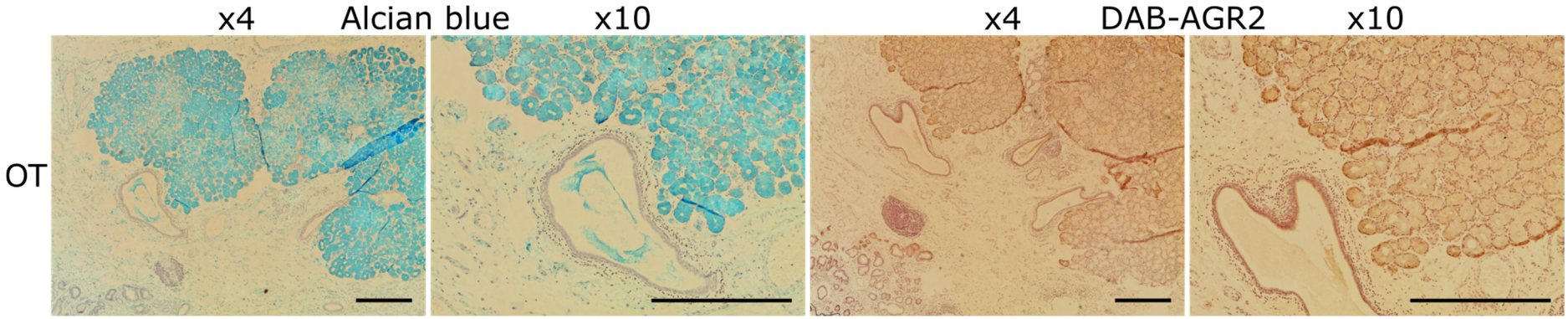

Figure 30: **Alcian Blue staining of mucins in oesophageal tumour tissue sections.**
Human tissue sections from oesophageal tumour (OT) were stained for mucin with Alcian Blue. Tissue was also stained with haematoxylin for cell nuclei. Similarly to Barrett's oesophagus in Figure 29, Alcian Blue staining can be seen in glandular clusters in oesophageal tumour tissues sections. Control oesophageal tumour sections displayed are Alcian Blue negative, but DAB stained for AGR2 as in Figures 27 & 28. Again, similar to BO in figure 29, glandular structures in OT display both Alcian Blue staining and DAB-AGR2 staining (brown) showing similarities in expression localisation. Scale bars represent 1 mm.

3.12 ER chaperone expression in OE19 vs OE33 cells

The OE19 oesophageal adenocarcinoma cell line was identified as pathological stage III (UICC) and showed moderate differentiation while the OE33 oesophageal adenocarcinoma cell line was identified as pathological stage IIA (UICC) and showed poor differentiation. This difference in cancer progression between these two cell lines allows the opportunity to study their differences and from that infer changes that may be brought about by cancer progression in human tissue.

Expression levels of a variety of ER chaperones were tested in both OE19 and OE33 cell lines by SDS-PAGE and western blotting (Figure 31). These included AGR2, PrdxIV, ERp29, PDI and calnexin, with β-actin used as a loading control. Quantification of western blotting signals was performed with ImageJ with densities being calculated relative to the cell line's β-actin density. These relative densities (OE19/OE33) can be seen in Table 5. AGR2 expression was significantly higher in OE19 cells. Looking at the western blotting results it may be possible there was over-spill from the OE19 lane into the OE33 lane, causing an increase in the OE33 signal. It also appears that the AGR2 band in OE19 was oversaturated and will therefore likely give an underestimation of AGR2 expression. Even considering this it is clear OE19 cells express AGR2 much stronger than OE33 cells.

PrdxIV levels were almost two-fold higher in OE19 cells and ERp29 saw an almost 50% increase when compared to OE33 cells. As a further progressed cancer cell line, OE19 may be overexpressing ER chaperones to keep up with the extra demand from a highly proliferating cell, which may be why we see increased levels of PrdxIV and ERp29. PDI levels were slightly but not significantly lower in OE19 and calnexin levels in OE19 were less than two thirds that of OE33 cells. As stated earlier it would be expected that the OE19 further progressed cancer cell line would have higher expression of ER chaperones when compared to the less progressed OE33 cancer cell line. From this data this appears not to be the case with PDI and calnexin. Calnexin does appear to have much lower expression in OE19 cells, however this may be due to the unusual shape of the band detected.

Overall it appears that chaperone expression is either increased in OE19 cells when compared to OE33 cells or the expression levels are relatively similar. This data serves to illustrate differences between these two cell lines, however, this was only one experiment, and only after repeating it multiple times would any significant conclusions about relative protein expression levels be deducible between these two cell lines.

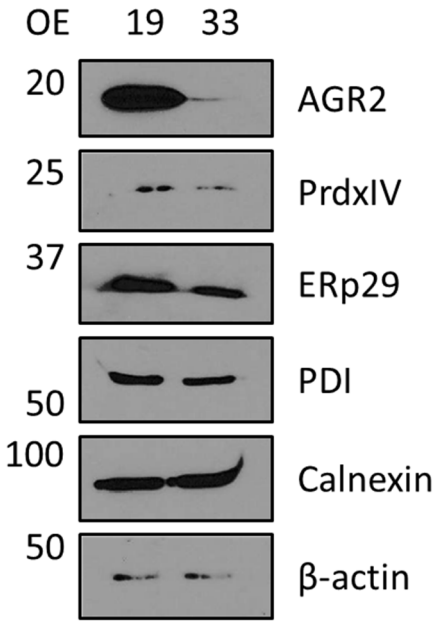

Figure 31: **Expression of ER chaperones in OE19 vs OE33 cells.**
Cell lysates made from OE19 and OE33 cells were analysed by SDS-PAGE and western blotting for the ER chaperones AGR2, PrdxIV, ERp29, PDI and calnexin. β-actin was used as a loading control.

Table 5: **Calculated relative densities of ER chaperone expression OE19 vs OE33 cells.**
Western blotting results show in Figure 31 were analysed and quantified using ImageJ and relative densities between OE19 and OE33 cells were calculated. ER chaperones expression was similar between the two cell lines with only AGR2 showing much greater expression in OE19 cells.

Protein	**Relative density (OE19/OE33)**
AGR2	24.79
PrdxIV	1.87
ERp29	1.49
PDI	0.96
Calnexin	0.64

4 Discussion

4.1 The intracellular localisation of AGR2

The presence of a signal sequence in the primary sequence of AGR2 (Figure 2 from introduction) dictates that it is translated into the ER lumen; the question of what happens to it after that is still up for debate. A sophisticated system of protein retrieval from the cis-Golgi compartment maintains levels of specific ER-resident proteins such as the chaperones within the ER. This is mediated by the C-terminal target peptide sequence KDEL, which is recognised by KDEL receptors in the cis-Golgi, after which retrograde transport is initiated and proteins are transported back to the ER lumen (Lewis and Pelham, 1990). AGR2 contains a non-optimal KTEL ER localisation signal which may allow localisation outside of the ER.

Immunofluorescence experiments performed in this study focused on OE19 oesophageal adenocarcinoma cells stained for both PDI and AGR2. PDI is a known ER-resident protein and therefore allowed visualisation of the ER in these cells. AGR2 staining within these cells showed a similar perinuclear profile of localisation to PDI supporting the claim that AGR2 is retained within the ER (Figures 5-8). A similar profile of immunofluorescence AGR2 expression was noted by (Dong et al., 2011) although they did not use an ER marker for comparison. Another experiment performed for this thesis involved co-staining of OE19 cells for both AGR2 and PrdxIV. Both proteins showed an almost identical pattern of localisation, which was again perinuclear. As PrdxIV is known to be an ER-resident protein (Tavender et al., 2008), this supports the claim that AGR2 is localised to the ER in OE19 cells. The ER localisation of AGR2 has been shown in other studies (Gupta et al., 2012; Higa et al., 2011; Park et al., 2009; Zhao et al., 2010) and therefore this observation is consistent with the literature. The question of whether AGR2 also leaves the ER to perform some of its functions remains possible. To answer this question higher resolution microscopy would be required.

4.2 AGR2 forms disulphide dependent complexes

AGR2 is a small member of the PDI family of proteins containing only one thioredoxin-like domain and one “active site” CXXS motif. Lacking the second cysteine residue, this motif does not allow for catalysed oxidase activity, as seen in PDI (Nørgaard and Winther, 2001). The presence of only one cysteine residue prompts the question of how this cysteine is involved in the interactions AGR2 makes with clients, co-chaperones and other interacting proteins. Through this cysteine residue, AGR2 can form disulphide bonds with itself, creating homodimers (Patel et al., 2013), as well as with client proteins, including MUC2 (Clarke et al., 2016).

The oxidant diamide was chosen to induce a change in the redox potential of the cells and promote disulphide bond formation. Diamide was initially discovered as an oxidiser of the intracellular pool of reduced glutathione (GSH), converting it to the glutathione disulphide (GSSG) (Kosower et al., 1969). As GSH reduces disulphide bonds, depletion of GSH promotes disulphide bond formation. Depletion of this GSH pool has been shown to result in cross-linking of certain proteins, such as PDI to IgM in lymphocytes (Roth and Pierce, 1987). Another early study showed that diamide may not be entirely specific to GSH and could also oxidise protein-SH groups resulting in non-specific modifications (Harris and Biaglow, 1972). These are all points to consider when using diamide to monitor protein-protein interactions as it moves cells away from physiological conditions. Other effects of diamide have also been noted, including depressed DNA synthesis and respiration (Harris and Biaglow, 1972). However, changes in protein expression due to these effects will not be noticeable for the short treatment time scales used in this thesis.

Through the use of diamide, in combination with the chemical NEM to alkylate free thiol groups and prevent disulphide bond reshuffling, it was possible to trap AGR2 complexes, visible through non-reducing western blotting (Figure 9). Induction of AGR2 complexes was rapid, occurring after only 5 minutes of treatment with diamide. Multiple bands were visible in the diamide treated non-reducing lanes in addition to smearing at the higher molecular weights representing a variety of AGR2 complexes. A distinct band appeared at ~34 kDa in the diamide treated non-reducing lanes which, due to its molecular weight, was assumed to be AGR2 in its homodimeric form, which is in line with the literature (Ryu et al., 2013). Determining the nature of the other complexes observed would require more advanced experimental techniques and was addressed by the mass spectrometry experiments described in section 3.4. A diamide recovery experiment was also performed to investigate the stability of these AGR2 complexes (Figure 9B). In the recovery experiments the majority of the induced AGR2 complexes persisted for 20 minutes with only one band clearly disappearing after recovery. Other studies have shown recovery of diamide induced loss of protein-SH groups occurs after just 15 minutes (Harris and Biaglow, 1972), in contrast to the results in this study. This may be due to differences in diamide concentrations used, the alkylation strategy, the cell type, or the cell-specific client range of AGR2 compared to other proteins.

Side by side comparison of reducing and non-reducing conditions clearly showed that the AGR2 complexes in OE19 cells are redox (disulphide) dependent as they are entirely absent under reducing conditions. As these AGR2 complexes are only visible under non-reducing condition they are very likely to occur through the single cysteine residue on AGR2.

4.3 The effect of ER stress on AGR2 complex formation

Previous experiments by Simpson and Benham (unpublished data) showed DTT modulated AGR2 complex formation. As DTT induces ER stress, one possibility was that these complexes may be induced by ER stress.

To test whether redox independent, ER stress-induced changes in AGR2 dependent complex formation could be detected, OE19 cells were treated with thapsigargin as well as a bile acid cocktail in low pH media. From western blotting results, thapsigargin treated samples did not show any sign of complex formation when probing for AGR2 (Figure 10A). Low pH media alone did not have an effect on AGR2 complexes (Figure 11C). When treating OE19 cells with low pH media supplemented with bile acids (Figure 11D), some additional bands were observed, although background signal partially obscured the results and bands also appeared in the reducing lanes. Overall these experiments indicated that ER stress, bile acids and pH did not affect AGR2 complex formation. This would suggest that the AGR2 complexes observed through non-reducing western blotting are not dependent on the redox state of the ER but not on ER stress.

It is, however, possible that prolonged ER stress may induce changes in gene expression, not visible in these experiments due to the short time scales. The chaperone BiP is one such protein that is induced after ER stress. As AGR2 has been shown to interact with BiP, it is possible that the AGR2-BiP interaction could be induced by elevated levels of the BiP protein resulting from ER stress. However, a series of experiments would need to be carried out over longer time scales to verify this.

4.4 AGR2 associates with mucins and other ER chaperones

Although it is well known that AGR2 plays an important role in a variety of different types of cancer and that it is required for correct synthesis and secretion of multiple mucin isoforms, the exact mechanism through which AGR2 performs these functions remains elusive. Previous interactions studies involving AGR2 have involved the use of yeast two-hybrid screens to detect potential novel interacting proteins. Proteins discovered through this technique include the DNA-binding protein Reptin (Maslon et al., 2010) along with the metastasis-associated GPI-anchored C4.4a protein and extracellular alpha-dystroglycan (DAG-1) (Fletcher et al., 2003). Due to the nature of these interacting proteins, these interactions are assumed to be involved in AGR2's oncogenic functions. However, the yeast two-hybrid approach does not take account of the topological issue imposed by the ER membrane.

The mechanisms though which AGR2 carries out its physiological function are less well known. Through knockout studies in mice, AGR2 has been shown to be essential for MUC2 synthesis and co-immunoprecipitation experiments have shown MUC2 is retained after AGR2 immunoprecipitation. Removal of the single cysteine residue in AGR2 prevents the interaction between AGR2 and MUC2 (Park et al., 2009). Further knockout studies showed that loss of AGR2 also resulted in a greater than 50% reduction in the levels of airway mucins MUC5AC and MUC5B (Schroeder et al., 2012). AGR2 has also been shown to associate with BiP through its dimeric form (Ryu et al., 2013). Although AGR2 has widely been described as an important part of the mucin synthesis machinery, the mechanism through which AGR2 is involved in mucin production are largely unknown.

Here we have demonstrated a trapping and immunoprecipitation approach for detecting AGR2 interacting proteins. The oxidising agent diamide was used to induce oxidising conditions and promote disulphide bond formation, and the alkylating agent NEM was used to alkylate free thiol groups on proteins and prevent disulphide bonds reshuffling. Additionally, cells were lysed using the non-ionic detergent Triton X-100, which was chosen as it is considered non-denaturing and generally less destructive to protein interactions when compared to harsher detergents. Through these conditions we have been able to preserve interactions of AGR2 and isolate AGR2 with its interacting partners.

Mass spectrometry analysis revealed both mucins MUC5AC and MUC5B were co-immunoprecipitated with AGR2 in all immunoprecipitated samples (Tables 1-4), consistent with the literature (Schroeder et al., 2012). Consistently high peptide counts for both of these mucin isoforms suggests that they are the primary clients for AGR2 in OE19 cells. Proteomic and western blotting analysis also revealed multiple ER chaperones were retained after AGR2 IP including: ERp29, ERp44, ERp57, PrdxIV, CNX, Ero1α and P5, as well as the previously known interactor BiP. The lectins GAL4 and PAUF/ZG16B were also detected in the MS data. Lectins bind to carbohydrates like those found on the highly glycosylated mucins and therefore hold the potential to be involved in AGR2/mucin interactions. However, low confidence in the MS results due to low peptide counts and negative results from immunoblotting of AGR2 immunoprecipitates meant that an interaction between AGR2 and GAL4 or ZG16B could not be confirmed.

Of the two mucin isoforms identified in the MS data MUC5AC was chosen for further analysis due to it having higher overall peptide counts. The presence of MUC5AC in the AGR2 immunoprecipitate was confirmed through western blotting of an AGR2 immunoprecipitation with a MUC5AC mAb. These results suggest that AGR2, in OE19 cells, is acting as a chaperone in the quality control of MUC5AC. The presence of MUC5AC in OE19 cells also suggests that this cell line has undergone the transition

similar to that found in Barrett's oesophagus, as Barrett's oesophagus is known to express MUC5AC (Arul et al., 2000). It is worth noting that the association between AGR2 and MUC5AC could be due to a direct interaction, or an indirect interaction with a third protein with which both AGR2 and MUC5AC interact. The high peptide counts obtained make the latter explanation unlikely, but this possibility could be resolved by performing re-immunoprecipitation studies. AGR2 may be part of a mucin folding complex, which has yet to be fully elucidated.

In both AGR2 immunoprecipitates from diamide treated OE19 cells, ERp29 was detected by mass spectrometry (Tables 2 & 4). ERp29 is a small ubiquitous ER-resident chaperone thought to play an important role in secretion. It is a component of the thyroglobulin folding complex; thyroglobulin being the major secretory product of the thyroid epithelial cells (Baryshev et al., 2006). ERp29 is not considered a protein disulphide isomerase as it does not contain an a domain and hence lacks the traditional thioredoxin motif found in PDI family members. Surprisingly, ERp29 was found to be retained after AGR2 immunoprecipitation only in samples treated with diamide, suggesting its presence was due to induced disulphide bonds or a change in the redox poise of the ER. It is possible that ERp29 co-associates with another protein retained in the IP, and that this protein has a diamide-induced interaction with AGR2.

Verification of MS results revealed several ER chaperones were retained after AGR2 immunoprecipitation and detectable by western blotting, supporting an interaction with AGR2. These included: ERp44, PrdxIV and CNX.

ERp44 is a chaperone protein preferentially binding client proteins in the acidic environment of the cis Golgi (Vavassori et al., 2013). It is known to forms mixed disulphide bonds with Ero1α, Ero1β and folding intermediates, including partially unfolded Ig subunits (Anelli et al., 2002, 2003). Through experiments with a truncated ribophorin mutant (Ri332) lacking cysteine residues, ERp44 has been shown to interact through formation of inter-chain disulphide bonds (Anelli et al., 2002). MS data from our study show ERp44 was only found in a diamide treated MS sample, suggesting that it was retained through interactions involving disulphide bonds, which is in line with the literature. ERp44 has also been shown to bind PrdxIV and Ero1α, retaining them in the ER as they lack the traditional KDEL ER localisation signal (Kakihana et al., 2013). As AGR2 does not contain a KDEL sequence, instead having a non-optimal KTEL ER localisation signal, it is possible that ERp44 also assists in retaining AGR2 in the ER compartments, which may be why we see it being retained after AGR2 immunoprecipitation.

PrdxIV, was also detected after AGR2 immunoprecipitation (Table 4 & Figure 19). PrdxIV is the ER-resident peroxiredoxin enzyme in humans and is capable of

metabolising hydrogen peroxide produced by Ero1α, oxidising itself and in turn allowing transfer of a disulphide bond to PDI or other PDI family members. PrdxIV was detected in our MS data with relatively high confidence – a peptide count of 7 and an unused value of 10.37, although only in the diamide treated sample of the second round. Validation of this result through western blotting of AGR2 immunoprecipitates resulted in a clear PrdxIV signal detected, but again only in the diamide treated sample. This suggests the interaction is redox dependent.

A concern when using an immortalised cell line to monitor protein-protein interactions is that interactions occurring in the immortalised cell line may not occur in tissues. To address this concern the PrdxIV and AGR2 interaction was tested in mouse stomach tissue as it is known to express both proteins. Unfortunately, testing this interaction *in vivo* was technically unsuccessful as the protein recovery method from mouse stomach tissue did not provide enough protein for the purposes of immunoprecipitation. This may have been partially due to stomach tissue not expressing AGR2 to the same degree as the OE19 adenocarcinoma cell line. Co-localisation immunofluorescence experiments were performed on OE19 cells to determine any overlap in intracellular localisation of these two proteins. When co-staining for both AGR2 and PrdxIV, an almost identical pattern of localisation occurred within OE19 cells, providing support to the claim that an interaction occurs between AGR2 and PrdxIV (Figure 22).

CNX was also successfully detected through western blotting of AGR2 immunoprecipitates (Figure 20). As a lectin chaperone known to assist in glycoprotein folding, it is possible that calnexin may play a role in the interactions and folding of mucins alongside AGR2. Previous studies have shown CNX does support mucin synthesis. Experiments in human colonic adenocarcinoma cells demonstrated CNX and the homologous lectin calreticulin (CRT) co-immunoprecipitated with MUC2, although no interaction was detected with MUC5AC for either of these proteins (McCool et al., 1999). As MUC5B was also detected in our MS analysis, it is possible that CNX could be interacting with MUC5B. Together, CNX and CRT cooperate in what is known as the CNX/CRT cycle of glycoprotein folding along with a range of other co-chaperones. One of these co-chaperones is ERp57, which was also detected in the MS data although could not be verified by western blotting due to technical issues. A direct interaction between ERp57/CNX and AGR2, if confirmed by immunoprecipitation, could imply that AGR2 is involved in the calnexin cycle to assist the folding of MUC5AC.

In summary, detection of proteins through MS analysis of diamide treated AGR2 immunoprecipitated OE19 lysates provides an unbiased approach for identifying AGR2 interacting proteins. Several new interacting partners for AGR2 have been identified, including ERp44, PrdxIV, and CNX, as well as several others that require

confirmation, including ERp29, ERp57, Ero1α and P5. A diagram summarizing these new AGR2 interacting partners is displayed in Figure 32. Here we have taken the first steps towards identifying novel players involved in AGR2 function and mucin quality control.

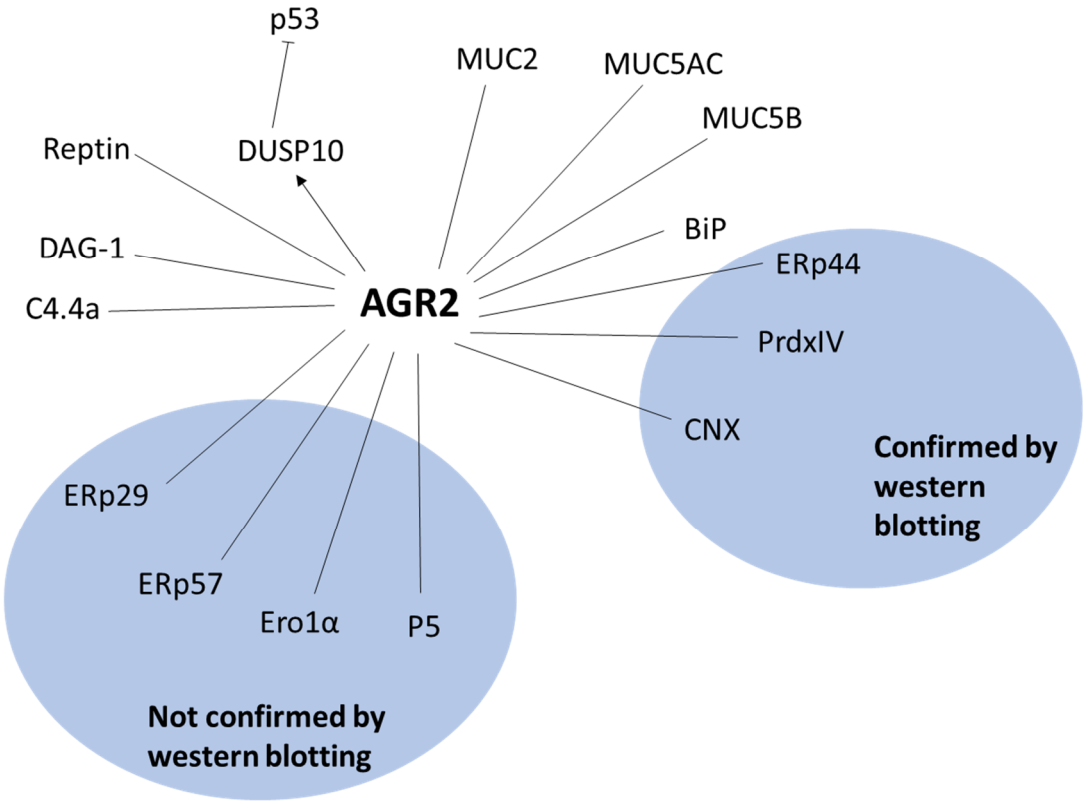

Figure 32: **Summary of interacting partners for AGR2.**
A diagram summarizing the major known interacting partners for AGR2 including ones discovered through this thesis. Straight lines indicate binding interactions (whether direct or indirect), arrows indicate upregulation of activity and flat ended lines indicate inhibition of activity. ERp29, ERp44, ERp57, PrdxIV, Ero1α, P5 and Calnexin were all detected through IP/MS during this investigation, and of those, ERp44, PrdxIV and CNX were confirmed through western blotting using antibodies specific to these new proteins.

4.5 Immunohistochemical and Alcian Blue analysis of oesophageal tissue sections

Oesophageal tissue, when transitioning into Barrett's oesophagus or oesophageal adenocarcinoma, exhibits changes in mucin expression along with derepression of AGR2 (Hao et al., 2006). Oesophageal tissue sections including normal oesophagus, Barrett's oesophagus, oesophageal junction tumour and oesophageal tumour were chosen to represent various stages of oesophageal tumour development and analysed for AGR2 and mucin expression. Staining for AGR2 with the AGR2 mAb D9V2F revealed strong AGR2 expression in Barrett's oesophagus, oesophageal junction tumour and oesophageal tumour tissues, but little to no expression in normal oesophageal tissue (Figure 27 & 28). These results are consistent with the findings from Hao et al., (2006) and morphologies of AGR2 expressing regions of the tissue sections show similarities to immunohistochemical images published by Dong et al., (2011).

Staining for mucins with Alcian Blue dye revealed large glandular structures in the tissue sections that appeared in all tissue types excluding normal oesophagus (Figures 29 & 30). Staining was very specific to these structures and did not occur to the same extent elsewhere in the tissue. These structures show similarities to Alcian Blue stained oesophageal gland ducts from patients with Barrett's oesophagus, observed in a study by Johnson et al., (2015). However, this study and others show Alcian Blue staining of Barrett's oesophagus with more even distribution than that observed in this project (Cabibi et al., 2014; Johnson et al., 2015; Voltaggio et al., 2011). This may be due to tissue samples that only express mucin in highly localised structures. When comparing these structures in Alcian Blue stained tissue with AGR2 stained tissue it was clear that these cells were also expressing AGR2. This overlapping localisation of AGR2 and mucins supports the co-immunoprecipitation data and is consistent with the assertion that AGR2 is a chaperone with mucin family proteins as its primary clients (Park et al., 2009; Schroeder et al., 2012).

4.6 ER chaperone expression in OE19 vs OE33 cells

There is increasing evidence that chaperone proteins play a pivotal role in maintaining cellular homeostasis in cancer cells. Gene expression microarray studies have shown increased expression of PDI in a variety of cancer types when compared to normal tissue (Xu et al., 2014), and cancer stem/progenitor cells from the bone marrow of breast cancer patients have shown overexpression of PDI, BiP and Grp94, demonstrating activation of the unfolded protein response (UPR) (Bartkowiak et al., 2010). The UPR has been implicated in hypoxia, a common form of cellular stress experienced by growing tumours (Wouters and Koritzinsky, 2008), and both the PERK

arm (Bi et al., 2005) and the XBP1 arm (Romero-Ramirez et al., 2004) of the UPR have been implicated in cell survival and tumour growth.

Considering the role ER chaperones have been shown to play in cancer cell progression, the expression levels of different ER chaperones were tested in both OE19 and OE33 cells. The OE19 cell line was derived from an oesophageal tumour classed as pathological stage III (UICC) while the OE33 cell line was derived from a tumour classed as pathological stage IIA (UICC). Therefore, by investigating expression levels between these two cell lines it was possible to observe differences in expression levels between two different stages in tumour progression (Figure 31 & Table 5). Most notable was the difference in AGR2 expression. OE19 cells strongly express AGR2 as shown in the earlier sections of this thesis but was almost entirely absent in OE33 cells. This expression profile may have been due to the poor differentiation of the OE33 cell line as AGR2 expression has been shown to occur in the vast majority of oesophageal adenocarcinomas (DiMaio et al., 2012). Expression levels of PrdxIV and ERp29 showed slight increases in expression in the OE19 cell line, with calnexin showing decreased expression and PDI showing little difference, when compared to the OE33 cell line. Overall a slight increase in ER chaperone expression was observed in the further progressed OE19 cancer cell line, which is in line with the literature, however, these experiments would need to be repeated before any significant changes could be claimed.

4.7 Future experiments

Experiments presented in this thesis have made considerable progress towards identifying AGR2 interacting proteins, the nature of these interactions and identification of the players involved in mucin synthesis in oesophageal adenocarcinoma. However, due to its short time scale, there are still many unanswered questions.

Early experiments in this thesis demonstrated AGR2 can form disulphide dependent complexes (Figure 9) and subsequently it was shown that AGR2 interacting partners could be identified through immunoprecipitation and mass spectrometry analysis (Tables 1-4). As the same conditions were used to trap these complexes in both sets of experiments, it is assumed that a large portion of the interactions seen were disulphide dependent. One possible way of determining whether or not these interactions were disulphide dependent would involve removal of the single cysteine residue in AGR2. This could be done by inserting a coding sequence representing AGR2, with the cysteine residue replaced with a serine, into an expression vector. This expression vector would then need to be transfected into OE19 cell with wild-type AGR2 expression inhibited, likely through shRNA silencing. Immunoprecipitation and mass spectrometry experiments, as described in this thesis, carried out with a

cell line expressing an AGR2 protein lacking cysteine residues would reveal whether these interactions are disulphide dependent. Any proteins retained after immunoprecipitation with this cell line would be assumed to associate with AGR2 independently of direct disulphide bonds with AGR2.

In experiments in this thesis, mucin visualisation through western blotting proved difficult, as demonstrated by the multiple attempts to improve mucin visualisation (Figures 23-25). This was due to the large size of the mucin proteins and their variable molecular weights caused by varying patterns of glycosylation. Western blotting is optimised for proteins between 20-200 kDa and mucins typically migrate well above this range. One method not attempted here would be to use gradient gels for SDS-PAGE separation. Gradient gels are harder to cast that traditional single concentration gels but provide much better separation for a wider range of protein molecular weights. These gels typically range from 4% to 20%, allowing larger proteins such as mucins to travel further into the gel as the initial acrylamide percentage is lower. Gradient gels may be an alternative method of visualising mucins and might allow for further experiments to be performed investigating mucins, such as determining expression levels between OE19 and OE33 cells to investigate the correlation between AGR2 expression and mucin expression.

Although ERp44, PrdxIV and CNX were all detected through western blotting of AGR2 immunoprecipitated lysates, several other proteins detected through mass spectrometry analysis were unable to be detected through western blotting. Identification of these proteins was hindered as the primary antibody used in western blotting would often react with the light and heavy chains of IgG used in immunoprecipitation, thus obscuring the signal of the protein of interest. These cross-reactivity issue would likely have been mitigated if the two antibodies used were raised in different species. For example, immunoprecipitation was carried out with an anti-rabbit AGR2 antibody. If western blotting detection of ERp29 was attempted with an anti-mouse ERp29 antibody it is possible the IgG light chain at ~25 kDa would be absent and the ERp29 band at ~29 kDa would be visible. Alternatively, 2D gel electrophoresis could have been implemented to further separate proteins before detection through immunoblotting.

Another experiment attempted with limited success was investigation into the in vivo interaction between AGR2 and PrdxIV, though the use of a mouse model. These experiments were halted as protein recovery from mouse stomach sections was limited do to their small size. One way around this would be to move to a larger animal such as a rat or rabbit. The larger stomach size of these animals would allow more protein to be recovered and hopefully allow an interaction to be observed between AGR2 and PrdxIV.

4.8 Conclusion

Experiments in this thesis have shown that AGR2 is strongly expressed in the OE19 oesophageal adenocarcinoma cell line, and that in this cell line it can form disulphide bond dependent complexes, visible through non-reducing western blotting. These complexes also appear to not be dependent on ER stress. With this knowledge, a novel, unbiased trapping and immunoprecipitation approach was implemented, and peptide identification by ESI mass spectrometry has revealed a variety of ER-resident proteins that associate with AGR2. The mucins MUC5AC and MUC5B have been identified as primary clients of AGR2 in the OE19 cell line, and associations with ER chaperones including PrdxIV, BiP, calnexin and ERp44 have been demonstrated and verified. Immunohistochemical analysis of oesophageal tissue sections has displayed the strong induction of AGR2 expression in the progression to Barrett's oesophagus and oesophageal adenocarcinoma and has revealed co-localisation between AGR2 and mucin secreting glands. Finally, experiments into ER chaperone expression have shown differences in expression between two cell lines representing different stages of oesophageal adenocarcinoma.

Identification of these novel AGR2 interactions has provided the basis for elucidation of a mucin quality control system within oesophageal adenocarcinoma and highlights potential therapeutic targets for AGR2-positive cancers.

5 References

Aberger, F., G. Weidinger, H. Grunz, and K. Richter. “Anterior Specification of Embryonic Ectoderm: The Role of the Xenopus Cement Gland-Specific Gene XAG-2.” *Mechanisms of Development* 72, no. 1–2: 115–30 (1998).

Anelli, Tiziana, Massimo Alessio, Angela Bachi, Leda Bergamelli, Gloria Bertoli, Serena Camerini, Alexandre Mezghrani, Elena Ruffato, Thomas Simmen, and Roberto Sitia. “Thiol-Mediated Protein Retention in the Endoplasmic Reticulum: The Role of ERp44.” *The EMBO Journal* 22, no. 19: 5015–22 (2003). https://doi.org/10.1093/emboj/cdg491.

Anelli, Tiziana, Massimo Alessio, Alexandre Mezghrani, Thomas Simmen, Fabio Talamo, Angela Bachi, and Roberto Sitia. “ERp44, a Novel Endoplasmic Reticulum Folding Assistant of the Thioredoxin Family.” *The EMBO Journal* 21, no. 4: 835–44 (2002). https://doi.org/10.1093/emboj/21.4.835.

Arul, G. S., M. Moorghen, N. Myerscough, D. A. Alderson, R. D. Spicer, and A. P. Corfield. “Mucin Gene Expression in Barrett’s Oesophagus: An in Situ Hybridisation and Immunohistochemical Study.” *Gut* 47, no. 6: 753–61 (2000). https://doi.org/10.1136/gut.47.6.753.

Bai, Zhigang, Yingjiang Ye, Bin Liang, Feng Xu, Hui Zhang, Yanbin Zhang, Jiarou Peng, et al. “Proteomics-Based Identification of a Group of Apoptosis-Related Proteins and Biomarkers in Gastric Cancer.” *International Journal of Oncology* 38, no. 2: 375–83 (2011). https://doi.org/10.3892/ijo.2010.873.

Bartkowiak, Kai, Katharina E. Effenberger, Sönke Harder, Antje Andreas, Friedrich Buck, Jasna Peter-Katalinic, Klaus Pantel, and Burkhard H. Brandt. “Discovery of a Novel Unfolded Protein Response Phenotype of Cancer Stem/Progenitor Cells from the Bone Marrow of Breast Cancer Patients.” *Journal of Proteome Research* 9, no. 6: 3158–68 (2010). https://doi.org/10.1021/pr100039d.

Baryshev, Mikhail, Ernest Sargsyan, and Souren Mkrtchian. “ERp29 Is an Essential Endoplasmic Reticulum Factor Regulating Secretion of Thyroglobulin.” *Biochemical and Biophysical Research Communications* 340, no. 2: 617–24 (2006). https://doi.org/10.1016/j.bbrc.2005.12.052.

Baumann, O., Walz, B. Endoplasmic reticulum of animal cells and its organization into structural and functional domains. Int. Rev. Cytol. 205, 149–214 (2001).

Benham, A. M., A. Cabibbo, A. Fassio, N. Bulleid, R. Sitia, and I. Braakman. “The CXXCXXC Motif Determines the Folding, Structure and Stability of Human Ero1-Lα.” *The EMBO Journal* 19, no. 17: 4493–4502 (2000). https://doi.org/10.1093/emboj/19.17.4493.

Bi, Meixia, Christine Naczki, Marianne Koritzinsky, Diane Fels, Jaime Blais, Nianping Hu, Heather Harding, et al. “ER Stress-Regulated Translation Increases Tolerance to Extreme Hypoxia and Promotes Tumor Growth.” *The EMBO Journal* 24, no. 19: 3470–81 (2005). https://doi.org/10.1038/sj.emboj.7600777.

Cabibi, D., A.G. Giannone, C. Mascarella, C. Guarnotta, M. Castiglia, G. Pantuso, and E. Fiorentino. “Immunohistochemical/Histochemical Double Staining Method in the Study of the Columnar Metaplasia of the Oesophagus.” *European Journal of Histochemistry : EJH* 58, no. 1 (2014). https://doi.org/10.4081/ejh.2014.2326.

Chen, Yunjia, Yong Zhang, Yanbin Yin, Ge Gao, Songgang Li, Ying Jiang, Xiaocheng Gu, and Jingchu Luo. “SPD--a Web-Based Secreted Protein Database.” *Nucleic Acids Research* 33, no. Database issue: D169-173 (2005). https://doi.org/10.1093/nar/gki093.

Clarke, David J., Euan Murray, Jakub Faktor, Aiman Mohtar, Borek Vojtesek, C. Logan MacKay, Pat Langridge Smith, and Ted R. Hupp. “Mass Spectrometry Analysis of the Oxidation States of the Pro-Oncogenic Protein Anterior Gradient-2 Reveals Covalent Dimerization via an Intermolecular Disulphide Bond.” *Biochimica Et Biophysica Acta* 1864, no. 5: 551–61 (2016). https://doi.org/10.1016/j.bbapap.2016.02.011.

Cowman, M. K., M. F. Slahetka, D. M. Hittner, J. Kim, M. Forino, and G. Gadelrab. “Polyacrylamide-Gel Electrophoresis and Alcian Blue Staining of Sulphated Glycosaminoglycan Oligosaccharides.” *The Biochemical Journal* 221, no. 3: 707–16 (1984).

Dias-Gunasekara, Sanjika, Marcel van Lith, J. A. Gareth Williams, Ritu Kataky, and Adam M. Benham. “Mutations in the FAD Binding Domain Cause Stress-Induced Misoxidation of the Endoplasmic Reticulum Oxidoreductase Ero1beta.” *The Journal of Biological Chemistry* 281, no. 35: 25018–25 (2006). https://doi.org/10.1074/jbc.M602354200.

DiMaio, Michael A., Shirley Kwok, Kelli D. Montgomery, Anson W. Lowe, and Reetesh K. Pai. “Immunohistochemical Panel for Distinguishing Esophageal Adenocarcinoma from Squamous Cell Carcinoma: A Combination of P63, Cytokeratin 5/6, MUC5AC, and AGR2 Allows Optimal Subtyping.” *Human Pathology* 43, no. 11: 1799–1807 (2012). https://doi.org/10.1016/j.humpath.2012.03.019.

Dong, Aiwen, Aparna Gupta, Reetesh K. Pai, May Tun, and Anson W. Lowe. “The Human Adenocarcinoma-Associated Gene, AGR2, Induces Expression of Amphiregulin through Hippo Pathway Co-Activator YAP1 Activation.” *The Journal of Biological Chemistry* 286, no. 20: 18301–10 (2011). https://doi.org/10.1074/jbc.M110.215707.

Dvorak, Katerina, Claire M Payne, Melissa Chavarria, Lois Ramsey, Barbora Dvorakova, Harris Bernstein, Hana Holubec, et al. “Bile Acids in Combination with

Low PH Induce Oxidative Stress and Oxidative DNA Damage: Relevance to the Pathogenesis of Barrett's Oesophagus." *Gut* 56, no. 6: 763–71 (2007). https://doi.org/10.1136/gut.2006.103697.

Fagerberg, Linn, Björn M. Hallström, Per Oksvold, Caroline Kampf, Dijana Djureinovic, Jacob Odeberg, Masato Habuka, et al. "Analysis of the Human Tissue-Specific Expression by Genome-Wide Integration of Transcriptomics and Antibody-Based Proteomics." *Molecular & Cellular Proteomics: MCP* 13, no. 2: 397–406 (2014). https://doi.org/10.1074/mcp.M113.035600.

Fessart, Delphine, Charlotte Domblides, Tony Avril, Leif A. Eriksson, Hugues Begueret, Raphael Pineau, Camille Malrieux, et al. "Secretion of Protein Disulphide Isomerase AGR2 Confers Tumorigenic Properties." *ELife* 5 30 (2016). https://doi.org/10.7554/eLife.13887.

Fletcher, G. C., S. Patel, K. Tyson, P. J. Adam, M. Schenker, J. A. Loader, L. Daviet, et al. "HAG-2 and HAG-3, Human Homologues of Genes Involved in Differentiation, Are Associated with Oestrogen Receptor-Positive Breast Tumours and Interact with Metastasis Gene C4.4a and Dystroglycan." *British Journal of Cancer* 88, no. 4: 579–85 (2003). https://doi.org/10.1038/sj.bjc.6600740.

Garbi, Natalio, Satoshi Tanaka, Frank Momburg, and Günter J. Hämmerling. "Impaired Assembly of the Major Histocompatibility Complex Class I Peptide-Loading Complex in Mice Deficient in the Oxidoreductase ERp57." *Nature Immunology* 7, no. 1: 93–102 (2006). https://doi.org/10.1038/ni1288.

Gupta, Aparna, Aiwen Dong, and Anson W. Lowe. "AGR2 Gene Function Requires a Unique Endoplasmic Reticulum Localization Motif." *The Journal of Biological Chemistry* 287, no. 7: 4773–82 (2012). https://doi.org/10.1074/jbc.M111.301531.

Hao, Ying, George Triadafilopoulos, Peyman Sahbaie, Harvey S. Young, M. Bishr Omary, and Anson W. Lowe. "Gene Expression Profiling Reveals Stromal Genes Expressed in Common between Barrett's Esophagus and Adenocarcinoma." *Gastroenterology* 131, no. 3: 925–33 (2006). https://doi.org/10.1053/j.gastro.2006.04.026.

Harris, J. W., and J. E. Biaglow. "Non-Specific Reactions of the Glutathione Oxidant 'Diamide' with Mammalian Cells." *Biochemical and Biophysical Research Communications* 46, no. 5: 1743–49 (1972). https://doi.org/10.1016/0006-291X(72)90045-9.

Higa, Arisa, Audrey Mulot, Frédéric Delom, Marion Bouchecareilh, Duc Thang Nguyên, Daniel Boismenu, Michael J. Wise, and Eric Chevet. "Role of Pro-Oncogenic Protein Disulfide Isomerase (PDI) Family Member Anterior Gradient 2 (AGR2) in the Control of Endoplasmic Reticulum Homeostasis." *The Journal of Biological Chemistry* 286, no. 52: 44855–68 (2011). https://doi.org/10.1074/jbc.M111.275529.

Ho, Melissa E., Sue-Ing Quek, Lawrence D. True, Roland Seiler, Achim Fleischmann, Lora Bagryanova, Sara R. Kim, et al. “Bladder Cancer Cells Secrete While Normal Bladder Cells Express but Do Not Secrete AGR2.” *Oncotarget* 7, no. 13: 15747–56 (2016). https://doi.org/10.18632/oncotarget.7400.

Hrstka, R., Bouchalova, P., Michalova, E., Matoulkova, E., Muller, P., Coates, P.J., Vojtesek, B., 2016. AGR2 oncoprotein inhibits p38 MAPK and p53 activation through a DUSP10-mediated regulatory pathway. Mol Oncol 10, 652–662 (2016). https://doi.org/10.1016/j.molonc.2015.12.003.

Johnson, Dennis R., Maisoun Abdelbaqui, Maryam Tahmasbi, Zoltan Mayer, Hung-Wei Lee, Mokenge P. Malafa, and Domenico Coppola. “CDX2 Protein Expression Compared to Alcian Blue Staining in the Evaluation of Esophageal Intestinal Metaplasia.” *World Journal of Gastroenterology* 21, no. 9: 2770–76 (2015). https://doi.org/10.3748/wjg.v21.i9.2770.

Kakihana, Taichi, Kazutaka Araki, Stefano Vavassori, Shun-ichiro Iemura, Margherita Cortini, Claudio Fagioli, Tohru Natsume, Roberto Sitia, and Kazuhiro Nagata. “Dynamic Regulation of Ero1α and Peroxiredoxin 4 Localization in the Secretory Pathway.” *The Journal of Biological Chemistry* 288, no. 41: 29586–94 (2013). https://doi.org/10.1074/jbc.M113.467845.

Ko, Wen-Chang, Keisuke Sugahara, Takumi Sakuma, Ching-Yu Yen, Shyun-Yeu Liu, Gwo-An Liaw, and Takahiko Shibahara. “Copy Number Changes of CRISP3 in Oral Squamous Cell Carcinoma.” *Oncology Letters* 3, no. 1: 75–81 (2012). https://doi.org/10.3892/ol.2011.418.

Kosower, N. S., E. M. Kosower, B. Wertheim, and W. S. Correa. “Diamide, a New Reagent for the Intracellular Oxidation of Glutathione to the Disulfide.” *Biochemical and Biophysical Research Communications* 37, no. 4: 593–96 (1969).

Lee, Ji Yun, Kyung Kim, Hyun Hwan Sung, Hwang Gyun Jeon, Byong Chang Jeong, Seong Il Seo, Seong Soo Jeon, et al. “Molecular Characterization of Urothelial Carcinoma of the Bladder and Upper Urinary Tract.” *Translational Oncology* 11, no. 1: 37–42 (2017). https://doi.org/10.1016/j.tranon.2017.10.008.

Lewis, M. J., and H. R. Pelham. “A Human Homologue of the Yeast HDEL Receptor.” *Nature* 348, no. 6297: 162–63 (1990). https://doi.org/10.1038/348162a0.

Liu, Dong, Philip S. Rudland, D. Ross Sibson, Angela Platt-Higgins, and Roger Barraclough. “Human Homologue of Cement Gland Protein, a Novel Metastasis Inducer Associated with Breast Carcinomas.” *Cancer Research* 65, no. 9: 3796–3805 (2005). https://doi.org/10.1158/0008-5472.CAN-04-3823.

Ma, Si-Rui, Wei-Ming Wang, Cong-Fa Huang, Wen-Feng Zhang, and Zhi-Jun Sun. “Anterior Gradient Protein 2 Expression in High Grade Head and Neck Squamous Cell Carcinoma Correlated with Cancer Stem Cell and Epithelial Mesenchymal

Transition." *Oncotarget* 6, no. 11: 8807–21 (2015). https://doi.org/10.18632/oncotarget.3556.

Magnuson, Brian, Emily K. Rainey, Thomas Benjamin, Mikhail Baryshev, Souren Mkrtchian, and Billy Tsai. "ERp29 Triggers a Conformational Change in Polyomavirus to Stimulate Membrane Binding." *Molecular Cell* 20, no. 2: 289–300 (2005). https://doi.org/10.1016/j.molcel.2005.08.034.

Maslon, Magdalena M., Roman Hrstka, Borek Vojtesek, and Ted R. Hupp. "A Divergent Substrate-Binding Loop within the pro-Oncogenic Protein Anterior Gradient-2 Forms a Docking Site for Reptin." *Journal of Molecular Biology* 404, no. 3: 418–38 (2010). https://doi.org/10.1016/j.jmb.2010.09.035.

McCool, D J, Y Okada, J F Forstner, and G G Forstner. "Roles of Calreticulin and Calnexin during Mucin Synthesis in LS180 and HT29/A1 Human Colonic Adenocarcinoma Cells." *Biochemical Journal* 341, no. Pt 3: 593–600 (1999).

Mezzacasa, Anna, and Ari Helenius. "The Transitional ER Defines a Boundary for Quality Control in the Secretion of TsO45 VSV Glycoprotein." *Traffic (Copenhagen, Denmark)* 3, no. 11: 833–49 (2002).

Nancarrow, Derek J., Andrew D. Clouston, B. Mark Smithers, David C. Gotley, Paul A. Drew, David I. Watson, Sonika Tyagi, et al. "Whole Genome Expression Array Profiling Highlights Differences in Mucosal Defense Genes in Barrett's Esophagus and Esophageal Adenocarcinoma." *PloS One* 6, no. 7 (2011): e22513. https://doi.org/10.1371/journal.pone.0022513.

Nørgaard, P., and J. R. Winther. "Mutation of Yeast Eug1p CXXS Active Sites to CXXC Results in a Dramatic Increase in Protein Disulphide Isomerase Activity." *The Biochemical Journal* 358, no. Pt 1: 269–74 (2001).

Park, Kyoungsook, Yong Jin Chung, Hyekyung So, Kwangsoo Kim, Junsoo Park, Mijoung Oh, Minwha Jo, et al. "AGR2, a Mucinous Ovarian Cancer Marker, Promotes Cell Proliferation and Migration." *Experimental & Molecular Medicine* 43, no. 2: 91–100 (2011). https://doi.org/10.3858/emm.2011.43.2.011.

Park, Sung-Woo, Guohua Zhen, Catherine Verhaeghe, Yasuhiro Nakagami, Louis T. Nguyenvu, Andrea J. Barczak, Nigel Killeen, and David J. Erle. "The Protein Disulfide Isomerase AGR2 Is Essential for Production of Intestinal Mucus." *Proceedings of the National Academy of Sciences of the United States of America* 106, no. 17: 6950–55 (2009). https://doi.org/10.1073/pnas.0808722106.

Patel, Pryank, Christopher Clarke, Dong Liu Barraclough, Thomas Adam Jowitt, Philip Spencer Rudland, Roger Barraclough, and Lu-Yun Lian. "Metastasis-Promoting Anterior Gradient 2 Protein Has a Dimeric Thioredoxin Fold Structure and a Role in Cell Adhesion." *Journal of Molecular Biology* 425, no. 5: 929–43 (2013). https://doi.org/10.1016/j.jmb.2012.12.009.

Pizzi, Marco, Matteo Fassan, Stefano Realdon, Mariangela Balistreri, Giorgio Battaglia, Cinzia Giacometti, Giovanni Zaninotto, Vittorina Zagonel, Michele De Boni, and Massimo Rugge. "Anterior Gradient 2 Profiling in Barrett Columnar Epithelia and Adenocarcinoma." *Human Pathology* 43, no. 11: 1839–44 (2012). https://doi.org/10.1016/j.humpath.2012.01.004.

Pohler, Elizabeth, Ashley L. Craig, James Cotton, Laura Lawrie, John F. Dillon, Pete Ross, Neil Kernohan, and Ted R. Hupp. "The Barrett's Antigen Anterior Gradient-2 Silences the P53 Transcriptional Response to DNA Damage." *Molecular & Cellular Proteomics: MCP* 3, no. 6: 534–47 (2004). https://doi.org/10.1074/mcp.M300089-MCP200.

Ramachandran, Vijaya, Thiruvengadam Arumugam, Huamin Wang, and Craig D. Logsdon. "Anterior Gradient 2 Is Expressed and Secreted during the Development of Pancreatic Cancer and Promotes Cancer Cell Survival." *Cancer Research* 68, no. 19: 7811–18 (2008). https://doi.org/10.1158/0008-5472.CAN-08-1320.

Romero-Ramirez, Lorenzo, Hongbin Cao, Daniel Nelson, Ester Hammond, Ann-Hwee Lee, Hiderou Yoshida, Kazutoshi Mori, et al. "XBP1 Is Essential for Survival under Hypoxic Conditions and Is Required for Tumor Growth." *Cancer Research* 64, no. 17: 5943–47 (2004). https://doi.org/10.1158/0008-5472.CAN-04-1606.

Ross, Christopher A., and Michelle A. Poirier. "Protein Aggregation and Neurodegenerative Disease." *Nature Medicine* 10 Suppl (2004): S10-17. https://doi.org/10.1038/nm1066.

Roth, R. A., and S. B. Pierce. "In Vivo Cross-Linking of Protein Disulfide Isomerase to Immunoglobulins." *Biochemistry* 26, no. 14: 4179–82 (1987).

Ryu, Joohyun, Sung Goo Park, Phil Young Lee, Sayeon Cho, Do Hee Lee, Gwang Hoon Kim, Jeong-Hoon Kim, and Byoung Chul Park. "Dimerization of Pro-Oncogenic Protein Anterior Gradient 2 Is Required for the Interaction with BiP/GRP78." *Biochemical and Biophysical Research Communications* 430, no. 2: 610–15 (2013). https://doi.org/10.1016/j.bbrc.2012.11.105.

Schroeder, Bradley W., Catherine Verhaeghe, Sung-Woo Park, Louis T. Nguyenvu, Xiaozhu Huang, Guohua Zhen, and David J. Erle. "AGR2 Is Induced in Asthma and Promotes Allergen-Induced Mucin Overproduction." *American Journal of Respiratory Cell and Molecular Biology* 47, no. 2: 178–85 (2012). https://doi.org/10.1165/rcmb.2011-0421OC.

Solaymani-Dodaran, M., R. F. A. Logan, J. West, T. Card, and C. Coupland. "Risk of Oesophageal Cancer in Barrett's Oesophagus and Gastro-Oesophageal Reflux." *Gut* 53, no. 8: 1070–74 (2004). https://doi.org/10.1136/gut.2003.028076.

Steedman, H. F. “Alcian Blue 8GS: A New Stain for Mucin.” *Journal of Cell Science* s3-91, no. 16: 477–79 (1950).

Tavender, Timothy J., Alyson M. Sheppard, and Neil J. Bulleid. “Peroxiredoxin IV Is an Endoplasmic Reticulum Localised Enzyme Forming Oligomeric Complexes in Human Cells.” *The Biochemical Journal* 411, no. 1: 191–99 (2008). https://doi.org/10.1042/BJ20071428.

Thompson, D. A., and R. J. Weigel. “HAG-2, the Human Homologue of the Xenopus Laevis Cement Gland Gene XAG-2, Is Coexpressed with Estrogen Receptor in Breast Cancer Cell Lines.” *Biochemical and Biophysical Research Communications* 251, no. 1: 111–16 (1998). https://doi.org/10.1006/bbrc.1998.9440.

Vavassori, Stefano, Margherita Cortini, Shoji Masui, Sara Sannino, Tiziana Anelli, Imma R. Caserta, Claudio Fagioli, et al. “A PH-Regulated Quality Control Cycle for Surveillance of Secretory Protein Assembly.” *Molecular Cell* 50, no. 6: 783–92 (2013). https://doi.org/10.1016/j.molcel.2013.04.016.

Vitello, Elizabeth A., Sue-Ing Quek, Heather Kincaid, Thomas Fuchs, Daniel J. Crichton, Pamela Troisch, and Alvin Y. Liu. “Cancer-Secreted AGR2 Induces Programmed Cell Death in Normal Cells.” *Oncotarget* 7, no. 31: 49425–34 (2016). https://doi.org/10.18632/oncotarget.9921.

Voltaggio, Lysandra, Elizabeth A. Montgomery, and Dora Lam-Himlin. “A Clinical and Histopathologic Focus on Barrett Esophagus and Barrett-Related Dysplasia.” *Archives of Pathology & Laboratory Medicine* 135, no. 10: 1249–60 (2011). https://doi.org/10.5858/arpa.2011-0019-RA.

Wang, Chao, Chen, S., Wang, X., Wang, L., Wallis, A.K., Freedman, R.B., Wang, Chih-chen. Plasticity of human protein disulfide isomerase: evidence for mobility around the X-linker region and its functional significance. J. Biol. Chem. 285, 26788–26797 (2010). https://doi.org/10.1074/jbc.M110.107839

Wilson, C. L., A. H. Sims, A. Howell, C. J. Miller, and R. B. Clarke. “Effects of Oestrogen on Gene Expression in Epithelium and Stroma of Normal Human Breast Tissue.” *Endocrine-Related Cancer* 13, no. 2: 617–28 (2006). https://doi.org/10.1677/erc.1.01165.

Wouters, Bradly G., and Marianne Koritzinsky. “Hypoxia Signalling through MTOR and the Unfolded Protein Response in Cancer.” *Nature Reviews. Cancer* 8, no. 11: 851–64 (2008). https://doi.org/10.1038/nrc2501.

Wu, H., Carvalho, P., Voeltz, G.K. Here, there, and everywhere: The importance of ER membrane contact sites. Science 361, eaan5835 (2018). https://doi.org/10.1126/science.aan5835

Xu, Shili, Saranya Sankar, and Nouri Neamati. “Protein Disulfide Isomerase: A Promising Target for Cancer Therapy.” *Drug Discovery Today* 19, no. 3: 222–40 (2014). https://doi.org/10.1016/j.drudis.2013.10.017.

Zhang, Jin-San, Aiyu Gong, John C. Cheville, David I. Smith, and Charles Y. F. Young. “AGR2, an Androgen-Inducible Secretory Protein Overexpressed in Prostate Cancer.” *Genes, Chromosomes & Cancer* 43, no. 3: 249–59 (2005). https://doi.org/10.1002/gcc.20188.

Zhang, Yuexing, Douglas Linn, Zhenqiu Liu, Jonathan Melamed, Fabio Tavora, Charles Y. Young, Angelika M. Burger, and Anne W. Hamburger. “EBP1, an ErbB3-Binding Protein, Is Decreased in Prostate Cancer and Implicated in Hormone Resistance.” *Molecular Cancer Therapeutics* 7, no. 10: 3176–86 (2008). https://doi.org/10.1158/1535-7163.MCT-08-0526.

Zhao, Fang, Robert Edwards, Diana Dizon, Jennifer R. Mastroianni, Mikhail Geyfman, André J. Ouellette, Bogi Andersen, and Steven M Lipkin. “Disruption of Paneth and Goblet Cell Homeostasis and Increased Endoplasmic Reticulum Stress in Agr2−/− Mice.” *Developmental Biology* 338, no. 2: 270–79 (2010). https://doi.org/10.1016/j.ydbio.2009.12.008.

Zheng, W., P. Rosenstiel, K. Huse, C. Sina, R. Valentonyte, N. Mah, L. Zeitlmann, et al. “Evaluation of AGR2 and AGR3 as Candidate Genes for Inflammatory Bowel Disease.” *Genes and Immunity* 7, no. 1: 11–18 (2006). https://doi.org/10.1038/sj.gene.6364263.

Zhu, Hong, David Chi Leung Lam, Kam Chu Han, Vicky Pui Chi Tin, Wai Sing Suen, Elaine Wang, Wah Kit Lam, Wei Wen Cai, Lap Ping Chung, and Maria Pik Wong. “High Resolution Analysis of Genomic Aberrations by Metaphase and Array Comparative Genomic Hybridization Identifies Candidate Tumour Genes in Lung Cancer Cell Lines.” *Cancer Letters* 245, no. 1–2: 303–14 (2007). https://doi.org/10.1016/j.canlet.2006.01.020.